UNIVERSITY OF CALIFORNIA SAN DIEGO

Modulation of RNA-dependent Interactions in Stress Granules Prevents Persistent TPD-43 accumulation in ALS/FTD

A dissertation submitted in partial satisfaction of the
requirements for the degree Doctor of Philosophy

in

Biomedical Sciences

by

Mark Yang Fang

Committee in charge:

Professor Gene W. Yeo, Chair
Professor Eric Bennett
Professor Don W. Cleveland
Professor Jens Lykke-Andersen
Professor Christina Sigurdson

2019

The Dissertation of Mark Yang Fang is approved, and it is acceptable in quality and form for publication on microfilm and electronically:

_____

_____

_____

_____

_____

Chair

University of California San Diego

2019

TABLE OF CONTENTS

LIST OF ABBREVIATIONS

AA	L-ascorbic acid
ALS	Amyotrophic lateral sclerosis
AoH	Arm of homology
Ars	Sodium arsenite
ATP	Adenosine triphosphate
BCA	Bicinchoninic acid
BDNF	Brain-derived neurotrophic factor
BSA	Bovine serum albumin
CAS	Chemical abstracts service
CH	CHIR99021
CHX	Cycloheximide
Cmpd	Compound
CNTF	Ciliary neurotrophic factor
CO_2	Carbon dioxide
CRISPR	Clustered regularly interspaced short palindromic repeats
Ctrl	Control
DAPI	4’,6-diamidino-2-phenylindole
DM	Dorsomorphin
DMEM	Dulbecco’s Modified Eagle Medium
DMSO	Dimethyl sulfoxide
EB	Embryoid body
EDTA	Ethylenediaminetetraacetic acid
EME	Emetine
ER	Endoplasmic reticulum

ERK	Extracellular signal regulated kinase
F12	F12 medium
FDA/IN	Food and Drug Administration/International approved drugs
FTD	Frontotemporal dementia
GABA	Gamma-aminobutyric acid
GDNF	Glial cell line-derived neurotrophic factor
GFP	Green fluorescent protein
HCS	High-content screening
hESC	Human embryonic stem cells
HRI	Human heme-regulated eukaryotic initiation factor 2alpha kinase
HRP	Horseradish peroxidase
HTS	High-throughput screening
Hygro	Hygromycin
IC50	50% inhibitor concentration
IDR	Intrinsically disordered region
IF	Immunofluorescence
IgG	Immunoglobulin G
iPSC	Induced pluripotent stem cell
iPS-MN	Induced pluripotent stem cell-derived motor neuron
IRES	Internal ribosome entry site
kDa	KiloDalton
LDS	Lithium dodecyl sulfate
LLPS	Liquid-liquid phase separation
MN	Motor neuron
MOA	Mechanism of action

mRNA	Messenger ribonucleic acid
mRNP	Messenger ribonucleoprotein
M.W.	Molecular weight
$NaAsO_2$	Sodium arsenite
NCBI	National Center for Biotechnology Information
Neg	Negative
NLS	Nuclear localization signal
NPC	Small molecular neural precursor cell
n.s.	Not significant
pA	Polyadenylation signal
PBS	Phosphate buffered saline
PDL	Poly-D-lysine
PERK	Protein kinase R-like endoplasmic reticulum kinase
PFA	Paraformaldehyde
PLA2	Phospholipase A2
PLO	Poly-L-ornithine
PMA	Purmorphamine
Pos	Positive
PrLD	Prion-like domain
PrP	Prion protein
puro	Puromycin
QC	Quality control
RBP	Ribonucleic acid binding protein
RFP	Red fluorescent protein
RIPA buffer	Radioimmunoprecipitation assay buffer

SB	SB431542
SG	Stress granule
SWIMMER	Statistical Workflow for Identification of Molecular Modulators of ribonucleoprotEins by Random variance modeling
TBST	Tris-buffered saline and Tween 20
thap	Thapsigargin
U	Unit
UTR	Untranslated region
v/v	Volume/volume ratio
WB	Western blot

LIST OF SYMBOLS

α	Alpha subunit of protein complex
Δ	Deletion of a region of DNA or protein

LIST OF FIGURES

LIST OF TABLES

ACKNOWLEDGEMENTS

I would like to acknowledge Professor Gene W. Yeo for his support as the chair of my committee. Through multiple drafts and many long nights, his guidance has proved to be invaluable.

I would also like to acknowledge Dr. Sebastian Markmiller, without whom my research would have no doubt taken five times as long. It is his support that helped me in an immeasurable way.

Chapters 1-3, in full, are adapted from material which has been submitted for publication as it may appear in Science Translational Medicine, 2019, M. Y. Fang, S. Markmiller, W. E. Dowdle, A. Q. Vu, P. J. Bushway, S. Ding, M. M. Mercola, J. W. Lewcock, G. W. Yeo. The dissertation author was the primary investigator and author of this paper.

VITA

2011	Bachelor of Sciences, Stanford University
2011-2012	Research Assistant, Stanford University
2012-2014	School of Medicine, University of California San Diego
2019	Doctor of Philosophy, University of California San Diego

PUBLICATIONS

P. Leucht, J. Jiang, D. Cheng, B. Liu, G. Dhamdhere, M. Y. Fang, S. D. Monica, J. J. Urena, W. Cole, L. R. Smith, A. B. Castillo, M. T. Longaker, J. A. Helms, Wnt3a reestablishes osteogenic capacity to bone grafts from aged animals. *J Bone Joint Surg Am* **95**, 1278-1288 (2013).

J. L. Whyte, A. A. Smith, B. Liu, W. R. Manzano, N. D. Evans, G. R. Dhamdhere, M. Y. Fang, H. Y. Chang, A. E. Oro, J. A. Helms, Augmenting endogenous Wnt signaling improves skin wound healing. *PLoS One* **8**, e76883 (2013).

G. R. Dhamdhere, M. Y. Fang, J. Jiang, K. Lee, D. Cheng, R. C. Olveda, B. Liu, K. A. Mulligan, J. C. Carlson, R. C. Ransom, W. I. Weis, J. A. Helms, Drugging a stem cell compartment using Wnt3a protein as a therapeutic. *PLoS One* **9**, e83650 (2014).

D. A. Nelles, M. Y. Fang, S. Aigner, G. W. Yeo, Applications of Cas9 as an RNA-programmed RNA-binding protein. *Bioessays* **37**, 732-739 (2015).

E. L. Van Nostrand, G. A. Pratt, A. A. Shishkin, C. Gelboin-Burkhart, M. Y. Fang, B. Sundararaman, S. M. Blue, T. B. Nguyen, C. Surka, K. Elkins, R. Stanton, F. Rigo, M. Guttman, G. W. Yeo, Robust transcriptome-wide discovery of RNA-binding protein binding sites with enhanced CLIP (eCLIP). *Nat Methods* **13**, 508-514 (2016).

D. A. Nelles, M. Y. Fang, M. R. O'Connell, J. L. Xu, S. J. Markmiller,, J. A. Doudna, G. W. Yeo, Programmable RNA Tracking in Live Cells with CRISPR/Cas9. *Cell* **165**, 488-496 (2016).

S. Markmiller, S. Soltanieh, K. L. Server, R. Mak, W. Jin, M. Y. Fang, E. C. Luo, F. Krach, D. Yang, A. Sen, A. Fulzele, J. M. Wozniak, D. J. Gonzalez, M. W. Kankel, F. B. Gao, E. J. Bennett, E. Lecuyer, G. W. Yeo, Context-Dependent and Disease-Specific Diversity in Protein Interactions within Stress Granules. *Cell* **172**, 590-604 e513 (2018).

FIELDS OF STUDY

Major Field: Bioengineering

Studies in Regenerative Medicine
Professor Jill A. Helms

Major Field: Neuroscience

Studies in Neurodegeneration
Professor Gene W. Yeo

ABSTRACT OF THE DISSERTATION

Modulation of RNA-dependent Interactions in Stress Granules Prevents Persistent TPD-43 accumulation in ALS/FTD

by

Mark Yang Fang

Doctor of Philosophy in Biomedical Sciences

University of California San Diego, 2019

Professor Gene W. Yeo, Chair

Stress granules (SG) form during cellular stress and have been linked to neurodegenerative diseases such as amyotrophic lateral sclerosis and frontotemporal dementia (ALS/FTD). Strategies to modulate SGs have the potential to yield insights into their role in pathophysiology. We performed a high-content screen to identify small molecules that alter SG properties in proliferative cells and iPSC-derived motor neurons (iPS-MNs). One major class of hit compounds are nucleic acid intercalating molecules that disrupt recruitment of ALS-associated RNA-binding proteins (RBPs), such as TDP-43 and FUS/TLS, into SGs and reduce accumulation of cytoplasmic TDP-43 in iPS-MNs from ALS patients.

These findings corroborate our biochemical results indicating that SGs accumulate ALS-associated RBPs in their shells in an RNA-dependent manner. Thus, SGs contribute to persistent accumulation of TDP-43, and nucleic acid intercalating compounds represent a promising new therapeutic approach for treating ALS/FTD.

INTRODUCTION

Stress granules (SGs) assemble transiently in response to cellular stresses such as oxidative damage, heat shock and environmental toxins, as an adaptive survival mechanism for cells (*1, 2*). SGs contain both proteins as well as cellular messenger RNAs, which are locked in a translationally stalled state induced by phosphorylation of serine 51 of the translation initiation factor eIF2α (*3, 4*). By modulating mRNA translation and recruiting intracellular signaling proteins, SGs are believed to triage intracellular activity toward an integrated stress response (*5-8*). SGs are highly dynamic, exhibiting liquid-like behaviors and begin to disassemble within minutes of removal of stress (*9*). These liquid-like properties are thought to be mediated by the intrinsically disordered regions (IDRs) common to many proteins found in SGs (*10-15*). Neurodegeneration-linked mutations in genes such as *FUS*, *HNRNPA2B1 and TARDBP* (encoding TDP-43), frequently cluster in areas corresponding to IDRs in the encoded proteins, potentially altering their liquid-like phase-separation properties (*16-18*). These mutations are implicated in hereditary forms of frontotemporal dementia (FTD) and amyotrophic lateral sclerosis (ALS) (*19-23*), a fatal, incurable disease characterized by progressive degeneration of motor neurons (MNs) (*24*). *In vitro* studies of recombinant IDRs carrying ALS-associated mutations report that phase-separated droplets of mutant IDRs can transition from a liquid-like state to a solid-like state resembling prion inclusion bodies and characterized by cross-beta sheet fibrils (*18, 19, 25-27*). To illustrate, recombinant mutant IDR from HNRNPA2B1 undergoes liquid-liquid phase separation (LLPS) followed by spontaneous maturation into insoluble fibers (*18, 19*). Therefore, these IDR mutations likely predispose assembly of inclusion bodies, and is speculated to cause toxic loss-of-function and contributing to disease pathophysiology. Indeed, a hallmark feature of nearly all ALS patients is the presence of cytoplasmic TDP-43-containing inclusion bodies

within MNs that contain SG-associated proteins such as PABPC1, TIA1, eIF3, ATXN2, HNRNPA2B1, and FUS (*19, 28-32*).

Recent studies that characterize the composition of SGs have revealed that a large fraction of protein components found in SG appear to be pre-assembled prior to stress (*11, 12*). Also, a super-resolution microscopy study reported the existence of substructures called SG cores, around which a halo of additional proteins forms, called the SG shell (*10*). It is very likely that cores and shells contain different protein components, with differences that may relate to pathogenesis of disease (*3, 10*). Excitingly, the modulation of some SG protein components appears to alleviate degenerative phenotypes in animal models of ALS (*11, 33-35*). Despite these advances, there still exists an urgent need to understand how ALS-associated proteins such as TDP-43 relate to SGs and for new tools that can readily perturb these relationships.

Thus, to accelerate our understanding of SGs and their connections to molecular pathophysiology in neurodegenerative disease, we conducted a high-content screen for small molecules that robustly modulate various aspects of SG biology. We identified several classes of compounds, including small molecules that act at cell surface targets such as ion channels, receptors, or lipid membranes, and compounds that modulate inflammatory signaling pathways. Interestingly, we also identified a large group of molecules with planar moieties such as nucleic acid intercalators, supporting the hypothesis that SG formation requires nucleic acid interactions. In parallel, we discovered that SGs accumulate ALS-associated proteins in an RNA-dependent manner, and that molecules with planar moieties disrupt this accumulation. We show SGs can induce persistent cytoplasmic localization of TDP-43 in an induced pluripotent stem cell-derived MN (iPS-MN) model of disease, and that iPS-MNs carrying ALS-associated mutations in *TARDBP* or *FUS* exhibit exacerbated cytoplasmic localization of TDP-43. Excitingly, nucleic acid intercalators with planar moieties

prevent co-localization of TDP-43 with SGs and reduce cytoplasmic localization of TDP-43 in mutant iPS-MNs. We believe our results expand our understanding of SG biology, establish a mechanistic relationship from SGs to disease pathophysiology, and pave the way to development of a new classes of therapeutics for ALS/FTD.

CHAPTER 1: High-content Screening Reveals Molecules with Planar Moieties as Small Molecule Modulators of Stress Granules

1.1: Generation of Robust SG Assays

G3BP1 is a key protein required for SG formation (*1, 36*). As G3BP1 is found in both the SG core and, to a lesser extent, the SG shell (*10*), we reasoned that identifying compounds that modulate G3BP1-positive puncta formation will unveil molecular principles of SG formation and point toward mechanistic links between SGs and disease pathophysiology. We used CRISPR/Cas9 genome editing in HEK293xT cells and the human induced pluripotent stem cell iPSC line CV-B to insert the coding sequence of green fluorescent protein (GFP) immediately upstream of the stop codon of the endogenous *G3BP1* locus. iPSCs were subsequently differentiated into neural precursor cells using a small molecule protocol (NPCs) or motor neurons (iPS-MNs; Figures 1.1.1-1.1.2 and 1.1.6). The G3BP1-GFP expressing HEK293xT cells, NPCs, and iPS-MNs robustly and reproducibly formed bright GFP-positive puncta upon exposure to sodium arsenite ($NaAsO_2$), which co-localized with immunofluorescence probing of SG-associated proteins UBAP2L, CAPRIN1, DDX3, and PABPC1 but not the negative control CYC, consistent with formation of G3BP1-containing SGs (Figures 1.1.3 and 1.1.7). These $NaAsO_2$-induced puncta were abrogated by pre-treatment with cycloheximide, which inhibits SG formation by stabilizing polysomes, as expected (Figures 1.1.3-1.1.4) (*1*). Our results indicate that these G3BP1-GFP expressing lines are robust SG reporter lines.

We conducted our primary SG screen in the HEK293xT and NPC reporter lines, as they can be expanded to large quantities and seeded in a monodisperse layer facilitating high-content image segmentation. The screening strategy entailed first pre-incubating cells with compounds before stressing the cells with $NaAsO_2$ (Figure 1.1.4). We performed the

screen with a compound-first, stress-second paradigm because this order of operations is most likely to capture both compounds that prevent SGs from forming as well as compounds that cause disassembly of SGs while they have already begun to assemble. Using cycloheximide as a positive control and DMSO vehicle as the negative control, we calculated Z' of 0.51 and 0.42 for the assay in HEK293xT cells and NPCs, respectively (Figure 1.1.5). We concluded from these Z' that the signal-to-noise ratio of the SG assay was sufficient for high-content screening (HCS) (*37*).

1.2: Identification of Diverse Classes of SG-modulating Compounds

We developed an experimental and computational pipeline to screen 3,350 and 5,910 compounds in biological duplicate in HEK293xT cells and NPCs, respectively (Figure 1.2.1). The screened compounds were sourced from five complex small molecule libraries spanning a diverse range of chemical structures and biological activities. Cells were pre-treated with screen compounds at 10μM, then stressed with $NaAsO_2$, fixed, stained with DAPI, and imaged. Screen images were segmented to identify DAPI-positive nuclei and G3BP1-GFP-positive SGs. To measure SG formation, the amount of SG formation per cell was quantified as the total image area enclosed in SGs divided by the total image area enclosed in nuclei. In addition to modulating the amount of SG formation per cell, these compounds may also alter the average SG size and/or the number of SGs per cell. We opined that a compound that inhibits the condensation of SG shell proteins onto SG cores may impair SG fusion and lead to on average smaller but more numerous SGs. We therefore computed two other metrics. The number of SGs formed per cell was quantified as the number of SG puncta divided by the total image area enclosed in nuclei, and the average size of SGs was quantified as the total image area enclosed in SGs divided by the number of SG puncta.

After normalizing the data, we performed a modified one sample Student's *t*-test to identify hit compounds that substantially alter one or more of these SG formation metrics.

We identified 40 and 27 compounds that reduced the amount of SG formation per cell in HEK293xT cells and NPCs, respectively (Figures 1.2.2-1.2.4 and 1.2.6). Additionally, we identified around 50 compounds which modulated SG formation in other ways, such as increasing or decreasing the average size of SGs or changing the number of SGs per cell (Figures 1.2.4 and 1.2.6-1.2.7). Hit compounds were then annotated with the compound name, skeletal formulae, and reported cellular targets using the National Center for Biotechnology Information PubChem database (Figures 1.2.5, 1.2.6, and Table 1.1.1). Supporting the validity of our screening approach, we confirmed that ribosomal inhibitors, such as anisomycin, the aminoglycoside neomycin, and the macrolide roxithromycin, strongly reduced the amount of SG formation per cell (Figures 1.2.3, 1.2.5-1.2.6, and Tables 1.1.2-1.1.4). This is consistent with the fact that ribosomal inhibitors, including cycloheximide and emetine which we included in the screen as positive controls, have been previously described to affect SG formation (*1*). We also confirmed that cytoskeleton targeting compounds, such as the vinka alkaloids vincristine and vinblastine, the microtubule stabilizing drug paclitaxel, and the actin filament stabilizer prieurianin, altered average SG size and/or the number of SGs per cell, consistent with previous reports that the cytoskeleton and cytoskeleton-associated molecular motors play key roles in SG migration, fusion, and maturation (Figures 1.2.3, 1.2.5-1.2.6, and Tables 1.1.2-1.1.4) (*38*).

Among our hit compounds which have not previously been reported to modulate SG formation, we identified many that act on targets at the surface of cells, such as ion channels, surface receptors, transporters, and lipid membranes (Figures 1.2.5-1.2.6 and Tables 1.1.2-1.1.4). Modulation of these plasma membrane targets has not previously been reported to directly modulate SGs. We identified a large group of cardiac glycosides including digitoxin

and proscillaridin A which inhibit the Na^+/K^+-ATPase, as well as the GABA-A chloride channel agonist ivermectin, compounds that bind to voltage gated Na^+ channels such as eslicarbazepine, and amphipathic molecules such as benzethonium which can disrupt lipid membranes (Figure 1.2.3 and Tables 1.1.2-1.1.4). Intriguingly, cardiac glycosides were previously shown to disperse nuclear TDP-43 foci in ALS patient-derived iPS-MNs, though it remains unclear how these compounds exert this effect and whether these nuclear TDP-43 foci are related to SGs (*39*). We also identified the receptor tyrosine kinase inhibitor tyrphostin A9 as a SG-modulating compound, which was reported in a prior study as increasing the survival of MNs carrying SOD1 mutations; however it is uncertain whether this survival effect is related to the ability of tyrphostin A9 to reduce the amount of SG formation per cell (*40*). Interestingly, the D2 receptor antagonist penfluridol reduced the amount of SG formation per cell in NPCs under $NaAsO_2$ stress but inversely modestly induced SG formation in the absence of stress (Figure 1.2.8). Overall, it is possible that several of these compounds which act on targets at the surface of cells modulate SGs by interfering with intracellular ion, solute, and/or osmolarity homeostasis. It has been reported that physical-chemical properties such as ionic content, tonicity, and concentration of hydrotrope solutes such as ATP regulate liquid-liquid phase transitions, which may be important for SG formation (*41, 42*). The divalent cation Zn^{2+} has also been recently reported to regulate the phase transition of the SG-associated protein TIA1 (*43*).

We also identified SG-modulating compounds that target a broad range of intracellular processes, including signaling pathways and transcription factors, metabolism, and inflammatory molecule biosynthesis pathways (Figures 1.2.5-1.2.6 and Tables 1.1.2-1.1.4). Several compounds modulate intracellular signaling pathways, including two compounds which target DYRK and RACK1, proteins at the intersection of SGs/mTOR signaling and SGs/SAPK signaling, respectively (*7, 8*). Some compounds modulate

intracellular metabolic processes which are known to regulate SGs, including heat shock proteins, autophagosomes, and proteasomes (*44-46*). We identified seven hit compounds that have anti-inflammatory activities, including quinacrine, an inhibitor of phospholipase A2 (PLA2), and oxyphenbutazone, a cyclooxygenase inhibitor (Figure 1.2.3 and Tables 1.1.2-1.1.4).

Strikingly, we identified a large group of SG modulatory compounds that contain extended planar molecular moieties, many of which act as nucleic acid intercalating molecules, including mitoxantrone, doxorubicin, and daunorubicin (Figures 1.2.5-1.2.6 and Tables 1.1.2-1.1.4). Molecules with planar moieties and nucleic acid intercalating compounds have not previously been reported to modulate SGs, but these compounds strongly reduced the amount of SG formation per cell, altered the average SG size, and/or changed the number of SGs per cell (Figure 1.2.3 and Tables 1.1.2-1.1.4). Interestingly, doxorubicin has recently been reported to modulate the phase transition diagram of RNA-only condensates containing CAG or CUG repeats *in vitro* and *in vivo* (*3, 47*). Furthermore, quinacrine, another molecule with planar moieties, has previously been reported to directly bind to the prion-like domain of the prion protein PrP and inhibit aggregation *in vitro* (*48*). It is possible these molecules with planar moieties modulate SGs by interacting with RNAs or protein IDRs contained therein.

1.3: Screen Hit Compounds Robustly Inhibit SG Formation Across Different Stress Contexts

We decided to evaluate the two most highly represented groups of hit compounds – molecules with planar moieties and cardiac glycosides. As it is unclear how these compounds modulate SGs, investigations with these compounds are likely to reveal molecular rules underlying SG biology. First, we tested 16 and 18 compounds (Tables 1.2.5-1.2.6) in their capacities to reduce the amount of SG formation per cell in HEK293xT cells

and NPCs, respectively, in a dose-dependent manner over a concentration range covering three orders of magnitude and spanning the initial screening concentration of 10 μM (Figure 1.3.1). We found that 11 and 12 compounds show concentration dependent inhibition of SG formation in HEK293xT cells and NPCs, respectively (Figures 1.3.2 and 1.3.9). After fitting logistic functions to the dose response data, we estimated the compounds' 50% inhibitory concentrations (IC50s; Figure 1.3.2). Most compounds' IC50s were in the single digit micromolar range, which suggests that their mechanisms of actions are unlikely a direct inhibition of one specific protein or target, but rather the sum of activities against several targets.

$NaAsO_2$ generates intracellular oxidative damage that leads to activation of the heme-regulated inhibitor (HRI) kinase, which phosphorylates eIF2α leading to SG assembly. On the other hand, heat shock and thapsigargin-induced endoplasmic reticulum stress stimulate the unfolded protein response, resulting in activation of protein kinase RNA-like endoplasmic reticulum kinase (PERK), which phosphorylates eIF2α (*2*). Thapsigargin also inhibits the autophagosome, hindering SG clearance through autophagy (*44*). We therefore tested whether the hit compounds inhibit SG formation induced by heat shock or the autophagosome and endoplasmic reticulum (ER) poison thapsigargin. We found that at least 10 compounds significantly reduced the amount of SG formation per cell under heat shock or thapsigargin poisoning in both HEK293xT cells and NPCs (Figures 1.3.3-1.3.4). These alternate stressors induce SG formation via signaling through orthogonal cellular stress pathways compared to $NaAsO_2$ (*2*). Because the hit compounds inhibited SG formation under these orthogonal stressors, the mechanisms of action for these compounds are broader than just antioxidants scavenging reactive radicals generated by $NaAsO_2$ or inhibitors of HRI kinase.

Lastly, we tested whether these hit compounds can disassemble pre-existing SGs, by pre-stressing cells with $NaAsO_2$ and then adding compounds after SGs have already developed. We identified 10 and 5 compounds which significantly disassembled pre-formed SGs in HEK293xT cells and NPCs, respectively (Figure 1.3.5). This confirms that our screening paradigm of adding compounds first and stressing second successfully identified compounds which prevent SG formation, but also compounds which induced disassembly of SGs after they have already begun to form. In summary, the compounds tested in the counterscreens, most of which are molecules with planar moieties or cardiac glycosides, robustly inhibited SGs across diverse stress conditions (Figures 1.3.6-1.3.7).

1.4: Hit Compounds Inhibit SG formation in a Manner Independent of eIF2α Phosphorylation

Next, we evaluated if our compounds that inhibit SG formation affected eIF2α phosphorylation or levels. Unexpectedly, most of the hit compounds did not alter $NaAsO_2$-induced phosphorylation of eIF2α at serine 51 or total levels of eIF2α, whereas our control GSK2606414, a selective PERK inhibitor, significantly reduced eIF2α phosphorylation as previously reported (Figures 1.3.8 and 1.3.11) (*34*). Oddly, in the absence of stress, the EBP1 kinase modulating compound WS3, the cardiac glycoside digitoxin, the ribosomal inhibitor anisomycin, and the planar heterocyclic molecule 8-hydroxyquinoline significantly increased phosphorylation of eIF2α above baseline without changing total levels of eIF2α, as did the PERK inhibitor GSK2606414, all without inducing SG formation (Figures 1.2.8, 1.3.10, and 1.3.12). These results indicate that these hit compounds likely act on SGs themselves rather than on upstream kinases or signaling pathways that lead to phosphorylation of eIF2α.

1.5: Screen Compounds Inhibit SG Formation in iPS-MNs

As our primary and counterscreens were performed in proliferative cells, we wanted to evaluate if the hit compounds can also inhibit SG formation in iPS-MNs terminally differentiated from iPSC lines. We utilized 4 iPSC lines from patients carrying ALS-linked mutations in the C-terminal IDR of TDP-43 (N352S and G298S), 2 iPSC lines from patients harboring mutations in the C-terminal NLS of FUS (R521G), and 4 control iPSC lines from healthy controls who are genetically related to the individuals carrying ALS-associated mutations (Figure 1.4.4). We selected 10 hit compounds that were validated as SG inhibiting compounds in the HEK293xT cell and NPC counterscreens and were also representative molecules spanning most of the hit compound classes identified in the screen, including several molecules with planar moieties (Table 1.3.7). We also included the positive control cycloheximide and the negative control DMSO (Table 1.3.7).

Puromycin which has previously been shown to robustly induce SG formation in MNs (*1, 11, 23, 45*) was utilized in our post-mitotic iPS-MNs. We observed that our compounds were effective at inhibiting SG formation across all lines, regardless of mutation status (Figures 1.4.1-1.4.3). Six (of 10) compounds – WS3, quinacrine, anisomycin, mitoxantrone, digitoxin, and pyrvinium – strongly reduced SG formation in all three stress contexts (Figures 1.4.1-1.4.3). Three of these compounds – quinacrine, mitoxantrone, and pyrvinium – are molecules with planar moieties. The remaining four compounds – 8-hydroxyquinoline, daunorubicin, penfluridol, and benzethonium – strongly reduced SG formation in two of three stress contexts (Figures 1.4.1-1.4.3). We concluded that our hit compounds are able to recapitulate their inhibition of SGs in patient-derived iPS-MNs.

1.6: Methods for HCS and Validation of Small Molecule Modulators of SGs

1.6.1: Generating Induced Pluripotent Stem Cells from Fibroblasts of Individuals Carrying ALS-associated Mutations in *TARDBP* or *FUS*

Human iPSC lines carrying ALS-associated mutations in *TARDBP* (N352S) and control individuals were previously reprogrammed from primary fibroblasts obtained by Dr. John Ravits (University of California, San Diego), as described (*49*). Lines carrying *TARDBP* (G298S) mutations were obtained courtesy of Kevin Eggan, as described (*50*). Lines carrying ALS-associated *FUS* (R521G) mutations were previously reprogrammed from primary fibroblasts obtained by Franca Cambi, Edward Kasarskis, and Haining Zhu (University of Kentucky), as described (*51*). Informed consent was obtained from all individuals prior to biopsy, and the use of human fibroblasts for this project was approved by the University of California, San Diego Institutional Review Board.

1.6.2: Generation of Human Induced Pluripotent Stem Cell-derived Small Molecule Neural Precursor Cells

Generation of small molecule neural precursor cells (NPC) from human iPSCs was adapted from a previously reported protocol (*52*). Briefly, iPSCs were dissociated into single cells with Accutase and 3×10^6 cells were seeded into one well of an uncoated 6-well plate. The plate was incubated on an orbital shaker at 90 rpm at 37°C, 5% CO_2 and the cells were grown in DMEM/F12, GlutaMAX supplement media containing N-2 Supplement (1:100 v/v), CTS B27 Supplement, XenoFree (1:50 v/v), L-ascorbic acid (150 μM), CHIR99021 (3 μM), purmorphamine (0.5 μM), Y-27632 (5 μM), as well as two small molecule SMAD inhibitors: SB431542 (10 μM) and dorsomorphin (1 μM). After 2 days, embryoid bodies (EB) formed, at which point 1/3 of the EBs were transferred to three wells of an uncoated 6-well plate to prevent overgrowth; Y-27632 was also withdrawn from the media. Following this passaging, half media changes were performed every 24 hours. At 6 days, formation of neuroepithelium was evident in the EBs, and a full media change was performed to media that omits SB431542 and dorsomorphin (NPC media, also described below). At 8 days, individual EBs

were picked and triturated into small fragments. These EB fragments were seeded onto 10 cm plates coated with Matrigel. These plates were prepared by adding 6 mL of Matrigel (diluted 1:60 v/v in DMEM/F12, GlutaMAX supplement) to each 10 cm plate and incubating for 60 min. EB fragments were maintained on these Matrigel plates as adherent cultures. After 4 days, these adherent EB fragments were dissociated into single cells with Accutase and passaged at a ratio of 1:6 to 1:8 onto new Matrigel plates. Every 3-6 days thereafter these cultures were passaged at a 1:10 to 1:15 ratio. After 5-6 passages, most non-NPCs disappear and homogeneous colonies of NPCs remained. These NPCs may be passaged at least 20 times at a 1:5 to 1:15 ratio.

1.6.3: Generation of Human iPS-MNs

Generation of iPS-MNs was adapted from a previous reported protocol (*23*). Briefly, iPSCs were dissociated into single cells with Accutase and 1×10^6 cells were seeded into one well of a Matrigel-coated 6-well plate. These Matrigel-coated plates were prepared by adding 1 mL of Matrigel (diluted 1:60 v/v in DMEM/F12, GlutaMAX supplement) to each well of a 6-well plate and incubating the plate for 60 min. The dissociated iPSCs were grown for 6 days in DMEM/F12, GlutaMAX supplement media containing N-2 Supplement (1:100 v/v), CTS B27 Supplement, XenoFree (1:50 v/v), L-ascorbic acid (150 μM), CHIR99021 (3 μM), as well as two small molecule SMAD inhibitors: SB431542 (10 μM) and dorsomorphin (1 μM). ROCK inhibitor (Y-27632) may also be added to the media to a final concentration of 5 μM to reduce cell death. Full media changes were performed every 24 hours. At 7 days, a full media change was performed in which CHIR99021 was withdrawn from the media and retinoic acid (1.5 μM) and Smoothened Agonist (200 nM) was added to the media. The cells were cultured for a further 8 days in this media with daily full media changes. At 15 days, the cells were dissociated: Cells were washed once with PBS and 3 mL of Accutase was added per

well of a 6-well plate. Cells were incubated with Accutase for 30 min. Next, each well of cells was triturated gently 4-5 times, transferred to 15 mL centrifuge tubes containing 6 mL of DMEM/F12, GlutaMAX supplement, and the cells pelleted by centrifuging for 5 min at 1000 g. The cell pellets should be resuspended and 1×10^7 cells seeded onto each 10 cm Matrigel-coated plate; the media should also be supplemented with 10 μM Y-27632 to reduce cell death. Full media changes were performed every 24 hours. At 20 days, the media was modified to reduce Y-27632 (2 μM) and to include three growth factors: recombinant human BDNF (2 ng/ml), recombinant human CNTF (2 ng/mL), and recombinant human GDNF (2 ng/ml). At 22 days, retinoic acid and Smoothened Agonist were withdrawn from the media and DAPT (2 μM) was added to aid maturation to iPS-MNs. At this point, full media changes were performed every 2 days. At 26 days, DAPT was withdrawn from the media. At 28 days, iPS-MN cultures were obtained that stained positive for known MN markers Hb9, Islet-1/2 and SMI-31.

1.6.4: Plasmid Construction and G3BP1-GFP Reporter Line Generation

To generate G3BP1-GFP SG reporter lines, the HR120PA-1 targeting vector (System Biosciences) was modified to include a 1.5 kilobase 5' arm of homology span part of intron 11 and exon 12 of the endogenous human G3BP1 locus, and a 1.5 kilobase 3' arm of homology from the 3' untranslated region of G3BP1. These arms of homology were amplified from genomic DNA and the modified G3BP1 targeting vector was assembled via Gibson assembly. HEK293xT cells were transfected with this targeting vector and the Cas9 expression vector PX458 using lipofectamine 2000. Human induced pluripotent stem cells were electroporated using an Amaxa Nucleofector with Stem Cell Kit 1 and pulse setting B-016. Cells were selected beginning two days after transfection with puromycin at 1 μg/ml for four days. After two weeks, G3BP1-GFP colonies were picked using a steromicroscope.

1.6.5: Cell Culture Conditions

Human induced pluripotent stem cells (iPSC) were maintained in mTeSR1 with supplement. iPSCs were clump dissociated and passaged using enzyme-free Cell Dissociation Buffer. HEK293xT cells were maintained in DMEM, high glucose supplemented with 10% fetal bovine serum, heat inactivated. HEK293xT cells were dissociated and passaged using TrypLE Express Enzyme dissociation buffer. Small molecule neural precursor cells (NPC) were maintained in DMEM/F12, GlutaMAX supplement, containing N-2 Supplement (1:100 v/v), CTS B27 Supplement, XenoFree (1:50 v/v), L-ascorbic acid (150 μM), CHIR99021 (3 μM), and purmorphamine (0.5 μM). NPCs were dissociated and passaged using Accutase solution. iPS-MNs were maintained in DMEM/F12, GlutaMAX supplement, containing N-2 Supplement (1:100 v/v), CTS B27 Supplement, XenoFree (1:50 v/v), L-ascorbic acid (150 μM), recombinant human BDNF (2 ng/mL), recombinant human CNTF (2 ng/mL), and recombinant human GDNF (2 ng/mL). iPS-MNs were dissociated and passaged using Accumax solution. All cell types were cultured in humidified incubators at 37°C, 5% CO_2.

1.6.6: Coating Plates for Cell Culture Maintenance

For HEK293xT cells, 10 cm tissue culture plates were coated with 4 ml aqueous solution of 0.001% w/v poly-D-lysine (PDL) hydrobromide and incubated for 5 min. The PDL was then aspirated and the plates washed once with sterile water. For human induced pluripotent stem cells and small molecule neural precursor cells (NPC), 10 cm tissue culture plates were coated with 6 mL of Matrigel (diluted 1:60 v/v in DMEM/F12, GlutaMAX supplement) and incubated for 60 min. The Matrigel was then aspirated and the plates seeded with cells. For iPS-MNs, 10 cm tissue culture plates were coated with 4 ml aqueous

solution containing 0.001% w/v PDL hydrobromide and 0.001% w/v poly-L-ornithine (PLO) hydrobromide and incubated overnight. The PDL/PLO was then aspirated and the plates washed once with sterile water. Next the plates were coated with 6 ml of mouse laminin (20 μg/ml in NPC media without CHIR99021 and purmorphamine) and incubated overnight. Finally, the laminin was aspirated and the plates were seeded with cells.

1.6.7: Coating Plates for Screening and Secondary Assays

For HEK293xT cells, 384-well plates were coated by adding 10 μL of 0.001% w/v poly-D-lysine (PDL) hydrobromide to each well and incubating overnight. The PDL was then aspirated and the wells washed once with sterile water. For small molecule neural precursor cells (NPC), 384-well plates were coated by adding 10 μL of 0.001% w/v PDL to each well and incubating overnight. The PDL was then aspirated and the wells washed once with sterile water. Next, 15 μL of mouse laminin (20 μg/ml in NPC media without CHIR99021 and purmorphamine) was added to each well and incubated overnight. Finally, the laminin was aspirated and the plates were seeded with cells. For iPS-MNs, 384-well plates were coated by adding 10 μl of 0.001% w/v PDL + 0.001% w/v poly-L-ornithine (PLO) hydrobromide to each well and incubating overnight. The PDL/PLO was then aspirated and the wells washed once with sterile water. Next, 15 μl of mouse laminin (20 μg/ml in NPC media without CHIR99021 and purmorphamine) was added to each well and incubated overnight. Finally, the laminin was aspirated and the plates were seeded with cells. Liquid handling was performed with a Hamilton Microlab STAR fluid handler.

1.6.8: Screen Assay for Identifying SG-modulating Compounds

Using a Hamilton Microlab STAR liquid handler, HEK293xT cells were plated at 7500 cells per well of 384-well plates in 20 μl of HEK293xT media, while the CV-B small molecule

neural precursor cells (NPC) were plated at 12000 cells per well of 384-well plates in 20 μl of NPC media without CHIR99021 or purmorphamine. Both cell types were then incubated overnight. After overnight incubation, cells were then pre-treated with screen compounds: Using a Labcyte ECHO 555 Liquid Handler, compounds were spotted into the wells in biological duplicate at a final concentration of 10 μM, and cells were incubated with compounds for 60 min. After compound pre-treatment, cells were stressed by using the Hamilton fluid handler to add $NaAsO_2$ diluted in 20 μl of DMEM to each well, to a final concentration of 500 μM or 250 μM of $NaAsO_2$ for HEK293xT cells or NPCs, respectively. Cells were incubated with $NaAsO_2$ for 60 min. Finally, cells were fixed by adding 24% paraformaldehyde in PBS to each well to a final concentration of 4% and incubated for 45 min at room temperature. After fixing, the plates were washed three times with PBS. Nuclei were stained with 30 μl DAPI (1:5000 v/v in PBS) per well and incubated overnight at 4°C, after which the plates were washed once with PBS. Finally, to preserve the plates 30 μl of 50% v/v glycerol in PBS was added to each well. Cells were imaged in this glycerol solution.

1.6.9: Robotic Imaging of Screen Plates

Screen plates were imaged using a Thermo Scientific CRS CataLyst-5 Express robotic plate loader coupled with a GE Healthcare IN Cell Analyzer 1000 plate imager. Four fields at the center of each well were imaged with a 10× objective through 460 nm and 535 nm emission filters for DAPI and G3BP1-GFP, respectively. Images at 460 nm and 535 nm were taken with 250 ms and 750 ms exposures, respectively.

1.6.10: Automated Image Segmentation and Feature Quantification

SG screen and secondary assay images were segmented and image features quantified using a custom CellProfiler pipeline (*53*). Briefly, nuclei were segmented and

identified in the DAPI fluorescence channel images using a diameter cutoff of 9-80 pixels for HEK293xT cells, small molecule neural precursor cells (NPC), and iPS-MNs. Cell bodies were then extrapolated by overlaying the GFP fluorescence channel images and tracing radially outward from the nuclei to the limits of the cytoplasmic G3BP1-GFP signal. The cell bodies were used as masks to eliminate imaging artifacts outside of cell boundaries, such as background fluorescence or dead cells. After masking, punctate structures were enhanced by image processing for speckle-like features that were 10 pixels in diameter for HEK293xT cells or 7 pixels in diameter for NPCs and iPS-MNs, and these punctate structures were then annotated as features such as G3BP1-GFP SG or TDP-43 foci. Finally, the total image area which was enclosed in each of the identified features (nuclei, punctate structures, or intersections of features) was calculated and output to spreadsheets.

1.6.11: Statistical Analysis of Screen Data

SG-modulating compounds were defined as hits that significantly decrease or increase one or more of three metrics:

1. Amount of SG formation per cell, defined as the total image area enclosed in SGs divided by the total image area enclosed in nuclei (SG area/nuclei area).
2. Number of SGs per cell, defined as the number of SG puncta divided by the total image area enclosed in nuclei (SG count/nuclei area).
3. Average size of SGs, defined as the total image area enclosed in SGs divided by the number of SG puncta (SG area/SG count).

To identify hit compounds for these three metrics, a custom computational pipeline, Statistical Workflow for Identification of Molecular Modulators of ribonucleoprotEins by Random variance modeling (SWIMMER; open source and available publicly on yeolab github page), was built following standard statistical practices for high-throughput screening (*54,*

55). The pipeline begins by interpolating sporadic missing values via K-nearest neighbors missing data imputation, using K = 10 nearest neighbors and Euclidean distances (*56*). To reduce batch effects, the pipeline then performs a two-way median polish, alternating across rows and columns over 10 iterations (*54, 57*). Next, normalization is performed by computing b-scores, in which post-polish residuals are divided by the median absolute deviation of all post-polish residuals of the screen (*58*). To increase the power of hypothesis tests performed on the b-scores and therefore improve calling of screen hits, the screen was performed in biological duplicate, sample variances across the duplicate b-scores were computed, and an inverse gamma distribution was fitted to the distribution of sample variances (*59*). Fitting an inverse gamma distribution enables performing a modified one sample Student's t-test which has increased statistical power for each screen compound (*54*). This modified t-test involves computing for each compound a modified t-statistic $\tilde{t} = \frac{\bar{x} - \mu_0}{\tilde{s}\sqrt{1 / K}}$, where $\bar{x}$ is the sample mean for the compound across K biological replicate b-scores, μ_0 is the mean under the null hypothesis, and $\tilde{s}^2$ is the modified sample variance for the compound across K biological replicate b-scores. In the present SG screen, $\mu_0 = 0$, $K = 2$, and $\tilde{s}^2 = \frac{(K-1)s^2 + 2a(ab)^{-1}}{(K-1) + 2a}$, where s^2 is the unmodified sample variance across K biological replicate b-scores and a and b are the fitted parameters of the inverse gamma distribution. Using these modified one sample Student's t-tests, hits were called using a significance cutoff of α = 0.001; calling hits using a family-wise error rate proved too stringent and resulted in too many false negatives. Quality control (QC) for called hits was performed by examining the raw screen images for imaging artifacts or confounding effects such as autofluorescence or out-of-focus wells. Screen hits that passed QC were manually annotated with the compound names, skeletal formulae, and previously reported cellular targets of the compounds using the National Center for Biotechnology Information PubChem database.

1.6.12: Computation of the Screen Assay Z'

To estimate whether the screen assay has adequate sensitivity and specificity for detecting hits in a high-throughput screening paradigm, the Z' was computed for the screen assay in each cell type: $Z' = 1 - \frac{3(\hat{\sigma}_p + \hat{\sigma}_n)}{|\hat{\mu}_p - \hat{\mu}_n|}$, where $\hat{\sigma}_p$ and $\hat{\sigma}_n$ are the sample standard deviations for the positive and negative controls, respectively, and $\hat{\mu}_p$ and $\hat{\mu}_n$ are the sample means for the positive and negative controls, respectively. The Z' is therefore a measure of the signal-to-noise in the screen assay, and an assay is suitable for high-throughput screen if the Z' is greater than 0.5 (*37*).

1.6.13: Counterscreen Assays

384-well plates were coated and cells were seeded as described above for 384-well screening plates. For dose response assays, hit compounds diluted in 20 μl DMEM were added to cells to final concentrations of 30, 10, 3.3, 1.1, 0.37, or 0.12 μM, and cells were incubated with compounds for 60 min. Cells were then stressed by adding $NaAsO_2$ diluted in 40 μl of DMEM to each well, to a final concentration of 500 μM or 250 μM for HEK293xT cells or CV-B small molecule neural precursor cells (NPC), respectively. Cells were incubated with $NaAsO_2$ for 60 min at 37°C, 5% CO_2, after which cells were fixed, DAPI stained, and imaged. For heat shock stress assays, hit compounds diluted in 20 μl DMEM were added to cells to final concentrations of 10 μM, and cells were incubated with compounds for 60 min. Cells were then heat shocked by incubating for 60 min at 43°C, 5% CO_2, after which cells were fixed, DAPI stained, and imaged. For thapsigargin stress assays, hit compounds diluted in 20 μL DMEM were added to cells to final concentrations of 10 μM, and cells were incubated with compounds for 60 min. Cells were then stressed by adding thapsigargin diluted in 40 μL

DMEM to a final concentration of 50 μM or 1 μM for HEK293xT cells or NPCs, respectively. Cells were then incubated with thapsigargin for 60 min at 37°C, 5% CO_2, after which cells were fixed, DAPI stained, and imaged. For the $NaAsO_2$ pre-stress assays, cells were first stressed by adding $NaAsO_2$ diluted in 20 μl DMEM to a final concentration of 500 μM or 250 μM for HEK293xT cells or NPCs, respectively. Cells were incubated with $NaAsO_2$ for 60 min. Then, hit compounds diluted in 40 μl DMEM were added to cells to a final concentration of 10 μM, and cells were incubated with compounds for 60 min at 37°C, 5% CO_2, after which cells were fixed, DAPI stained, and imaged.

1.6.14: Estimating IC50s of SG Inhibiting Compounds

IC50s were estimated from logistic functions fitted to the dose response data of SG inhibiting compounds. Least squares regression was used to fit logistic functions of the type: $f(x) = \frac{L}{1 + e^{-k(x - x_0)}}$, where L is the maximum value of the curve, k is the steepness of the curve and x_0 is the midpoint of the curve. From these fitted logistic functions, the IC50 estimates are therefore the fitted x_0 parameters, representing the midpoints of the dose-response transfer curves.

1.6.15: Western Blotting and Quantification of eIF2α Serine 51 Phosphorylation

12-well plates were coated as described above for 384-well primary screening plates but scaled to 12-well plates. $2*10^5$ HEK293xT cells or CV-B small molecule neural precursor cells (NPC) were seeded into each well and incubated overnight. Screen hit compounds diluted in DMEM were added to cells to final concentrations of 10 μM and incubated with cells for 60 min. Cells were then stressed by adding $NaAsO_2$ diluted in DMEM to final concentrations of 500 μM or 250 μM for HEK293xT cells or NPCs, respectively, and

incubated for 40 min. Next, the media was aspirated and cells were washed once with PBS at room temperature. Cells were lysed for 10 min on ice with 100 μL per well of ice-cold RIPA Buffer Solution (Teknova) supplemented with cOmplete, EDTA-free Protease Inhibitor Cocktail (1 tab/50 ml), PhosSTOP phosphatase inhibitor cocktail (1 tab/10 mL), and Benzonase nuclease cocktail (1:1000). A Pierce BCA Protein Assay Kit was used to quantify protein concentrations in lysates and 1 μg of total protein from each lysate was loaded for gel electrophoresis and Western blotting. Western blot membranes were blocked with 1% bovine serum albumin (BSA) in TBST for 60 min at room temperature, probed for serine 51 phosphorylate eIF2α using rabbit anti-EIF2S1 (Phospho-Ser51) primary antibody diluted 1:1000 in 0.5% BSA in TBST overnight at 4°C, and probed with secondary antibody diluted 1:2000 in 0.5% BSA in TBST for 60 min at room temperature. As control, total eIF2α was probed using rabbit anti-EIF2S1 primary antibody. Western blot band sizes were quantified by densitometry in ImageJ: Equally sized boxes were drawn around bands and pixel intensities were integrated over the box areas to give the band sizes (*60*).

1.6.16: Hit Compound Inhibition of $NaAsO_2$, Thapsigargin, or Puromycin-induced SGs in iPS-MNs

iPS-MNs were differentiated and seeded into pre-coated 384-well plates as described above. iPS-MNs were allowed to adhere by incubating for 48 hours at 37°C, 5% CO_2; iPS-MNs were fed 24 hours after seeding by adding 20 μL of iPS-MN media to each well to a final volume of 40 μL per well. For $NaAsO_2$ stress assays, hit compounds diluted in 20 μL media were added to iPS-MNs to a final concentration of 10 μM, and cells were incubated with compounds for 80 min. iPS-MNs were then stressed by adding $NaAsO_2$ diluted in 20 μL iPS-MN media to a final concentration of 100 μM and incubated for 120 min at 37°C, 5%

CO_2, after which cells were fixed. For thapsigargin stress assays, hit compounds diluted in 20 μl iPS-MN media were added to iPS-MNs to final concentrations of 10 μM, and cells were incubated with compounds for 80 min. iPS-MNs were then stressed by adding thapsigargin diluted in 20 μl iPS-MN media to a final concentration of 250 nM and incubated for 120 min at 37°C, 5% CO_2, after which cells were fixed. For puromycin stress assays, hit compounds and puromycin were diluted in 40 μl iPS-MN media and added to iPS-MNs to final compound concentrations of 5 μM and final puromycin concentration of 5 μg/ml. iPS-MNs were incubated with compounds and puromycin for 12 hours at 37°C, 5% CO_2, after which cells were fixed. G3BP1 and TDP-43 were probed by immunofluorescence according to the procedure described above for immunofluorescence probing of SG-enriched fractions and nuclei were stained with DAPI. iPS-MNs were imaged as described above for imaging 384-well primary screening plates.

Chapter 1, in full, is adapted from material which has been submitted for publication as it may appear in Science Translational Medicine, 2019, M. Y. Fang, S. Markmiller, W. E. Dowdle, A. Q. Vu, P. J. Bushway, S. Ding, M. M. Mercola, J. W. Lewcock, G. W. Yeo. The dissertation author was the primary investigator and author of this paper.

CHAPTER 2: SGs are Composed of mRNP Cores Surrounded by a Proteinaceous Shell; Assembly of the Shell Depends on RNA-RBP Interactions and may be Disrupted by Molecules with Planar Moieties

2.1: ALS-associated RNA-binding Proteins are Recruited as SG Shells

Contemporaneous with our small molecule screen, we utilized our G3BP1-GFP reporter lines to evaluate if ALS-associated RBPs such as TDP-43, FUS, HNRNPA2B1 and TIA1 were present in SGs and if so, in which subcompartment i.e. SG core or shell. Using a previously reported protocol (*10*), we isolated SG-enriched fractions from our G3BP1-GFP expressing HEK293xT cells and NPCs. As expected, we found that fractions isolated from $NaAsO_2$-stressed cells contained distinct GFP-positive spherical bodies, whereas those from unstressed cells showed diffuse GFP signal (Figure 2.5.9). Additionally, gel electrophoresis and subsequent silver staining of these fractions from stressed and unstressed cells revealed changes in band intensity for numerous proteins upon $NaAsO_2$ stress, likely representing increased levels of SG shell proteins and proportionally decreased levels of SG core proteins as SG composition becomes more complex (Figure 2.5.10).

Next, we performed Western blot analysis of fractions from stressed and unstressed cells to determine the relative abundances of well-known SG-associated proteins, including G3BP1, ATAXIN2, CAPRIN1, UBAP2L, PABPC1, DDX3, and USP10, as well as ALS-associated RBPs, including TDP-43, FUS, HNRNPA2B1, and TIA1. Surprisingly, we found that the relative abundances of SG-associated proteins in these fractions decreased upon $NaAsO_2$ stress, whereas the relative abundances of the four ALS-associated proteins TDP-43, FUS, HNRNPA2B1, and TIA1 increased upon $NaAsO_2$ stress (Figures 2.5.1-2.5.2). CAPRIN1, UBAP2L, and USP10 are SG proteins that have been shown to directly interact with G3BP1 and can affect SG formation (*11, 12, 36*). ATAXIN2 binds mRNAs and altered

levels of this protein can disrupt SG formation, while PABPC1 and DDX3 are ubiquitous RBPs that are bound to the 3'UTR and 5'UTR of most mRNAs, respectively (*46, 61*). Supporting and further extending recent proximity-labeling proteomic studies of SGs (*11, 12*), our Western blot results indicate that SG-associated proteins already pre-exist in a core-like complex with G3BP1 even in the absence of stress but other proteins such as ALS-associated RBPs are further recruited to SGs (and are present in the shell) during stress.

Immunofluorescence probing of SG-enriched fractions from $NaAsO_2$-stressed HEK293xT cells and NPCs also confirm that ALS-associated RBPs join G3BP1 subcomplexes under stress. We found significant co-localization between G3BP1-GFP-positive SGs and ALS-associated proteins TDP-43, FUS, HNRNPA2B1, and TIA1 (Figures 2.5.3-2.5.4). As positive controls, we found significant co-localization for several SG-associated proteins including UBAP2L, PABPC1, CAPRIN1, and USP10 (Figures 2.5.3-2.5.4 and 2.5.11). The negative control CYCS did not co-localize with SGs in these fractions (Figures 2.5.3-2.5.4). These results confirm that ALS-associated RBPs such as TDP-43, FUS, HNRNPA2B1, and TIA1 assemble onto G3BP1-positive SG cores.

2.2: Assembly of ALS-associated RBPs onto SGs is RNA-dependent

Since SGs contain RNA and the ALS-associated proteins TDP-43, FUS, and HNRNPA2B1 are RBPs, we hypothesized that assembly of these proteins is RNA-dependent. Indeed, we showed by Western blotting that RNase I digestion of fractionated SG-enriched fractions from $NaAsO_2$-stressed HEK293xT cells and NPCs led to reduction of HNRNPA2B1 from SGs in a dose-dependent manner in both cell types. We also found that RNase I digestion reduced TDP-43 and FUS from SGs in fractions from NPCs and HEK293xT cells, respectively (Figures 2.5.5-2.5.6). This is in contrast to the SG-associated

RBPs UBAP2L and CAPRIN1, which were resistant to RNase I digestion (Figures 2.5.5-2.5.6).

Immunofluorescence staining of SG-enriched fractions in the absence or the presence of RNase I digestion indicated that co-localization of TDP-43, FUS, and HNRNPA2B1 with G3BP1-GFP-positive SGs decreased following RNase I digestion in HEK293xT cells, but not co-localization of G3BP1 or UBAP2L (Figures 2.5.7-2.5.8). This decrease in co-localization of TDP-43, FUS, and HNRNPA2B1 with G3BP1-GFP-positive SGs followed a dose-dependent relationship with increasing amounts of RNase I, while on the other hand there was a compensatory increase in co-localization of G3BP1 and UBAP2L with increasing amounts of RNase I digestion (Figure 2.5.12). Furthermore, by first incubating SG-enriched fractions with 1,6-hexanediol to disrupt hydrophobic interactions followed by RNase I digestion, we demonstrate decreased co-localization of FUS and HNRNPA2B1 with G3BP1-GFP-positive SGs in NPCs (Figure 2.5.13). These Western blot and immunofluorescence microscopy results suggest that the assembly of HNRNPA2B1, and to a lesser extent TDP-43 and FUS, onto SGs is RNA-dependent.

2.3: Molecules with Planar Moieties Reduce ALS-associated RBPs from SGs

As our small molecule screen demonstrated that molecules with planar moieties, such as mitoxantrone, doxorubicin, and daunorubicin, decreased the average size of SGs while increasing the number of SGs per cell (Figure 1.2.6), we reasoned that these molecules likely modulate SG fusion by interfering with proper formation of SG shells (*9*). As these planar moiety-containing molecules had been reported to be nucleic acid intercalating molecules that directly bind to RNA (*62-67*), we further reasoned that these compounds may reduce the RNA-dependent assembly of ALS-associated RBPs into SGs .

Indeed, immunofluorescence probing of SG-enriched fractions incubated in the absence or the presence of mitoxantrone demonstrated a significant decrease of co-localization of TDP-43, FUS, and HNRNPA2B1 with G3BP1-GFP-positive SGs. Co-localization of G3BP1 or UBAP2L was not affected (Figures 2.6.1-2.6.2). Similarly, we observed a reduction of co-localization of FUS and HNRNPA2B1 with G3BP1-GFP-positive SGs following incubation of SG-enriched fractions with quinacrine, doxorubicin, or daunorubicin, all molecules with planar moieties (Figure 2.6.6). In contrast, incubation of SG-enriched fractions with cycloheximide, digitoxin, WS3, or ISRIB, all compounds which do not have planar moieties, did not result in decreased co-localization of TDP-43, FUS, and HNRNPA2B1 with G3BP1-GFP-positive SGs (Figure 2.6.7).

Western blotting analysis of SG-enriched fractions incubated with mitoxantrone and daunorubicin also indicated reduction of TDP-43 from SGs (Figure 2.6.9). Two other compounds with planar moieties, pyrvinium and pararosaniline, additionally reduced FUS and HNRNPA2B1 from SGs in fractions from HEK293xT cells, and reduced TDP-43 from SGs in fractions from NPCs (Figure 2.6.8). By contrast, SG proteins G3BP1 and CAPRIN1 were not reduced from SGs during overnight incubation with any of these SG-modulating compounds with planar moieties (Figure 2.6.8). Incidentally, many of these compounds appear brightly colored under visible light due to the presence of aromatic rings with extended conjugated pi-bond systems, and we were readily able to observe their association with pelleted SGs with the naked eye (Figure 2.6.9). In summary, these results indicate that molecules with planar moieties, such as the nucleic acid intercalators mitoxantrone, daunorubicin, pyrvinium, and pararosaniline, reduce ALS-associated RBPs from SGs *in vitro*.

2.4: Planar Moiety-containing Compounds Inhibit TDP-43 Accumulation in SGs in TDP-43ΔNLS cells

Since compounds with planar moieties reduce TDP-43 from SGs *in vitro*, we next evaluated these compounds in disease-relevant cellular models that harbor mislocalized TDP-43 protein. In H4 neuroglioma cells that express G3BP1-mCherry and GFP-TDP-43ΔNLS (86-414), $NaAsO_2$ or thapsigargin treatment strongly induced formation of G3BP1-mCherry SGs as well as GFP-TDP-43ΔNLS foci that essentially co-localized completely with the G3BP1-mCherry SGs (Figures 2.6.3-2.6.4 and 2.6.10; for consistency, G3BP1-mCherry false colored green and GFP-TDP-43ΔNLS false colored red).

As expected from our results above, pre-treatment with each of four SG inhibiting compounds anisomycin, mitoxantrone, doxorubicin, or GSK2606414 significantly reduced the amount of SG formation per cell (Figures 2.6.3-2.6.4). Excitingly, pre-treatment with mitoxantrone, which has planar moieties, strongly inhibited co-localization of GFP-TDP-43ΔNLS with residual SGs (Figures 2.6.3 and 2.6.5). In contrast, pre-treatment with PERK inhibitor GSK2606414 inhibited SG formation but had no effect on cytoplasmic GFP-TDP-43ΔNLS foci, which were not co-localized with G3BP1-mCherry (Figures 2.6.3-2.6.4 and 2.6.10). These results demonstrate that planar nucleic acid intercalators such as mitoxantrone can inhibit accumulation of TDP-43 in SGs in live cells.

2.5: Methods for *In Vitro* and *In Vivo* Characterization of SG Core/Shell Structures

2.5.1: Isolation of SG-enriched Fractions

SG-enriched fractions were isolated as described previously (*10*). Briefly, cells were grown in 10 cm plates to 75-90% confluency and stressed with $NaAsO_2$ as described above. The media was then aspirated, cells were washed once with PBS at room temperature, and then lysed for 10 minutes on ice with 6 mL ice-cold NP-40 lysis buffer per 10 cm plate; formulation of this lysis buffer is as previously described (*10*). Lysed cells were scraped and collected in 15 ml centrifuge tubes in 3 ml aliquots. Lysates were sonicated using a

Diagenode Bioruptor Plus for two cycles of 10 s on low power and one cycle of 10 s on high power. After each sonication cycle, lysates were chilled on ice for 20 s. Following sonication, the lysates were centrifuged at 1000 g for 5 min at 4°C to pellet nuclei. The supernatants were then collected into 1.5 ml centrifuge tubes and centrifuged at 18000 g for 20 min at 4°C to pellet SGs. The pellets were resuspended by trituration in 1/10 of the original volume of ice-cold NP-40 lysis buffer. The resuspended samples were finally centrifuged at 850 g for 2 min at 4°C to pellet membrane-bound organelles and other large debris. The remaining supernatants were collected as the SG-enriched fractions. The same fractionation procedure was performed on unstressed cells as a control.

2.5.2: Western Blotting and Quantification of RBPs in SG-enriched Fractions

A Pierce BCA Protein Assay Kit was used to quantify protein concentrations in SG-enriched fractions and 1 μg of total protein from each sample was loaded for gel electrophoresis and Western blotting. For input controls, 1 μg of total protein from whole cell lysates was also loaded. After transfer and blotting, Western blot band sizes were quantified by densitometry in ImageJ as described above. SG-enriched fraction band sizes were normalized by dividing by the band sizes of the corresponding input controls.

2.5.3: Immunofluorescence Probing and Microscopy of SG-enriched Fractions

In each well of a 96-well plate, 2 μg of total protein from SG-enriched fractions was added to 40 μl of ice-cold NP-40 lysis buffer and SGs in these fractions were allowed to settle by incubating overnight at 4°C. To fix the SGs, 8% paraformaldehyde (PFA) in PBS was added to each well to a final concentration of 4% PFA and plates were incubated for 10 min at room temperature. The PFA was aspirated and the wells were washed three times with PBS at room temperature. Next the wells were simultaneously permeabilized and

blocked by adding 80 μL of 0.1% v/v Triton X-100 + 5% v/v serum (of the same species as secondary antibody) in PBS to each well and incubating the plates for 45 min at room temperature. The plates were then washed once with wash buffer (0.01% v/v Triton X-100 in PBS) before probing with primary antibody. Primary antibody was diluted in wash buffer containing 1% w/v bovine serum albumin (BSA). 40 μl of primary antibody solution was added per well and plates were overnight at 4°C. Plates were then washed five times with wash buffer. Secondary antibody was diluted in wash buffer containing 1% w/v BSA. 40 μl of secondary antibody solution was added per well and plates were incubated overnight at 4°C. Plates were washed 10 times with wash buffer and preserved by adding 80 μl of 50% v/v glycerol in PBS per well. Plates were then imaged at 20× magnification on a ZEISS Axio Vert.A1 inverted microscope.

2.5.4: Quantifying Co-localization of SGs and Immunofluorescence-probed RBPs in SG-enriched Fractions

Images were first pre-processed in ImageJ, to subtract background using the rolling ball method with a radius of 50 pixels (required for subsequent Manders Correlation Coefficient calculations), and then to transform the dynamic range of the brightness to 2-10 (arbitrary units). Co-localization of G3BP1-GFP SGs with RBPs probed with Alexa-555 conjugated antibodies was then quantified using Manders' algorithm in the Fiji plugin Coloc2 to calculate the unthresholded Manders' Correlation Coefficient between the GFP fluorescence channel image and the Alexa-555 fluorescence channel image (*68, 69*). In this way, co-localization is defined as the fraction of G3BP1-GFP-positive pixels that coincide with Alexa-555-positive pixels.

2.5.5: Disrupting SG-RBP Association in SG-enriched Fractions

For digestion of SG-enriched fractions with RNase I, 10 μg of total protein from SG-enriched fractions was incubated with 0, 2, 8, or 32 Units of RNase I in 1.5 mL centrifuge tubes and shaken at 1200 rpm for 5 min at 37°C using an Eppendorf Thermomixer R. For incubation with 1,6-hexanediol, 10 μg of total protein from SG-enriched fractions was incubated with 1,6-hexanediol to a final concentration of 5% and nutated overnight at 4°C using a Fisherbrand Mini-Tube Rotator. After overnight incubations, the SG-enriched fractions were centrifuged at 18000 × g for 20 min at 4°C to pellet remaining SG-like structures. The pellets were resuspended in equal volume lysis buffer and analyzed by Western blotting and immunofluorescence probing as described above. For incubation with compounds, 10 μg of total protein from SG-enriched fractions was incubated with a screen hit compound to a final concentration of 100 μM and nutated overnight at 4°C using a Fisherbrand Mini-Tube Rotator. After overnight incubations, the samples were plated, fixed, and analyzed by immunofluorescence probing as described above, or centrifuged at 18000 × g for 20 min at 4°C to pellet remaining SG-like structures. The pellets were resuspended in equal volume lysis buffer and analyzed by Western blotting as described above.

2.5.6: Disrupting TDP-43ΔNLS (86-414) Association with SGs in H4 Cells

H4 cells were stably transduced with lentivirus encoding G3BP1-mCherry and doxycycline-inducible GFP-TDP-43ΔNLS (86-414) made from pLVX-CMV_IRES-Hygro (Clontech) and pLVX-TetOne_IRES-Puro (Clontech), respectively. Cells were maintained in DMEM, high glucose supplemented with 10% fetal bovine serum, heat inactivated, and grown on 10 cm PDL coated plates, prepared as described above. H4 cells were dissociated and passaged using TrypLE Express Enzyme dissociation buffer. $2*10^5$ cells in 50 μL media were seeded into each well of a 96-well plate (Perkin-Elmer). Following overnight incubation

in a humidified incubator at 37°C, 5% CO_2, the cells were induced with doxycycline (1 ng/mL) for 24 hours. After doxycycline induction, hit compounds diluted in 50 μl media were added to final concentrations of 5 μM, and cells were incubated with compounds for 30 min. Cells were then stressed by adding $NaAsO_2$ or thapsigargin diluted in 100 μl media to a final concentration of 500 μM or 5 μM, respectively, and incubated for 60 min. Cells were then fixed, stained with DAPI, and imaged at 40× magnification on an Opera Phenix high content imaging system (Perkin Elmer).

Chapter 2, in full, is adapted from material which has been submitted for publication as it may appear in Science Translational Medicine, 2019, M. Y. Fang, S. Markmiller, W. E. Dowdle, A. Q. Vu, P. J. Bushway, S. Ding, M. M. Mercola, J. W. Lewcock, G. W. Yeo. The dissertation author was the primary investigator and author of this paper.

CHAPTER 3: Following SG Formation, ALS Patient-derived iPS-MNs Exhibit Persistent Cytoplasmic Accumulation of TDP-43, a Disease-associated Phenotype which is Reduced by Molecules with Planar Moieties

3.1: Puromycin Stress Induces Persistent Cytoplasmic TDP-43 in ALS Patient-derived iPS-MNs

Next, we evaluated if molecules with planar moieties mitigate ALS-associated phenotypes using iPS-MNs. First, we determined whether SG formation leads to persistent cytoplasmic accumulation of TDP-43 in motor neurons, as has been reported for HeLa cells (*70-74*). We treated *TARDBP* mutant and control iPS-MNs with puromycin and then washed out the puromycin to allow the cells to recover from stress. We found that during stress, significantly more TDP-43 accumulated in SGs in the *TARDBP* mutant iPS-MNs than in the controls (Figures 3.7.1-3.7.2). During recovery from stress following washout of puromycin, significantly more TDP-43 remained localized in the cytoplasm of the *TARDBP* mutants than in the controls (Figures 3.7.1-3.7.2). This cytoplasmic TDP-43 persisted for at least 24 hours after washout of the stressor. Furthermore, biochemically isolated SG-enriched fractions from mutant iPS-MNs contained significantly more TDP-43, FUS, and G3BP1 than fractions from control iPS-MNs during recovery after stress (Figures 3.7.3 and 3.7.10-3.7.13). Similarly, significantly more TDP-43 accumulated in SGs in iPS-MNs harboring ALS-associated *FUS* mutations than in the control iPS-MNs (Figures 3.7.4-3.7.5). During recovery from stress, we observed a dramatic increase in cytoplasmic TDP-43 in the *FUS* mutant iPS-MNs compared to controls (Figures 3.7.4-3.7.5). This increase in cytoplasmic TDP-43 in the *FUS* mutant iPS-MNs manifested in roughly 10-20% of cells as large cytoplasmic puncta that did not co-localize with G3BP1 (Figure 3.7.4).

3.2: Planar Moiety-containing Compounds Reduce Puromycin-induced Persistent Cytoplasmic TDP-43

Encouraged that iPS-MNs carrying ALS-associated mutations exhibit a clear ALS-associated molecular phenotype, we next incubated iPS-MNs from controls, *TARDBP* and *FUS* mutants with DMSO control, cycloheximide, or planar compound mitoxantrone in the presence of puromycin stress. As mentioned above, cycloheximide and mitoxantrone strongly inhibited SG formation compared to the DMSO treatment (Figure 1.4.3). Importantly, mitoxantrone also significantly abrogated cytoplasmic localization of TDP-43 in both control and *TARDBP* mutant iPS-MNs, whereas DMSO and cycloheximide largely did not (Figures 3.7.6-3.7.7 and 3.7.14-3.7.15). Furthermore, mitoxantrone and pyrvinium, another planar moiety-containing molecule, reduced accumulation of cytoplasmic TDP-43 during six hours of puromycin stress, which lasted at least seven hours into stress recovery after washout of puromycin (Figures 3.7.8-3.7.9 and 3.7.16-3.7.17). On the other hand digitoxin, a SG-inhibiting compound which does not contain extended planar moieties, did not produce this lasting effect of reducing accumulation of cytoplasmic TDP-43 during six hours of puromycin stress and recovery after washout (Figure 3.7.18). These results indicate that molecules with planar moieties can prevent the ALS-associated phenotype of persistent cytoplasmic TDP-43 induced by cellular stress.

3.3: Methods for Inducing SG-associated Persistent Cytoplasmic Accumulation of TDP-43 in ALS-derived iPS-MNs

3.3.1: iPS-MN Puromycin Stress and Recovery Assays

iPS-MNs were generated from human induced pluripotent stem cells as described above. Day 28 iPS-MNs were dissociated into single cells by adding 3 mL Accumax into each well of a 6-well plate of iPS-MNs and incubating for 60 min. The iPS-MNs were then

gently triturated 10-15 times with a P1000 pipette, and then incubated for a further 15 min at 37°C, 5% CO_2 to complete the dissociation. The iPS-MNs were transferred to 15 ml centrifuge tubes containing 6 ml DMEM/F12, GlutaMAX supplement and cells were pelleted by centrifuging for 4 min at 200× g. The cell pellet was then resuspended in 1 ml iPS-MN media supplemented with 10 μM Y-27632 (media formulation described above) by gently triturating 10-20 times with a P1000 pipette, and cell clumps were filtered out using a 40 μm filter. 10^4 iPS-MNs were seeded into each well of a laminin-coated 384-well plate; plate coating was as described above. Cells were allowed to adhere by incubating overnight at 37°C, 5% CO_2 and then stressed by adding puromycin diluted in 20 μl of iPS-MN media to a final concentration of 5 μg/ml. After incubation with puromycin for 24 hours, three half-media changes with iPS-MN media were performed to wash out the stressor. The iPS-MNs were then incubated for 24 hours at 37°C, 5% CO_2, after which cells were fixed and DAPI stained. iPS-MNs were also fixed at intermediate time points to generate a time course for SG and TDP-43 foci assembly/disassembly dynamics during puromycin stress and stress recovery. G3BP1 and TDP-43 were probed by immunofluorescence according to the procedure described above for immunofluorescence probing of SG-enriched fractions. iPS-MNs were imaged as described above for imaging 384-well primary screening plates. SG-enriched fractions were also isolated from iPS-MNs following the protocol described above.

3.3.2: iPS-MN Puromycin Stress and Recovery Assays in the Presence of Mitoxantrone

Mutant *TARDBP*, mutant *FUS*, and control iPS-MNs were generated from human induced pluripotent stem cells and seeded into 384-well plates as described above. Cells were pre-incubated with mitoxantrone, digitoxin, or pyrvninium diluted in 20 μl of iPS-MN media to a final concentration of 2 μM and incubated at 37°C, 5% CO_2 for 60 min, after which

cells were stressed by adding puromycin diluted in 40 μl of iPS-MN media to a final concentration of 5 μg/ml. After incubation with puromycin for 6 hours, three half-media changes with iPS-MN media were performed to wash out the stressor and mitoxantrone. The cells were then incubated for 7 hours at 37°C, 5% CO_2, after which cells were fixed and DAPI stained. G3BP1 and TDP-43 were probed by immunofluorescence according to the procedure described above for immunofluorescence probing of SG-enriched fractions. iPS-MNs were imaged as described above for imaging 384-well primary screening plates.

Chapter 3, in full, is adapted from material which has been submitted for publication as it may appear in Science Translational Medicine, 2019, M. Y. Fang, S. Markmiller, W. E. Dowdle, A. Q. Vu, P. J. Bushway, S. Ding, M. M. Mercola, J. W. Lewcock, G. W. Yeo. The dissertation author was the primary investigator and author of this paper.

DISCUSSION

In this study, a high-content small molecule screen was performed in which we identified approximately 100 compounds consisting of eight compound classes that modulate SG formation, six of which have not previously been reported to affect SGs. These include 50 compounds that act at cell surface targets such as ion channels, receptors, or lipid membranes; seven compounds that modulate inflammatory signaling pathways; and 20 compounds that are molecules with planar moieties. This diversity of SG-modulating compounds greatly expands the toolbox of molecular compounds with which to probe the relationship between SGs and disease. Previous studies of SGs in disease models have relied on a handful of SG modulators: cycloheximide, the PERK inhibitor GSK2606414, or ISRIB, a small molecule SG inhibitor identified in a translation-based screen (*5, 11, 34, 74, 75*). This study offers a host of alternative compounds that act through orthogonal mechanisms which may prove useful in dissecting the role of SGs in disease models.

This study is also the first high-content screen in which compounds (two-thirds of the hits) were identified to not only modulate the overall amount of SG formation, but also SG size and the numbers of SGs per cell. Surprisingly, we observed that molecules with planar moieties such as nucleic acid intercalators not only inhibit SG formation, but also alter SG size and the numbers of SGs per cell in proliferative cells as well as patient-specific and control post-mitotic iPS-MNs. We reasoned that the nuanced effects of these compounds on SGs may reveal the molecular rules underlying SG formation. Specifically, molecules with planar moieties likely act by inhibiting SG shell formation which would lead to defects in SG fusion and maturation across a diverse range of stressors, thus manifesting as smaller and more numerous SGs (*9*). Interestingly, we demonstrate that eight compounds – five of which are molecules with planar moieties – reduce total SG formation without altering

phosphorylation of eIF2α. This is surprising since phosphorylation of eIF2α is a committing step towards SG formation. This study therefore also offers SG-inhibiting compounds that act through orthogonal mechanisms, which will be useful in future dissection of the role of SGs in disease models.

To evaluate a potential molecular mechanism for how particular compounds affect specific subcompartments of SGs such as SG shells, we leveraged a recently published biochemical approach (*10*). We fractionated stressed cells and used the SG-enriched fractions as an *in vitro* model system (*10*). Using a combination of silver staining and Western blot analysis, we found that fractions from stressed cells were depleted or enriched for particular proteins compared to fractions from unstressed cells. Among the depleted proteins were proteins reported to be SG-associated proteins such as CAPRIN1, UBAP2L, and USP10, whereas the enriched proteins included ALS-associated proteins such as TDP-43, FUS/TLS, HNRNPA2B1 and TIA1. We observed that the depleted proteins consist of components of cores in SG that is pre-existing in mRNP complexes prior to cellular stress (*11*). The relative representation of these SG core proteins is reduced upon stress due to assembly of a complex array of SG shell proteins onto the cores. These SG shell proteins are enriched for the ALS-associated proteins whose representation becomes higher relative to the SG core proteins. This represents the first look into differences in protein compositions between cores and shells, and paves the way for systematic enumeration of core versus shell proteins as well as functional high-content screens to assess the differential contributions of core and shell proteins to SG formation.

By treating SG-enriched fractions with RNase I, we further demonstrated that the assembly of several of these SG shell proteins is RNA-dependent, revealing for the first time how SG shell proteins may be recruited to SGs. This is consistent with recent RNA-seq analyses of SG-enriched fractions where RNAs in these preparations were enriched for the

RNA binding motifs of putative SG shell proteins TDP-43 and TIA1 (*3*). Furthermore, a recent systematic survey of the protein interactome for HNRNPA2B1 revealed that this RBP associates with a large number of other RBPs indirectly via RNA-RBP interactions (*13*). Similarly, HNRNPA2B1 may indirectly associate with SG core proteins via RNA-RBP interactions. Finally, it has been recently reported that RNA can regulate the phase separation of RBPs, consistent with the hypothesis that SGs may be assembled in part through phase separation processes (*76, 77*).

Finally, comparing incubation of SG-enriched fractions with mitoxantrone, doxorubicin, or WS3 to incubation with DMSO control, we found that mitoxantrone and doxorubicin, but not WS3 or DMSO, dislodged the putative SG shell proteins TDP-43, FUS, and HNRNPA2B1 from SGs. Given that mitoxantrone and doxorubicin are both nucleic acid intercalating molecules reported to directly interact with RNA, we reasoned that these two compounds interfere with RNA-RBP interactions to dislodge putative SG shell proteins (*47, 62-65*). IDRs, including prion-like domains (PrLDs), are often enriched in amino acids with large aromatic side chains (*78*), and coacervation of charged aromatic side chains help regulate phase separation of IDR-containing proteins. Mitoxantrone, doxorubicin, and other molecules with planar moieties may interact with these aromatic side chains via π-π stacks (*2, 79*). For example, acridine derivatives such as quinacrine are largely planar molecules that directly interact with prion protein and amyloid beta inclusions (*48, 80*). Given that SG formation has been reported to cause altered nucleocytoplasmic shuttling and localization of ALS-associated RBPs (*74*), these compounds which can dislodge ALS-associated RBPs from SGs raises the possibility that these compounds represent a new therapeutic approach for disease.

To investigate this hypothesis, we developed a model system of ALS/FTD, in which iPS-MNs are exposed to 24h of stress by puromycin treatment, followed by washout and

recovery in medium without puromycin. We demonstrated increased cytoplasmic accumulation of TDP-43 during puromycin stress, which persisted for at least 24 hours into the recovery period in *TARDBP* and *FUS* mutant, but not in control iPS-MNs. This represents the first disease model showing motor neurons exhibit a persistent molecular TDP-43 phenotype resembling the cytoplasmic mislocalization of TDP-43 in patient tissues (*70*-*73*), and ties together SGs with disease pathophysiology. Excitingly, when we treated the cells with mitoxantrone, a molecule with planar moieties, we not only reduced SG formation, but also reduced cytoplasmic accumulation of TDP-43. This reduction in cytoplasmic accumulation of TDP-43 by mitoxantrone lasted for at least seven hours into stress recovery after washout of puromycin, and could be replicated with pyrvinium, another planar moiety-containing molecule, but not digitoxin, a SG-inhibiting compound which does not have extended planar moieties. Further corroborating these results, we found that mitoxantrone also decreased association of TDP-43 with SGs in H4 cells engineered with a TDP-43ΔNLS (86-414) expression cassette.

Overall, our results in this study point us towards a two-step model for SG formation (Figure 3.8.1): In the first step, cellular stress signaling leads to phosphorylation of eIF2α, freezing ribosomes in the 48S pre-initiation stage at the 5' untranslated regions (UTRs) of mRNAs. Actively translating polysomes eventually run off the ends of mRNAs, while at the same time the SG scaffold protein G3BP1 can directly bind to the 40S ribosome subunit. G3BP1 can undergo homotypic interactions via IDRs near the C-terminus and catalyze the formation of a SG core. In the second step of SG formation, RBPs assemble onto SGs through RNA-dependent interactions. Many of these RBPs contain IDRs, which can also mediate assembly of additional proteins through heterotypic IDR contacts to form a SG shell in a phase-transition process. We posit that this second step of SG formation is most relevant to disease pathophysiology. Mutations in the IDRs of RBPs or other SG shell

proteins may accumulate in local high concentrations in the SG shell, and over a lifetime of stress, SG shells could nucleate the formation of pathological aggregations of mutant proteins, such as those seen in the spinal cord MNs of ALS patients (*29*). In this context molecules with planar moieties such as nucleic acid intercalating molecules directly interact with RNAs, disrupting recruitment of ALS-associated RBPs to the SG shell. Thus, disruption of RNA-RBP interactions in SG shells is a potential therapeutic strategy for ALS/FTD.

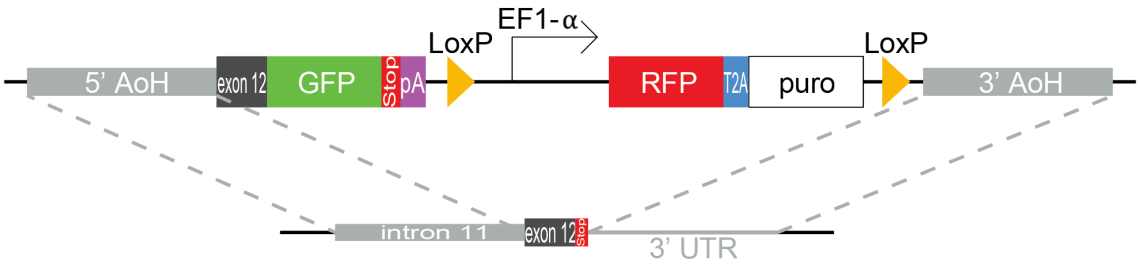

Figure 1.1.1: Schematic showing the GFP construct inserted in the C-terminus of the endogenous G3BP1 gene locus using CRISPR/Cas9-mediated homology directed repair. The puromycin selection cassette was removed by Cre-mediated recombination of flanking LoxP sequences. AoH: arm of homology, pA: polyadenylation sequence, puro: puromycin resistance cassette, UTR: untranslated region.

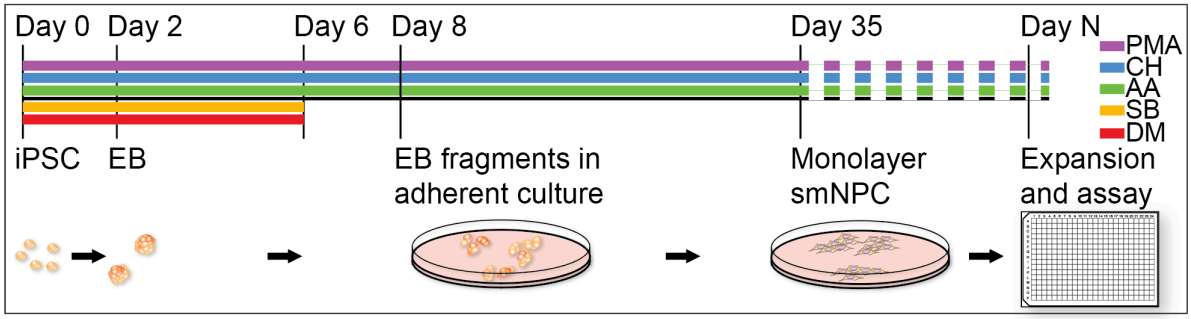

Figure 1.1.2: Timeline for the generation of small molecule neural precursor cells used in screening. iPSC: induced-pluripotent stem cells, EB: embryoid bodies, NPC: small molecule neural precursor cells, PMA: Purmorphamine, CH: CHIR99021, AA: L-Ascorbic acid, SB: SB431542, DM: Dorsomorphin.

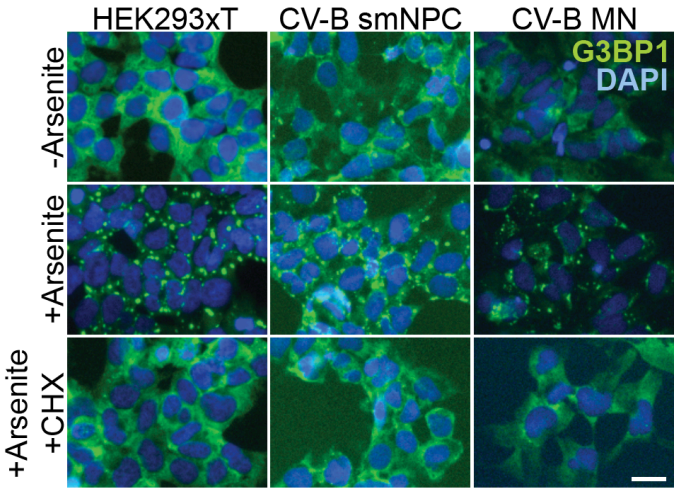

Figure 1.1.3: Representative wide-field fluorescence microscopy of G3BP1-GFP SG reporter lines under unstressed, $NaAsO_2$-stressed, and stressed but with cycloheximide pretreatment conditions. Scale bar is 50 μm. MN: motor neurons.

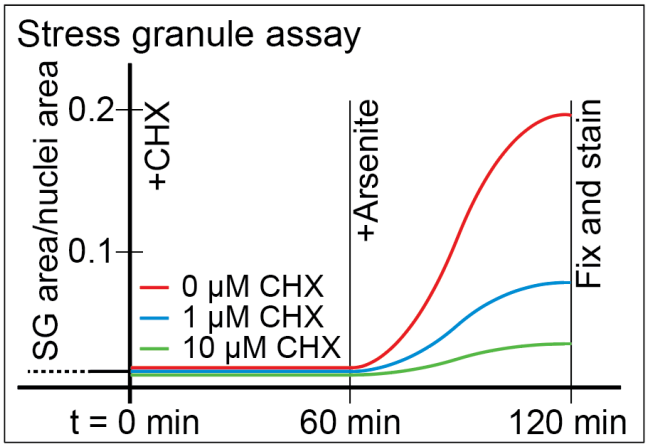

Figure 1.1.4: Overview of the screening paradigm, in which cells are pretreated with compounds such as cycloheximide for one hour, after which $NaAsO_2$ is added to stress cells for one hour. CHX: cycloheximide.

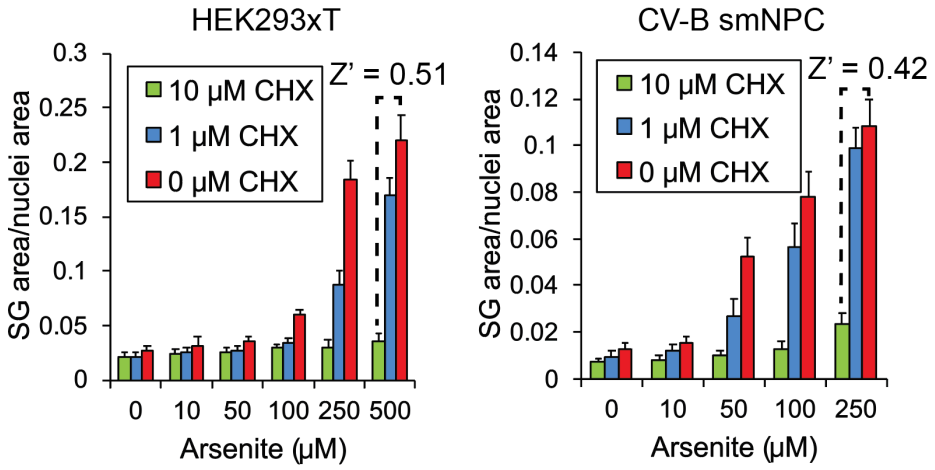

Figure 1.1.5: Histograms showing SG area/nuclei area at varying $NaAsO_2$ concentrations in the absence and presence of cycloheximide pretreatment, a positive control SG inhibiting compound. The Z' for the screen assay conditions are shown in the upper right and are used to estimate whether the screen assays have adequate sensitivity and specificity for high-throughput screening: $Z' = 1 - \frac{3(\hat{\sigma}_p + \hat{\sigma}_n)}{|\hat{\mu}_p - \hat{\mu}_n|}$, where $\hat{\sigma}_p$ and $\hat{\sigma}_n$ are the sample standard deviations for the positive and negative controls, respectively, and $\hat{\mu}_p$ and $\hat{\mu}_n$ are the sample means for the positive and negative controls, respectively. Error bars are sample standard deviations from four biological replicates.

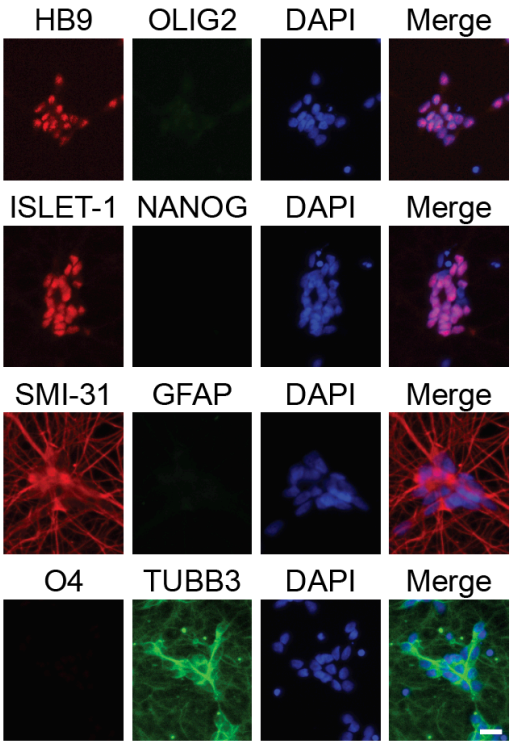

Figure 1.1.6: Representative wide-field fluorescence microscopy of CV-B iPS-MNs probed by immunofluorescence for MN markers HB9, ISLET-1, and SMI-31; neuronal marker TUBB3; and non-neuronal markers OLIG2 (oligodendrocytes), NANOG (induced-pluripotent stem cells), GFAP (astrocytes), and O4 (oligodendrocytes). Nuclei are stained with DAPI. Scale bar is 20 μm.

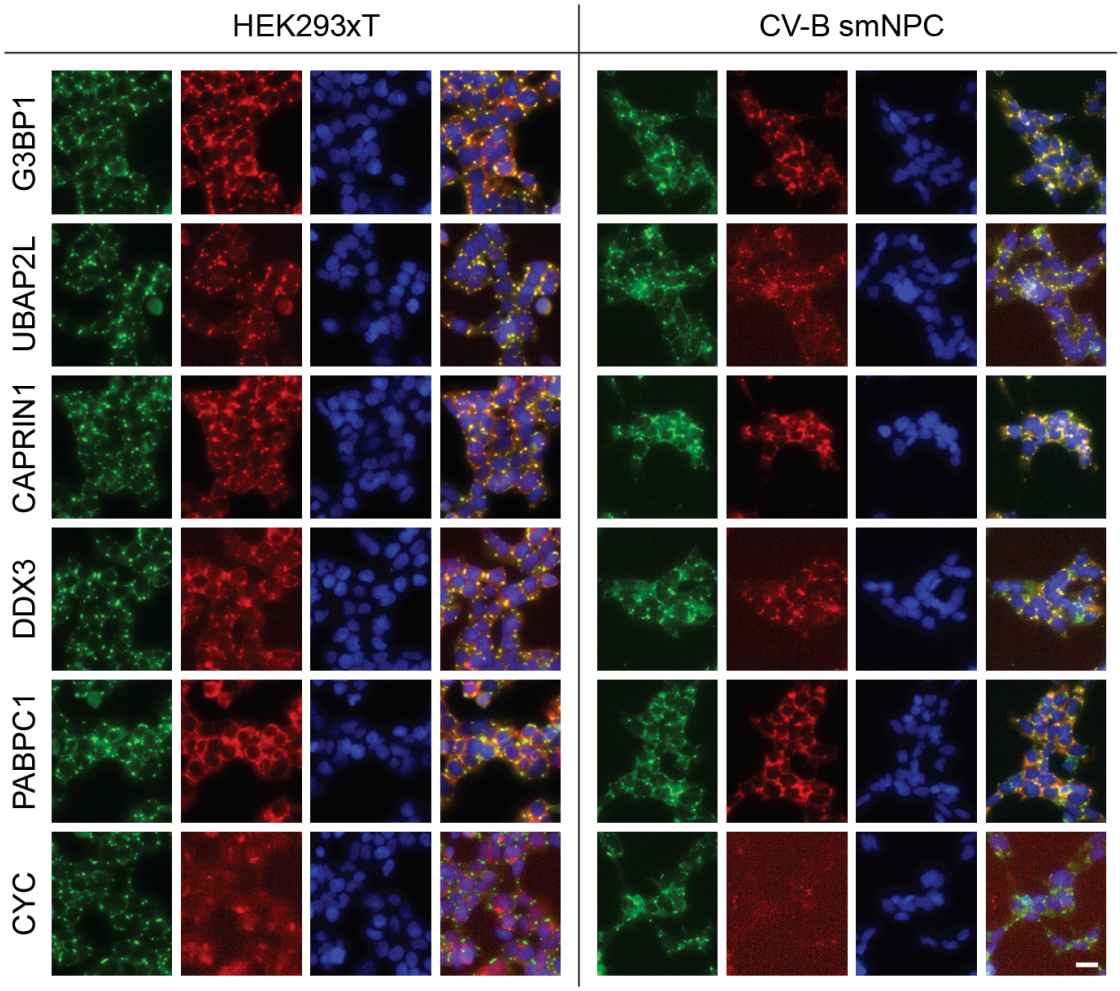

Figure 1.1.7: Representative wide-field fluorescence microscopy of G3BP1-GFP HEK293xT cells and NPCs stressed with $NaAsO_2$ and immunofluorescence probing for SG-associated proteins G3BP1, UBAP2L, CAPRIN1, DDX3, and PABPC1 as well as the negative control CYC. Nuclei are stained with DAPI. Scale bar is 20 μm. NPC: small molecule neural precursor cells.

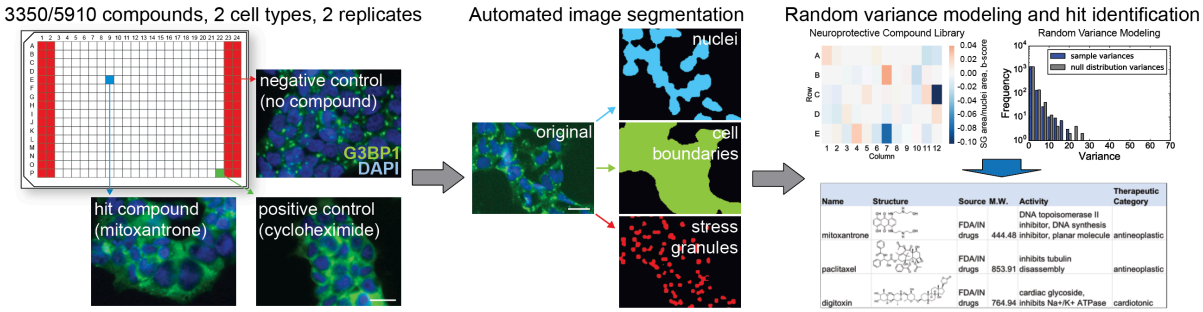

Figure 1.2.1: Schematic depicting the experimental and computational workflow of the small molecule screen for SG-modulating compounds. Scale bar is 50 μm.

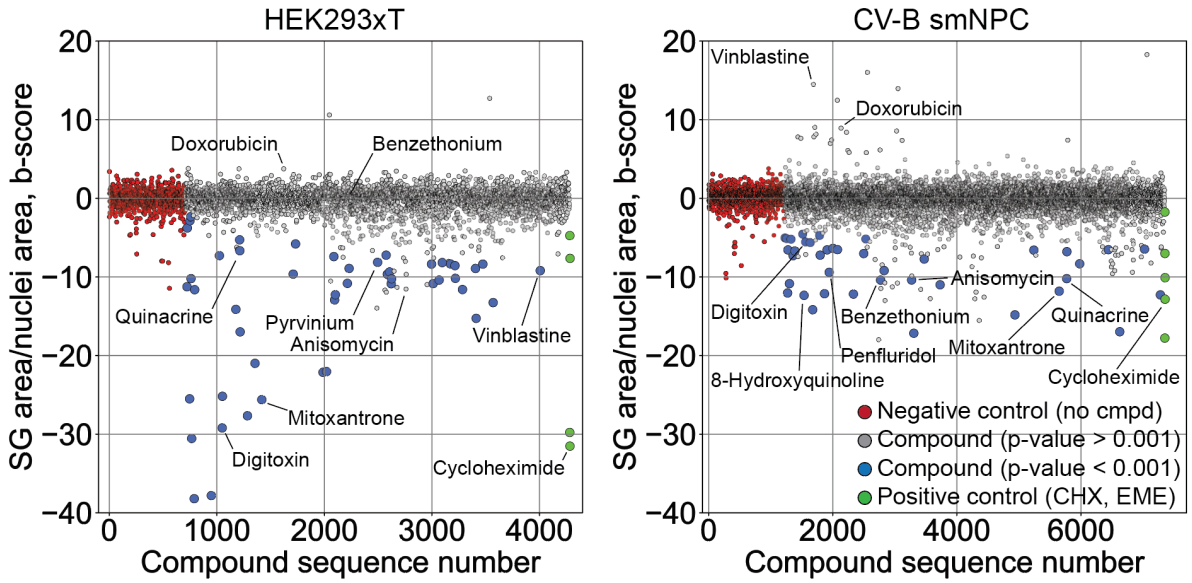

Figure 1.2.2: Scatterplot showing the amount of SG formation for each compound screened, computed as a b-score: SG area/nuclei area is processed through a two-way row/column median polish and the residuals are divided by the median absolute deviation of all post-polish residuals of the screen. For each compound, the mean of biological duplicate b-scores is represented. The red points on the left are negative controls in which no compounds were added. The green points on the right are positive controls in which either cycloheximide or emetine was added. The blue points are compounds identified as significantly reducing the amount of SG formation ($p < 0.001$) and the grey points are compounds that did not significantly reduce the amount of SG formation ($p > 0.001$). Significance levels are from one sample Student's t-tests against a null hypothesis mean of zero. SG: stress granule, NPC: small molecule neural precursor cells, CHX: cycloheximide, EME: emetine.

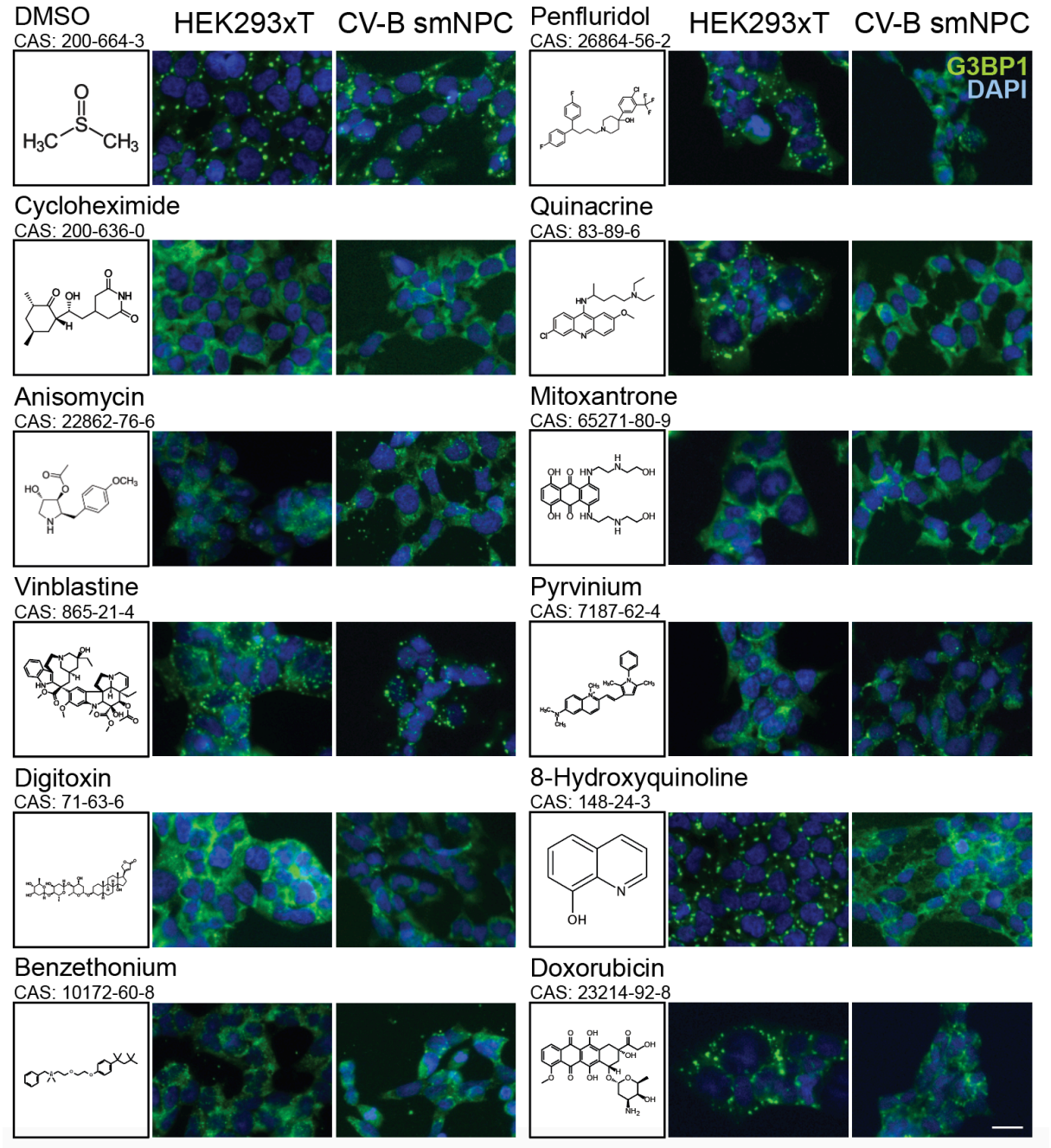

Figure 1.2.3: Representative wide-field fluorescence microscopy of HEK293xT and CV-B small molecule neural precursor cell SG reporter lines treated with SG-modulating compounds. Included are the skeletal formulae of the compounds. Scale bar is 50 μm.

	HEK293xT	CV-B smNPC	Both
Compounds screened	3350	5910	3350
Decreased:			
SG area/nuclei area	40	27	11
SG count/nuclei area	24	21	8
Average SG size	32	15	9
Increased:			
SG area/nuclei area	1	15	0
SG count/nuclei area	4	9	2
Average SG size	2	25	0

Figure 1.2.4: Summarizing the number of compounds which either decreased or increased the amount of SGs per cell defined as SG area/nuclei area, the number of SGs per cell defined as SG count/nuclei area, or the average size of SGs defined as SG area/SG count. Some compounds were included in more than one library screened; these were counted only once each.

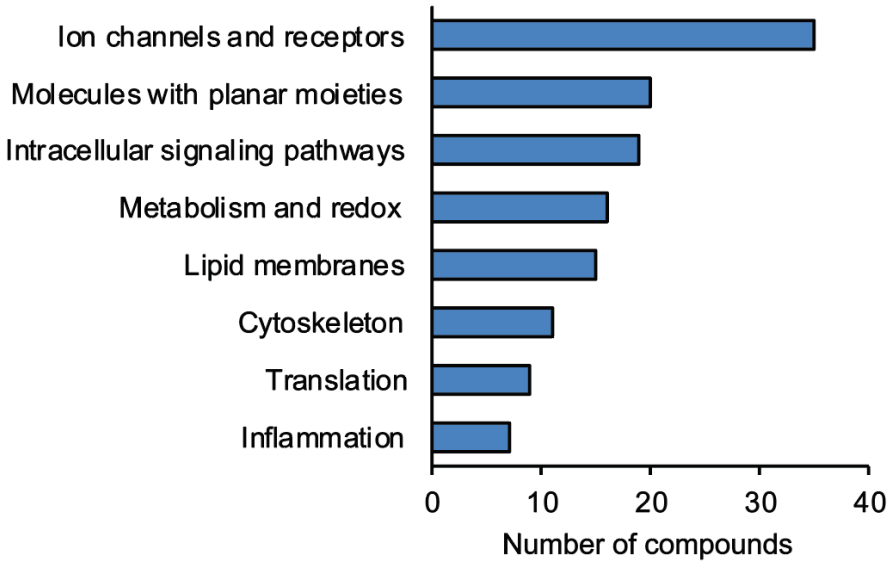

Figure 1.2.5: Histogram classifying hit compounds from Figure 1.2.4 by the known cellular targets of the compounds. Classification was performed by manual annotation from the National Center for Biotechnology Information PubChem database.

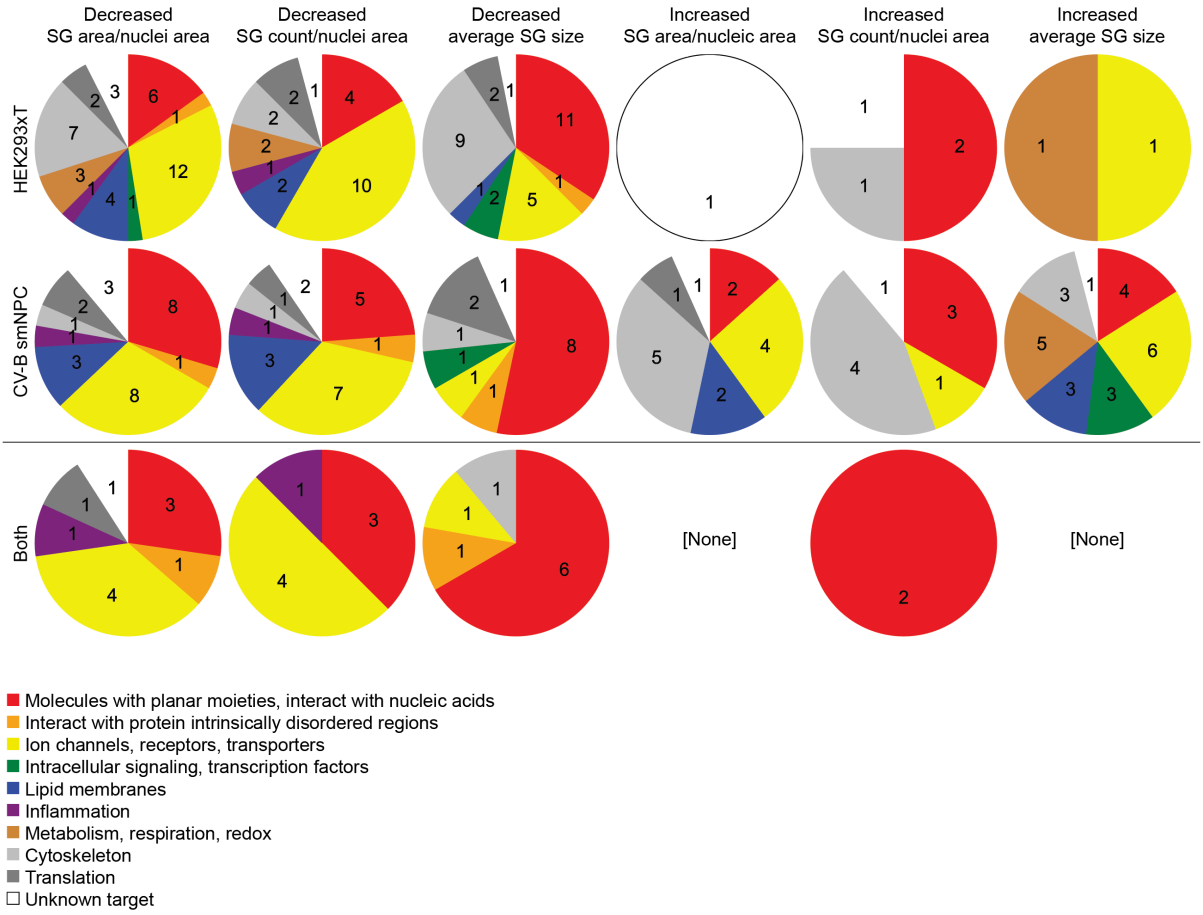

Figure 1.2.6: Pie charts representing the known cellular targets of SG-modulating compounds, corresponding Figure 1.2.4. Classification, including for compounds with more than one annotated cellular target class, was performed by manual annotation from the NCBI PubChem database. SG: stress granule, NPC: small molecule neural precursor cells.

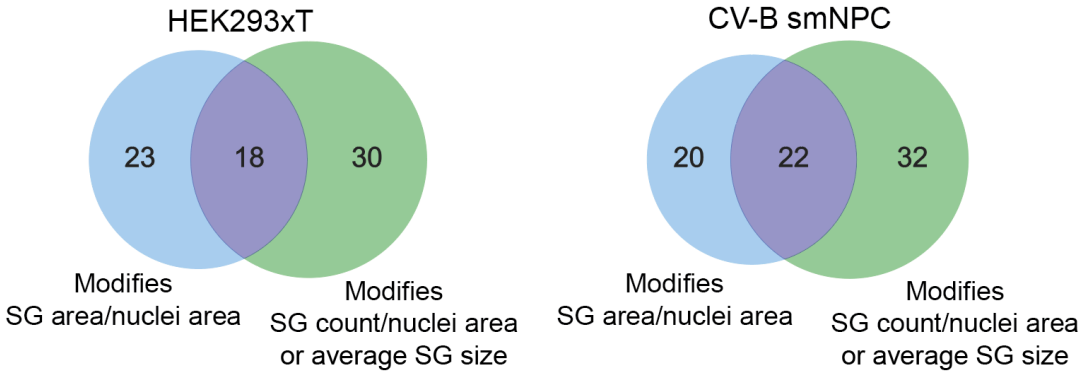

Figure 1.2.7: Venn diagrams representing the proportions of compounds that modulate SG area/nuclei area only, compounds that do not alter SG area/nuclei area but more subtly affect SG count/nuclei area and/or average SG size (defined as SG area/SG count), or compounds that modulate both SG area/nuclei area and SG count/nuclei area and/or average SG size.

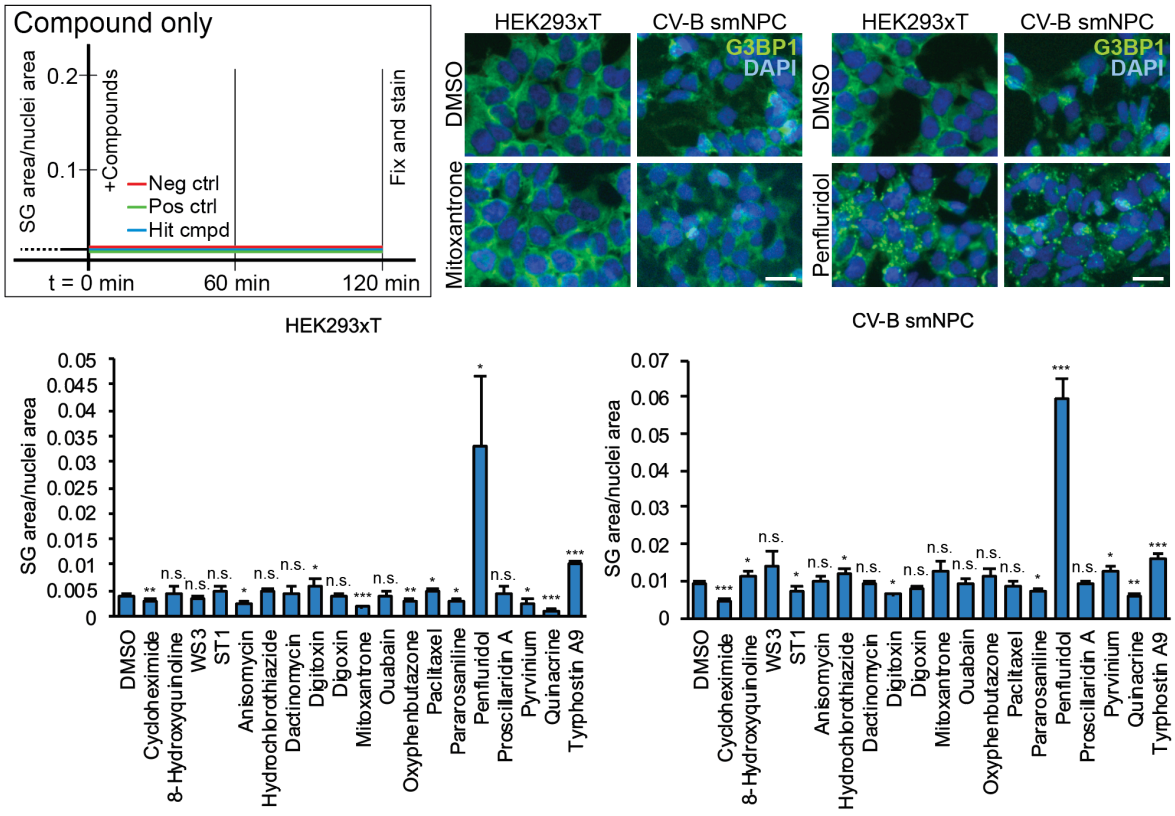

Figure 1.2.8: Overview of the assay used to test whether compounds alone induce SG formation in the absence of stress. Representative wide-field fluorescence microscopy of HEK293xT cells and CV-B small molecule neural precursor cells treated with a nucleic acid intercalating molecule mitoxantrone or the dopaminergic receptor antagonist penfluridol versus DMSO control in the absence of stress. Histograms showing SG area/nuclei area in HEK293xT cells and CV-B small molecule neural precursor cells treated with hit compounds in the absence of stress. Significance levels are from two-tailed two sample Student's t-tests to DMSO control: * $p < 0.05$, ** $p < 0.01$, *** $p < 0.001$. Error bars are sample standard deviations from four biological replicates. Scale bar is 50 μm.

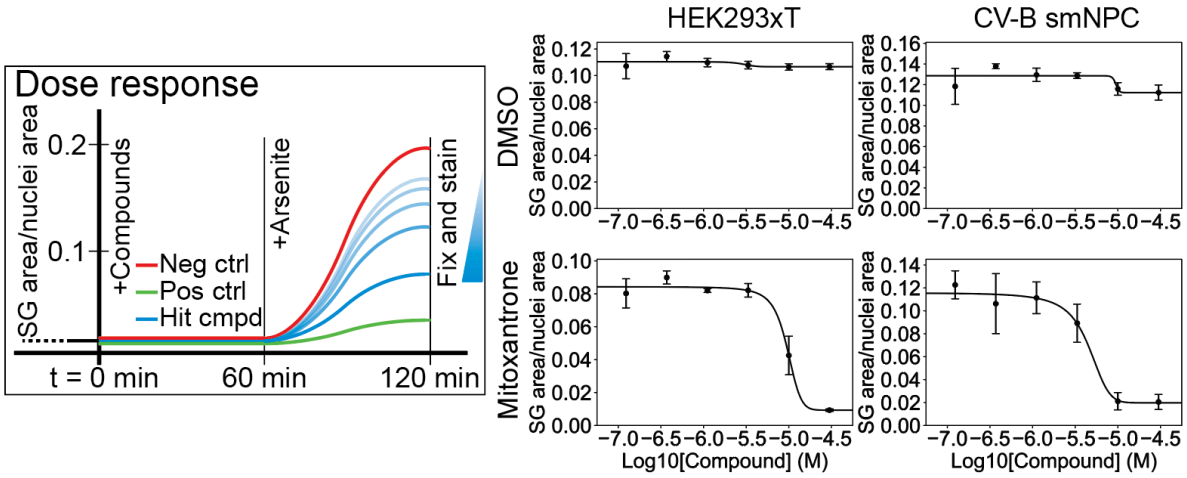

Figure 1.3.1: Overview of the assay used to demonstrate dose-dependent inhibition of SG formation by SG screen hit compounds. Scatterplot and logistic regression showing dose-dependent reduction of SG area/nuclei area by a nucleic acid intercalating molecule mitoxantrone but not by the vehicle control DMSO. Error bars are sample standard deviations from four biological replicates. SG: stress granule, NPC: small molecule neural precursor cells.

HEK293xT		CV-B smNPC	
Compound	**IC50 (µM)**	**Compound**	**IC50 (µM)**
Anisomycin	<1	8-Hydroxyquinoline	1.32
WS3	1.01	Anisomycin	<1
Digitoxin	0.63	WS3	2.77
Digoxin	1-3	Digitoxin	1-3
Gitoxigenin	3-10	Digoxin	1-3
Mitoxantrone	9.55	Gitoxigenin	3-10
Ouabain	1-3	Mitoxantrone	4.49
Proscillaridin A	1-3	Ouabain	9.97
Pyrvinium	3-10	Pyrvinium	10.69
Quinacrine	8.48	Quinacrine	4.38
ST1	3.16	ST1	0.85
		Tyrphostin A9	2.5

Figure 1.3.2: Summarizing the estimated IC50s of SG inhibiting compounds, determined from the midpoints of logistic regression functions fitted to dose response scatterplots.

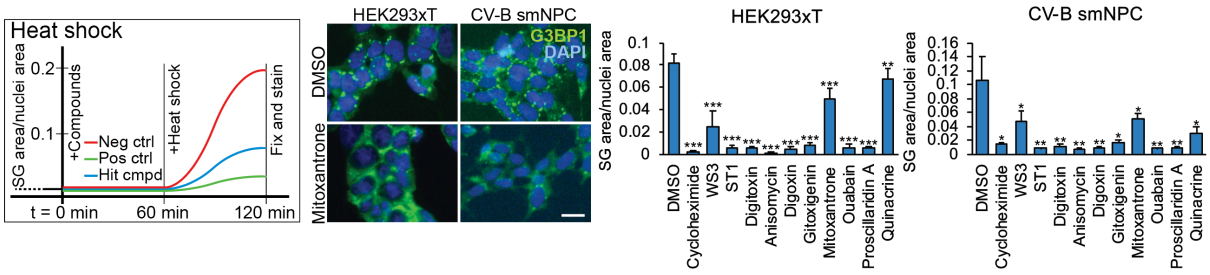

Figure 1.3.3: Overview of the assay used to test the efficacy of compounds to inhibit SG formation under heat shock stress. Representative wide-field fluorescence microscopy of HEK293xT cells and CV-B small molecule neural precursor cells treated with a nucleic acid intercalating molecule mitoxantrone versus DMSO control under heat shock stress. Histograms showing the reduction in SG area/nuclei area in HEK293xT cells and CV-B small molecule neural precursor cells treated with hit compounds under heat shock stress. Significance levels are from two-tailed two sample Student's t-tests to DMSO control: * $p < 0.05$, ** $p < 0.01$, *** $p < 0.001$. Error bars are sample standard deviations from four biological replicates. Scale bar is 50 μm.

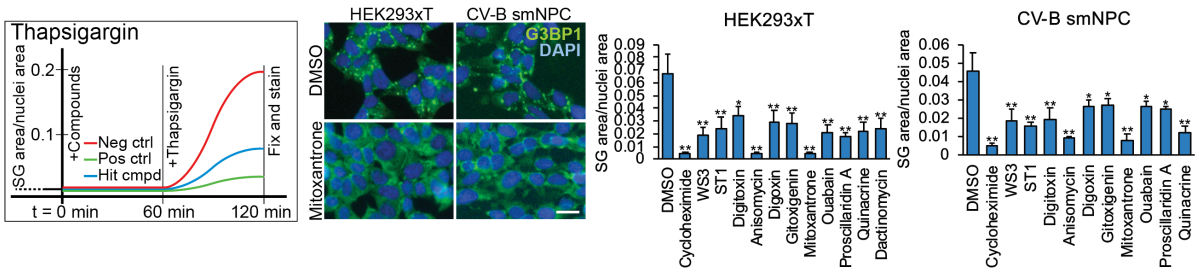

Figure 1.3.4: Overview of the assay used to test the efficacy of compounds to inhibit SG formation under thapsigargin stress. Representative wide-field fluorescence microscopy of HEK293xT cells and CV-B small molecule neural precursor cells treated with a nucleic acid intercalating molecule mitoxantrone versus DMSO control under thapsigargin stress. Histograms showing the reduction in SG area/nuclei area in HEK293xT cells and CV-B small molecule neural precursor cells treated with hit compounds under thapsigargin stress. Significance levels are from two-tailed two sample Student's t-tests to DMSO control: * $p < 0.05$, ** $p < 0.01$, *** $p < 0.001$. Error bars are sample standard deviations from four biological replicates. Scale bar is 50 μm.

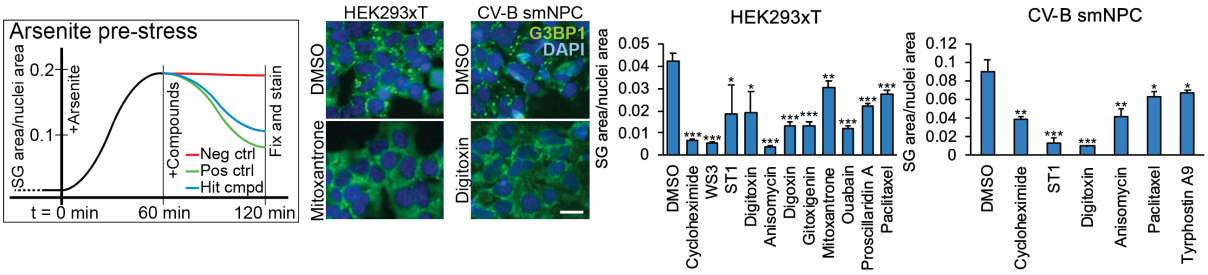

Figure 1.3.5: Overview of the assay used to test the efficacy of compounds to reverse SG formation after cells have been pre-stressed by $NaAsO_2$ for one hour. Representative wide-field fluorescence microscopy of HEK293xT cells and CV-B small molecule neural precursor cells treated with a nucleic acid intercalating molecule mitoxantrone or Na^+/K^+-ATPase inhibitor digitoxin versus DMSO control after one hour of $NaAsO_2$ pre-stress. Histograms showing the reduction in SG area/nuclei area in HEK293xT cells and CV-B small molecule neural precursor cells when hit compounds are added after $NaAsO_2$ stress. Significance levels are from two-tailed two sample Student's t-tests to DMSO control: * $p < 0.05$, ** $p < 0.01$, *** $p < 0.001$. Error bars are sample standard deviations from four biological replicates. Scale bar is 50 μm.

	HEK293xT	CV-B smNPC
Primary screen hits tested	16	18
Dose response	11	12
Heat shock	10	10
Thapsigargin	11	10
Arsenite pre-stress	10	5

Figure 1.3.6: Summarizing the number of compounds that reduced SG area/nuclei area in each of the counterscreen assays.

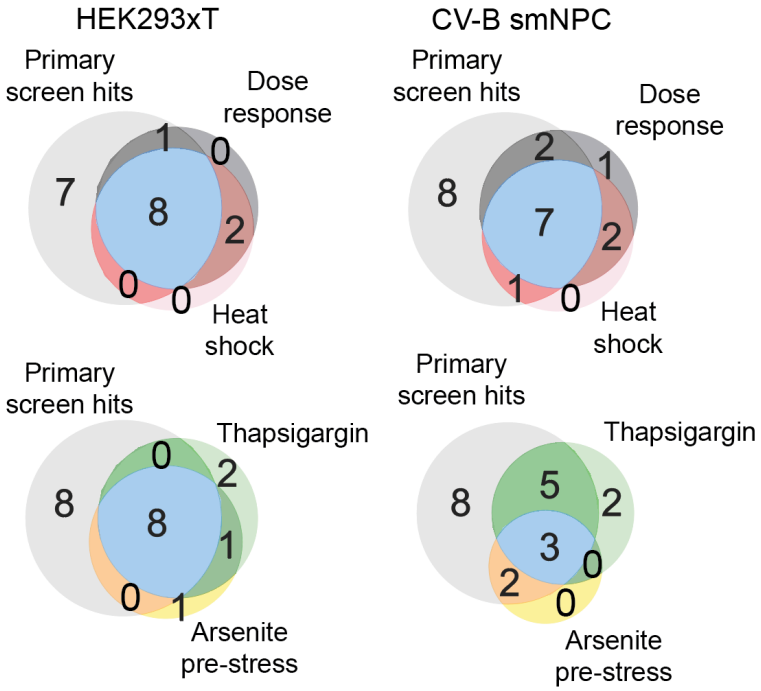

Figure 1.3.7: Venn diagrams representing the number of compounds that reduced SG area/nuclei area in more than one counterscreen assay.

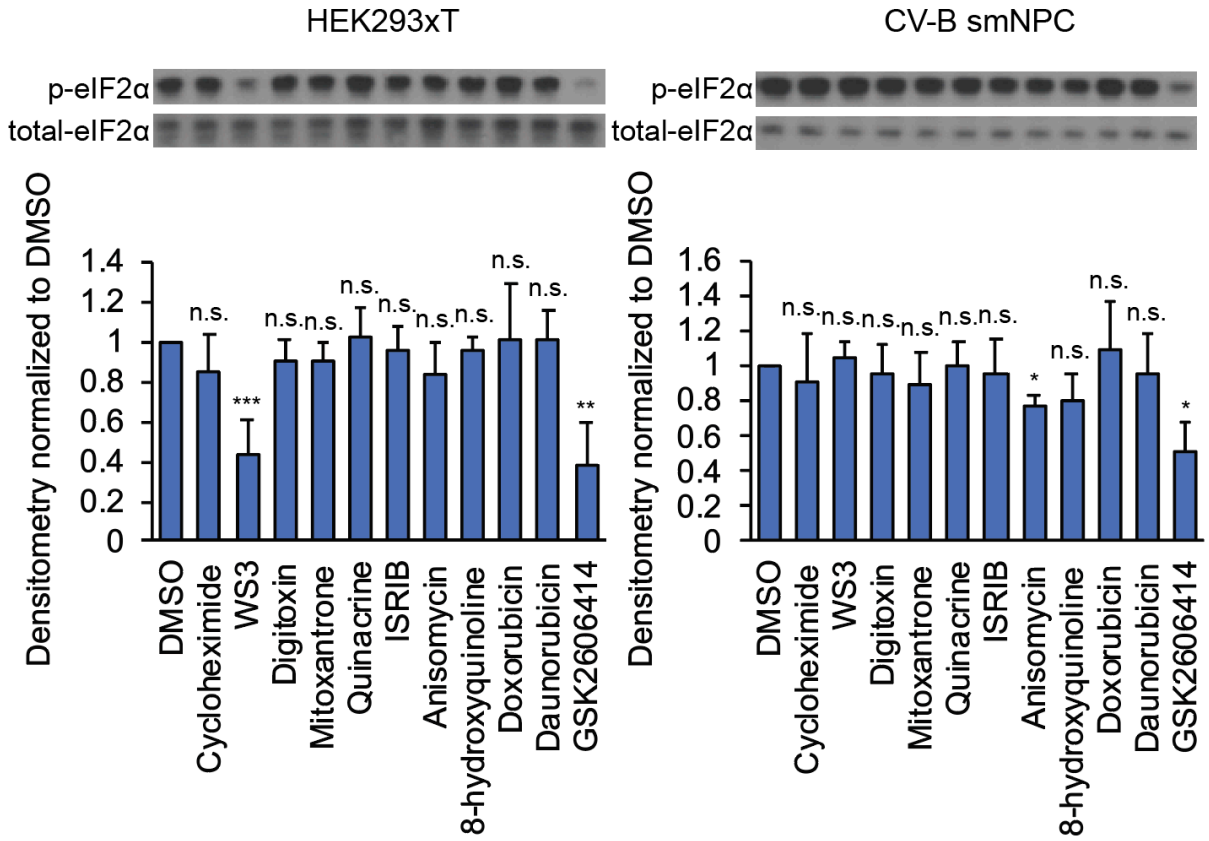

Figure 1.3.8: Representative Western blots of eIF2α phosphorylated at serine 51 versus total eIF2α protein in cells treated with hit compounds and under $NaAsO_2$ stress. Histograms quantifying the amount of eIF2α protein phosphorylated at serine 51 in HEK293xT cells and CV-B small molecule neural precursor cells treated with SG inhibiting compounds under $NaAsO_2$ stress. Histogram values are normalized to samples treated with the vehicle control DMSO. Significance levels are from two-tailed one sample Student's t-tests: * $p < 0.05$, ** $p < 0.01$, *** $p < 0.001$. Error bars are sample standard deviations from at least four biological replicates.

Figure 1.3.9: Scatterplots and logistic regressions showing dose-dependent reduction of SG area/nuclei area by SG screen hit compounds but not by the vehicle control DMSO. Error bars are sample standard deviations from four biological replicates. SG: stress granule, NPC: small molecule neural precursor cells.

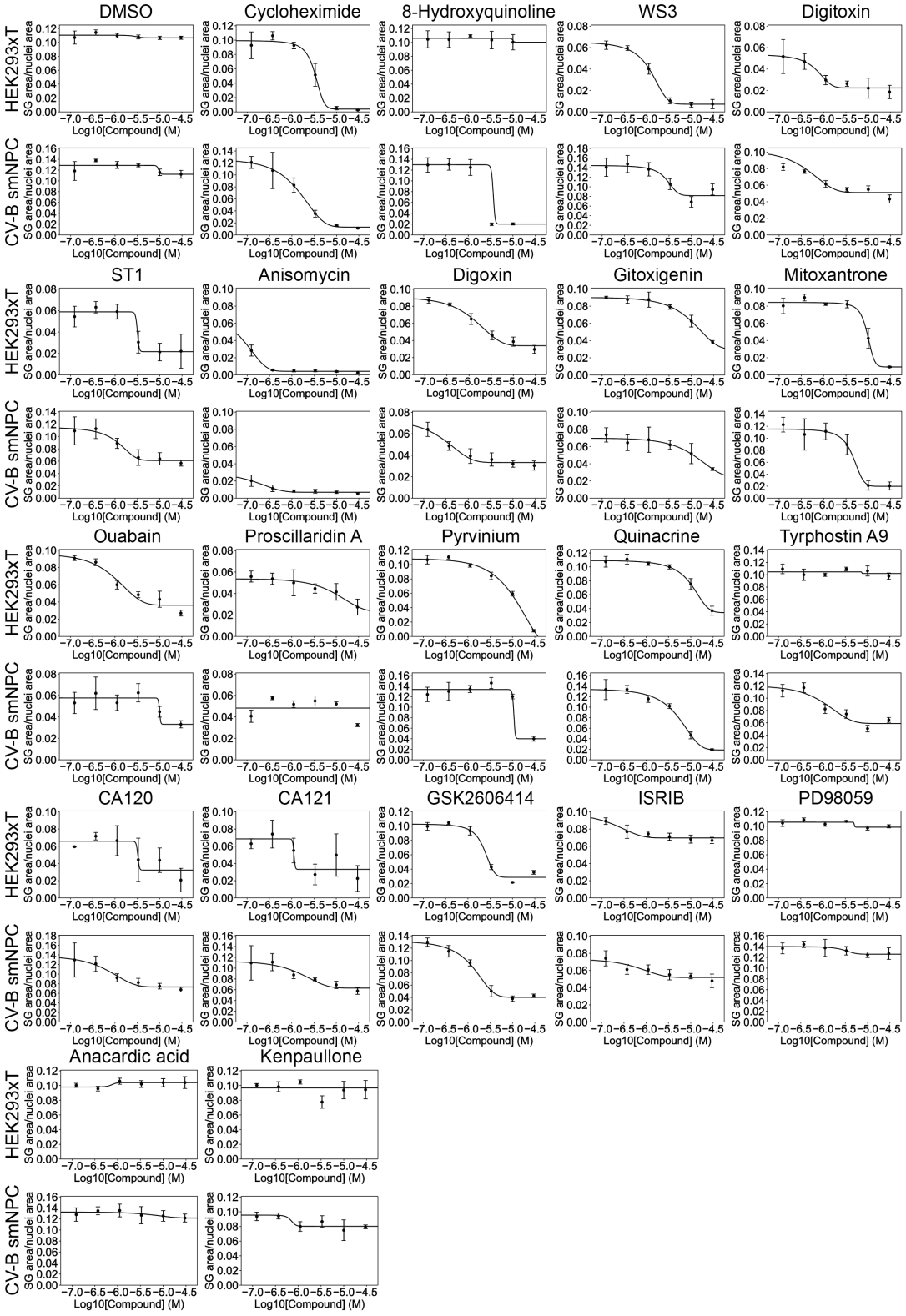
DMSO
Cycloheximide
8-Hydroxyquinoline
WS3
Digitoxin
ST1
Anisomycin
Digoxin
Gitoxigenin
Mitoxantrone
Ouabain
Proscillaridin A
Pyrvinium
Quinacrine
Tyrphostin A9
CA120
CA121
GSK2606414
ISRIB
PD98059
Anacardic acid
Kenpaullone
HEK293xT
CV-B smNPC
SG area/nuclei area
Log10[Compound] (M)

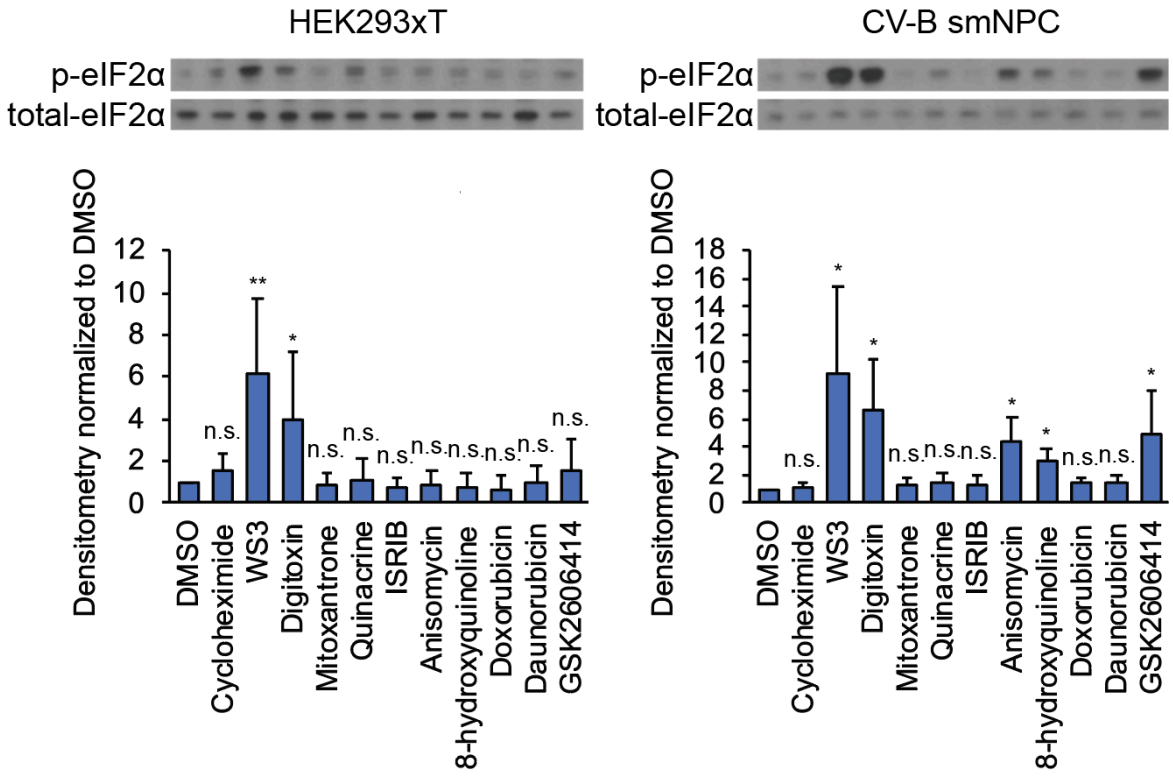

Figure 1.3.10: Representative Western blots of eIF2α phosphorylated at serine 51 versus total eIF2α protein in unstressed cells treated with hit compounds. Histograms quantifying the amount of eIF2α protein phosphorylated at serine 51 in unstressed HEK293xT cells and NPCs treated with SG inhibiting compounds. Histogram values are normalized to samples treated with the vehicle control DMSO. Significance levels are from two-tailed one sample Student's t-tests: * $p < 0.05$, ** $p < 0.01$. Error bars are sample standard deviations from at least three experimental replicates.

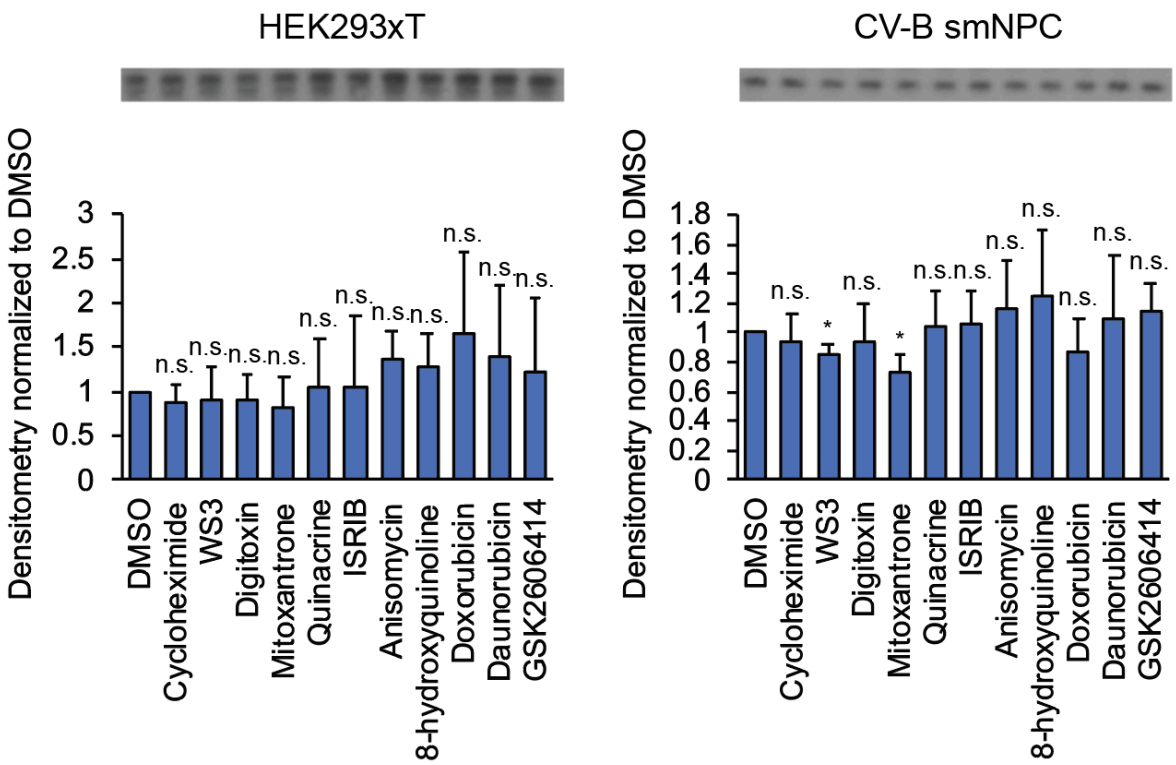

Figure 1.3.11: Representative Western blots of total eIF2α in cells treated with hit compounds and under $NaAsO_2$ stress, reproduced from Figure 1.3.8. Histograms quantifying the total eIF2α in HEK293xT cells and CV-B small molecule neural precursor cells treated with SG inhibiting compounds under $NaAsO_2$ stress. Histogram values are normalized to samples treated with the vehicle control DMSO. Significance levels are from two-tailed one sample Student's t-tests: * $p < 0.05$, ** $p < 0.01$. Error bars are sample standard deviations from at least three experimental replicates.

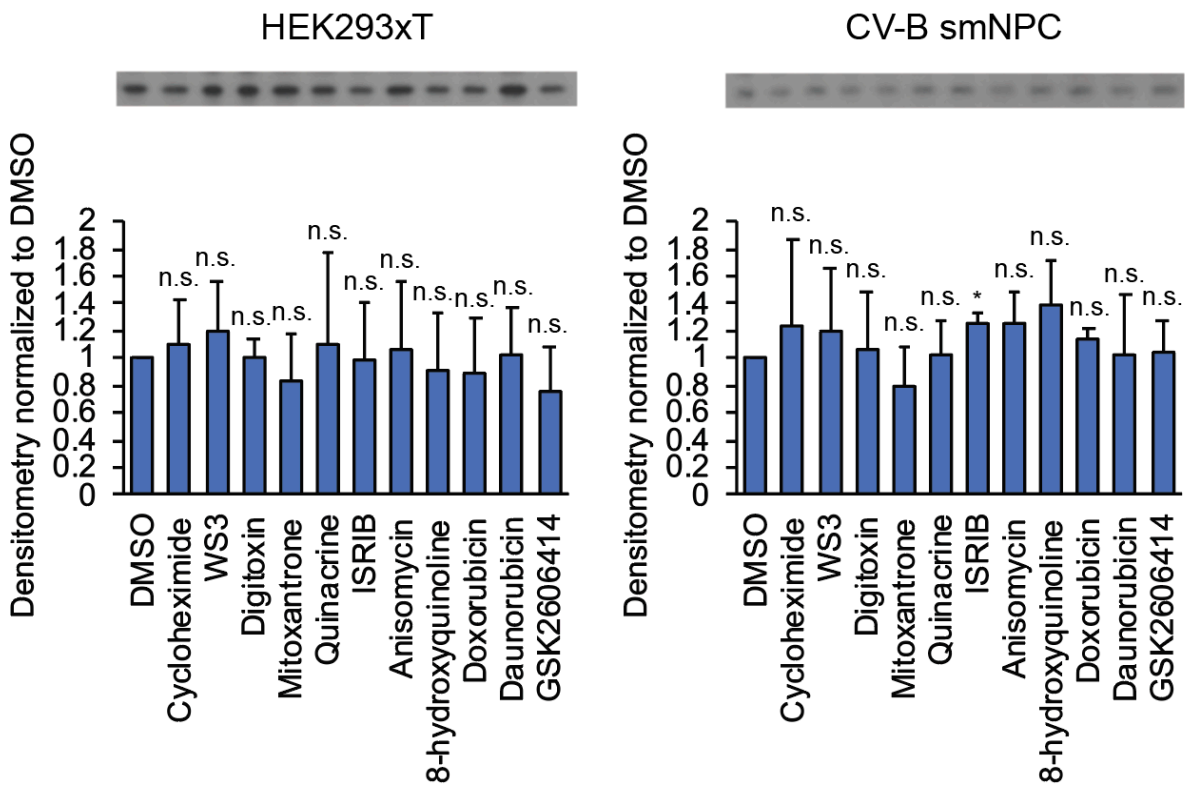

Figure 1.3.12 Representative Western blots of total eIF2α in unstressed cells treated with hit compounds, reproduced from Figure 1.3.10. Histograms quantifying the total eIF2α in unstressed HEK293xT cells and CV-B small molecule neural precursor cells treated with SG inhibiting compounds. Histogram values are normalized to samples treated with the vehicle control DMSO. Significance levels are from two-tailed one sample Student's t-tests: * $p < 0.05$, ** $p < 0.01$. Error bars are sample standard deviations from at least three experimental replicates.

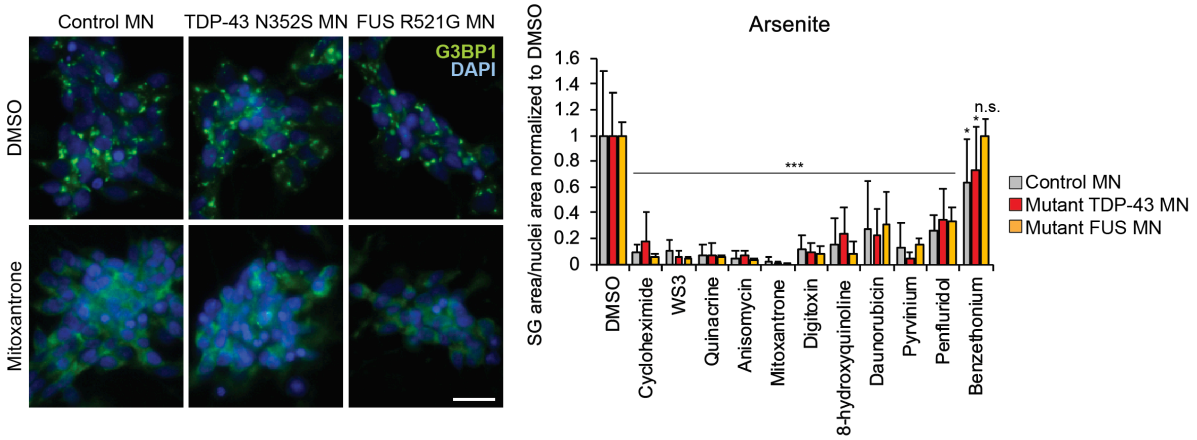

Figure 1.4.1: Representative wide-field fluorescence microscopy of control iPS-MN line and iPS-MNs lines carrying ALS-associated mutations in *TARDBP* and *FUS*, respectively, treated with a nucleic acid intercalating molecule mitoxantrone versus DMSO control under $NaAsO_2$ stress. Histograms showing the reduction in SG area/nuclei area in four control lines, four *TARDBP* mutant lines, and two *FUS* mutant lines treated with hit compounds under $NaAsO_2$ stress. MN: motor neuron, SG: stress granule. Histogram values are normalized to cells treated with the vehicle control DMSO. Significance levels are from two-tailed two sample Student's t-tests to DMSO control: * $p < 0.05$, ** $p < 0.01$, *** $p < 0.001$. Error bars are sample standard deviations from at least five biological replicates of four control lines, four *TARDBP* mutant lines, and two *FUS* mutant lines. Scale bars are 20 μm.

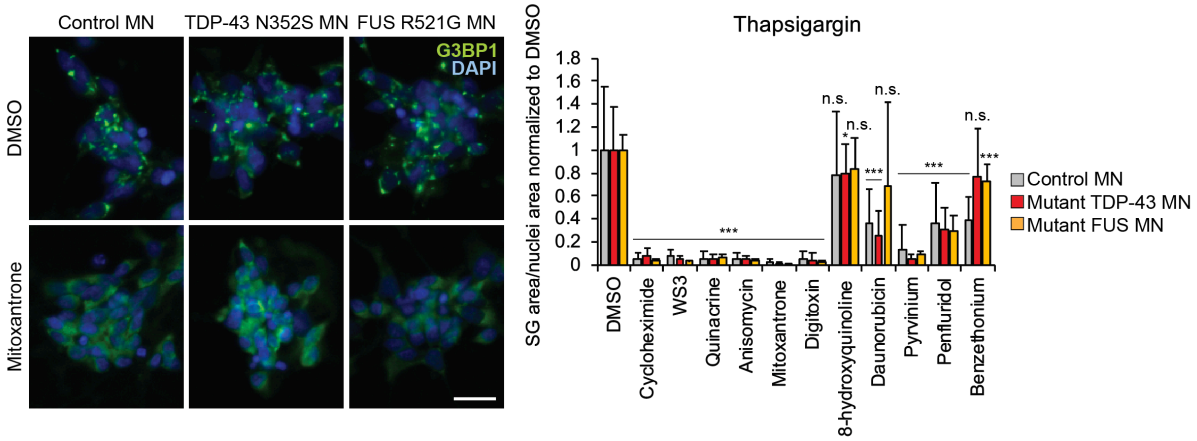

Figure 1.4.2: Representative wide-field fluorescence microscopy of control iPS-MN line and iPS-MNs lines carrying ALS-associated mutations in *TARDBP* and *FUS*, respectively, treated with a nucleic acid intercalating molecule mitoxantrone versus DMSO control under thapsigargin stress. Histograms showing the reduction in SG area/nuclei area in four control lines, four *TARDBP* mutant lines, and two *FUS* mutant lines treated with hit compounds under thapsigargin stress. Histogram values are normalized to cells treated with the vehicle control DMSO. Significance levels are from two-tailed two sample Student's t-tests to DMSO control: * $p < 0.05$, ** $p < 0.01$, *** $p < 0.001$. Error bars are sample standard deviations from at least five biological replicates of four control lines, four *TARDBP* mutant lines, and two *FUS* mutant lines. Scale bars are 20 μm.

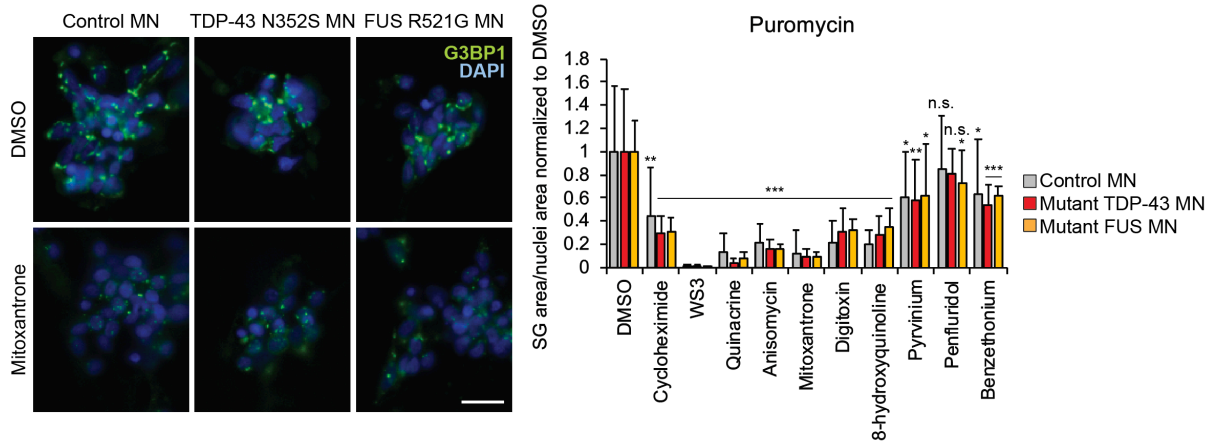

Figure 1.4.3: Representative wide-field fluorescence microscopy of control iPS-MN line and iPS-MNs lines carrying ALS-associated mutations in *TARDBP* and *FUS*, respectively, treated with a nucleic acid intercalating molecule mitoxantrone versus DMSO control under puromycin stress. Histograms showing the reduction in SG area/nuclei area in four control lines, four *TARDBP* mutant lines, and two *FUS* mutant lines treated with hit compounds under puromycin stress. Histogram values are normalized to cells treated with the vehicle control DMSO. Significance levels are from two-tailed two sample Student's t-tests to DMSO control: * $p < 0.05$, ** $p < 0.01$, *** $p < 0.001$. Error bars are sample standard deviations from at least five biological replicates of four control lines, four *TARDBP* mutant lines, and two *FUS* mutant lines. Scale bars are 20 μm.

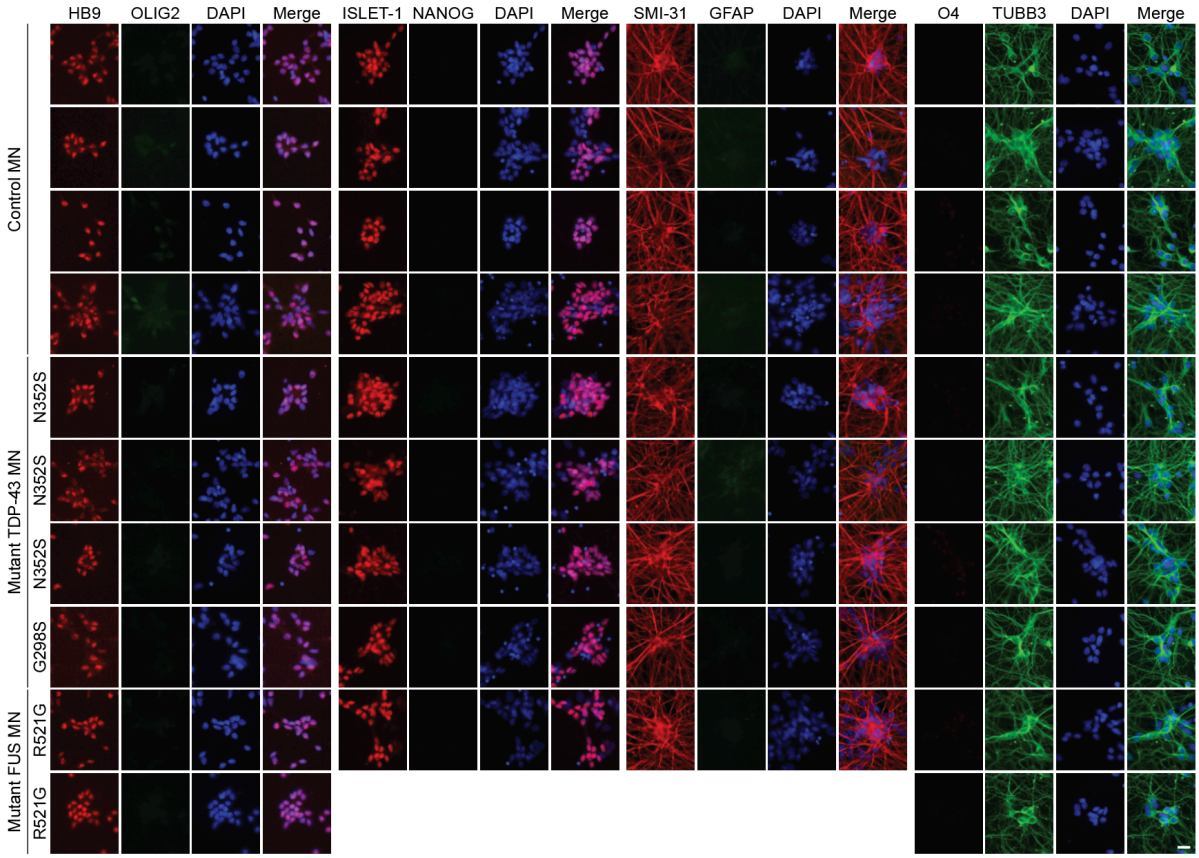

Figure 1.4.4: Representative wide-field fluorescence microscopy of iPS-MN lines: four control lines, four lines carrying ALS-associated mutations in *TARDBP*, and four lines carrying ALS-associated mutations in *FUS*. The iPS-MNs are probed by immunofluorescence for MN markers HB9, ISLET-1, and SMI-31; neuronal marker TUBB3; and non-neuronal markers OLIG2 (oligodendrocytes), NANOG (induced-pluripotent stem cells), GFAP (astrocytes), and O4 (oligodendrocytes). Nuclei are stained with DAPI. Scale bar is 20 μm. MN: motor neuron.

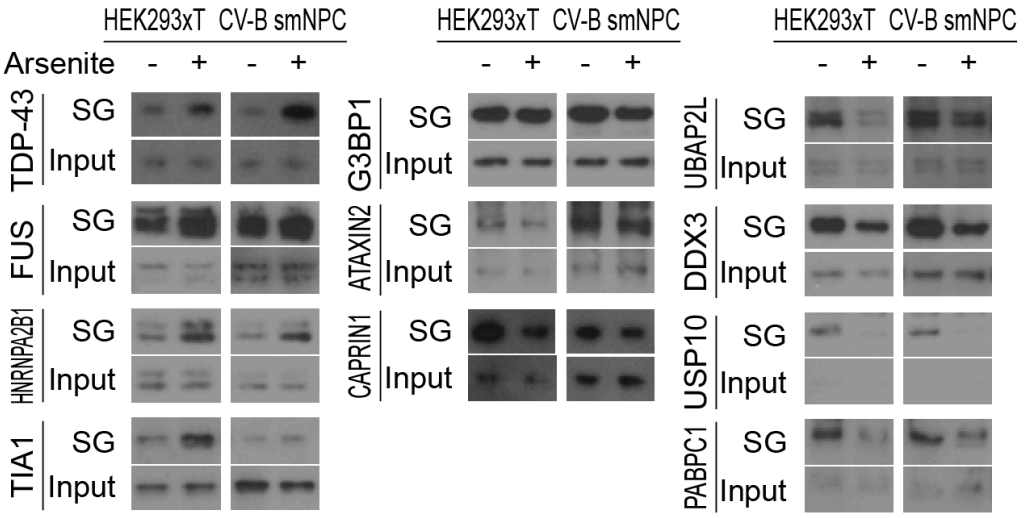

Figure 2.5.1: Representative Western blots of ALS-associated RBPs and SG-associated proteins in SG-enriched fractions or whole-cell lysate input from unstressed versus $NaAsO_2$-stressed cells. SG-enriched fractions were isolated from G3BP1-GFP HEK293xT cells and CV-B small molecule neural precursor cells. SG: stress granule, NPC: small molecule neural precursor cells.

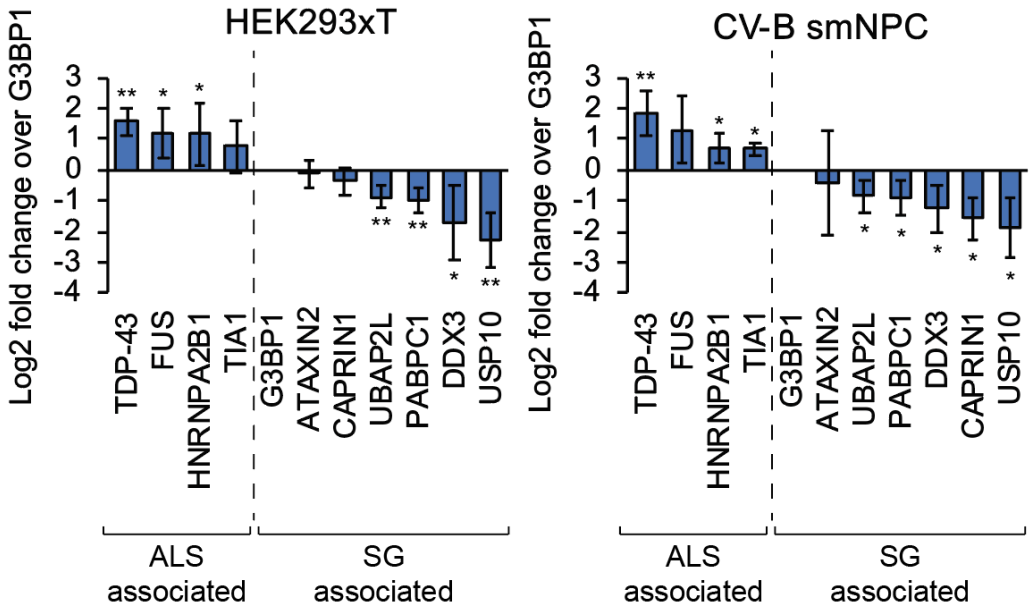

Figure 2.5.2: Histograms quantifying the Western blotting in Figure 2.5.1 of ALS-associated RBPs and SG-associated proteins in SG-enriched fractions from unstressed versus $NaAsO_2$-stressed cells. Histogram values are ratios of Western blot band intensities from stressed fractions divided by unstressed fractions, normalized to G3BP1, and log_2-transformed. Significance levels are from two-tailed one sample Student's t-tests: * $p < 0.05$, ** $p < 0.01$. Error bars are sample standard deviations from three experimental replicates.

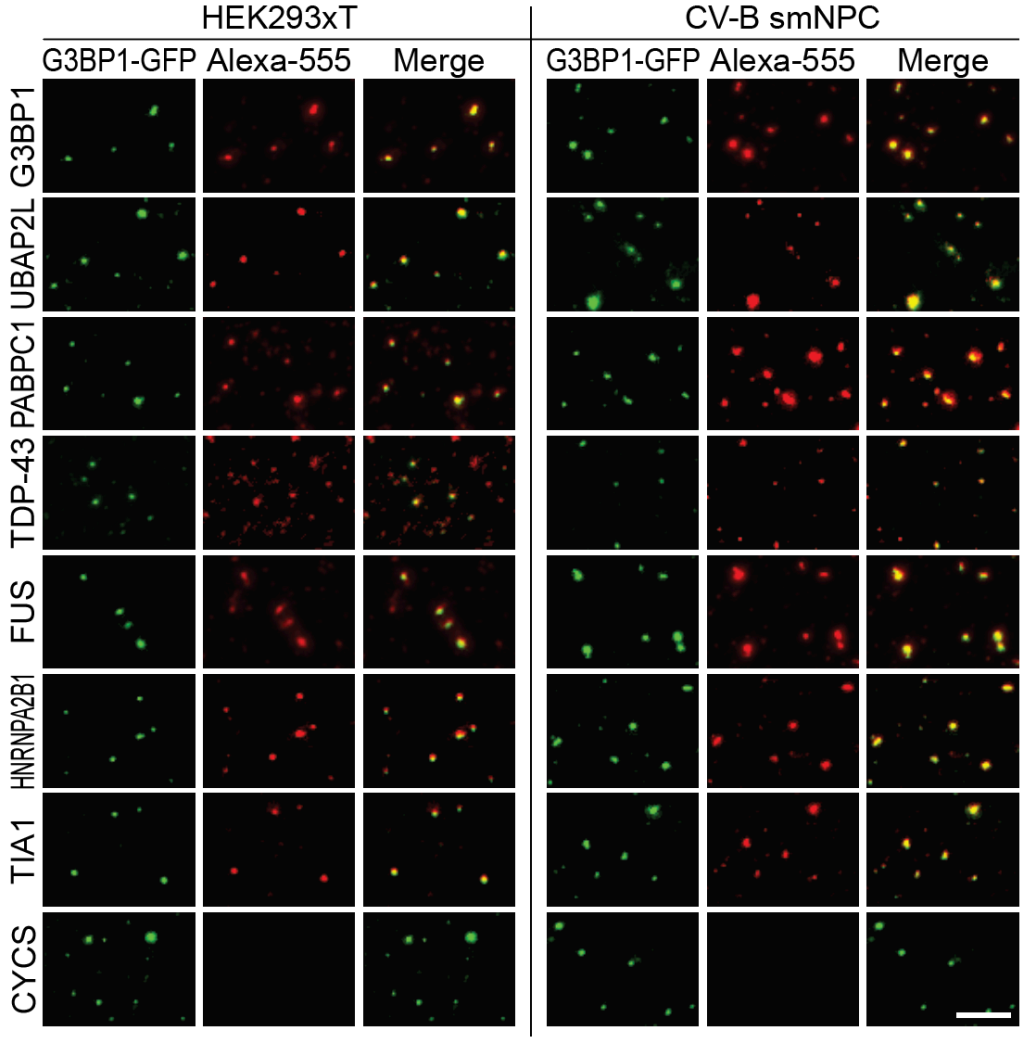

Figure 2.5.3: Representative wide-field fluorescence microscopy of $NaAsO_2$ SG-enriched fractions probed by immunofluorescence for ALS-associated RBPs and SG-associated proteins. G3BP1 was probed as a positive control and CYCS was probed as a negative control. Scale bar is 10 μm.

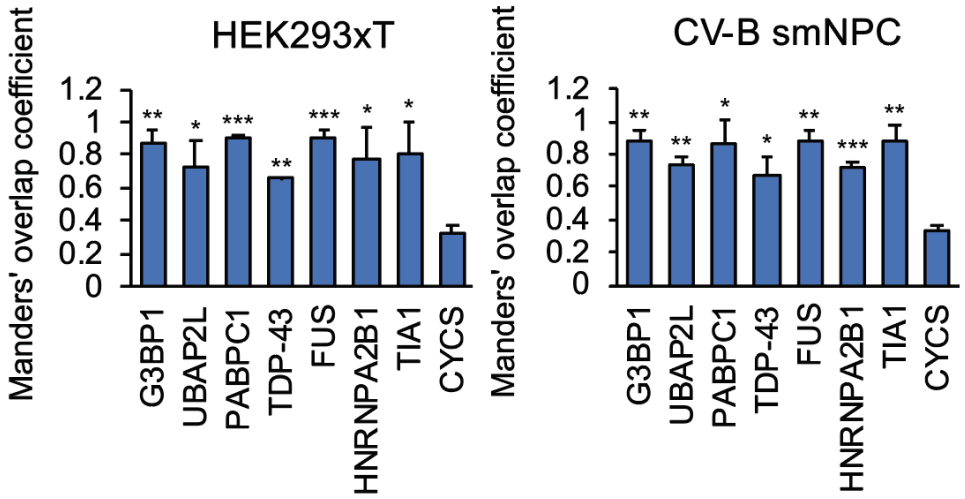

Figure 2.5.4: Histograms quantifying the co-localization in Figure 2.5.3 of G3BP1-GFP SGs and immunofluorescence probing of ALS-associated RBPs and SG-associated proteins in $NaAsO_2$ SG-enriched fractions. Significance levels are from two-tailed two sample Student's t-tests to CYC: * $p < 0.05$, ** $p < 0.01$, *** $p < 0.001$. Error bars are sample standard deviations from three experimental replicates.

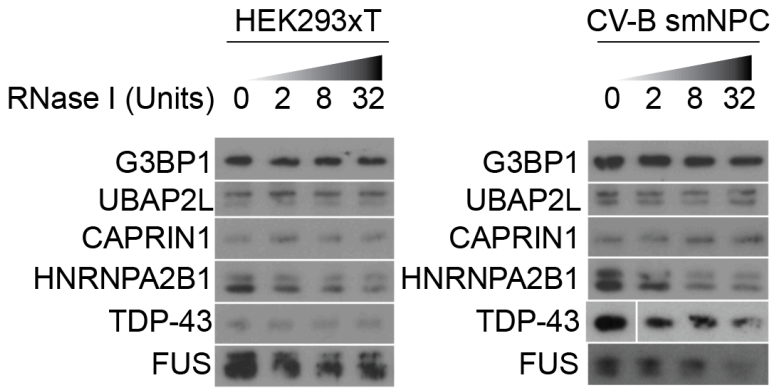

Figure 2.5.5: Representative Western blots of ALS-associated RBPs and SG-associated proteins in $NaAsO_2$ SG-enriched fractions after digestion with increasing amounts of RNase I.

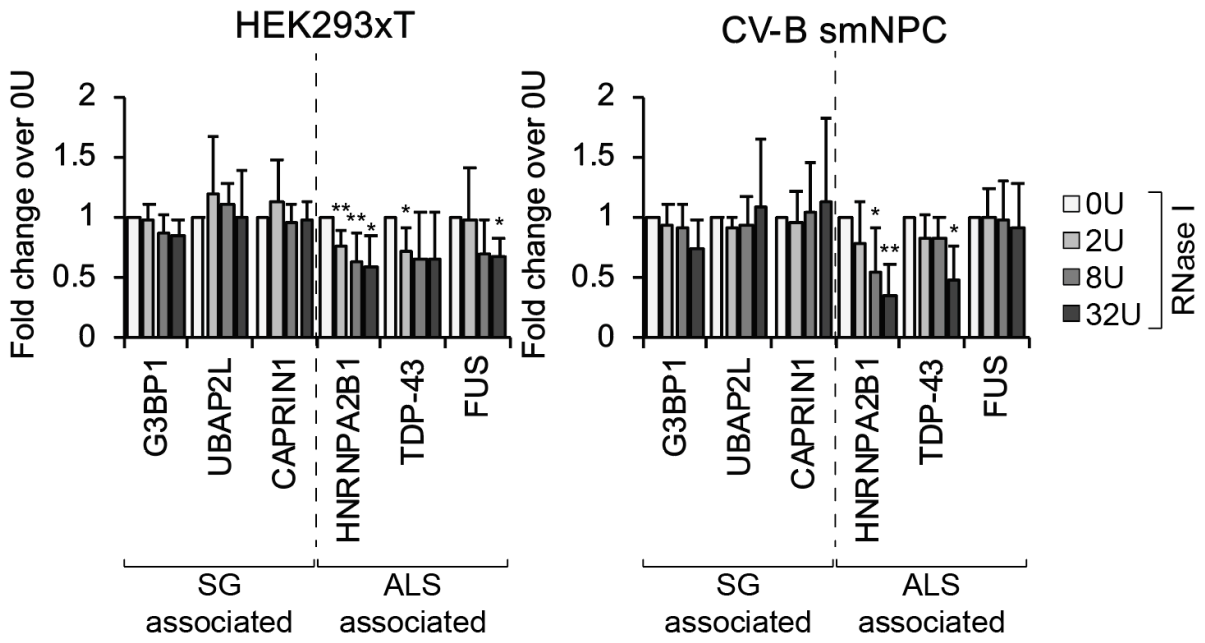

Figure 2.5.6: Histograms quantifying the Western blotting in Figure 2.5.5 of ALS-associated RBPs and SG-associated proteins in $NaAsO_2$ SG-enriched fractions after digestion with increasing amounts of RNase I. Histogram values are normalized to samples treated with 0 Units of RNase I. Significance levels are from two-tailed one sample Student's t-tests: * $p < 0.05$, ** $p < 0.01$. Error bars are sample standard deviations from three experimental replicates.

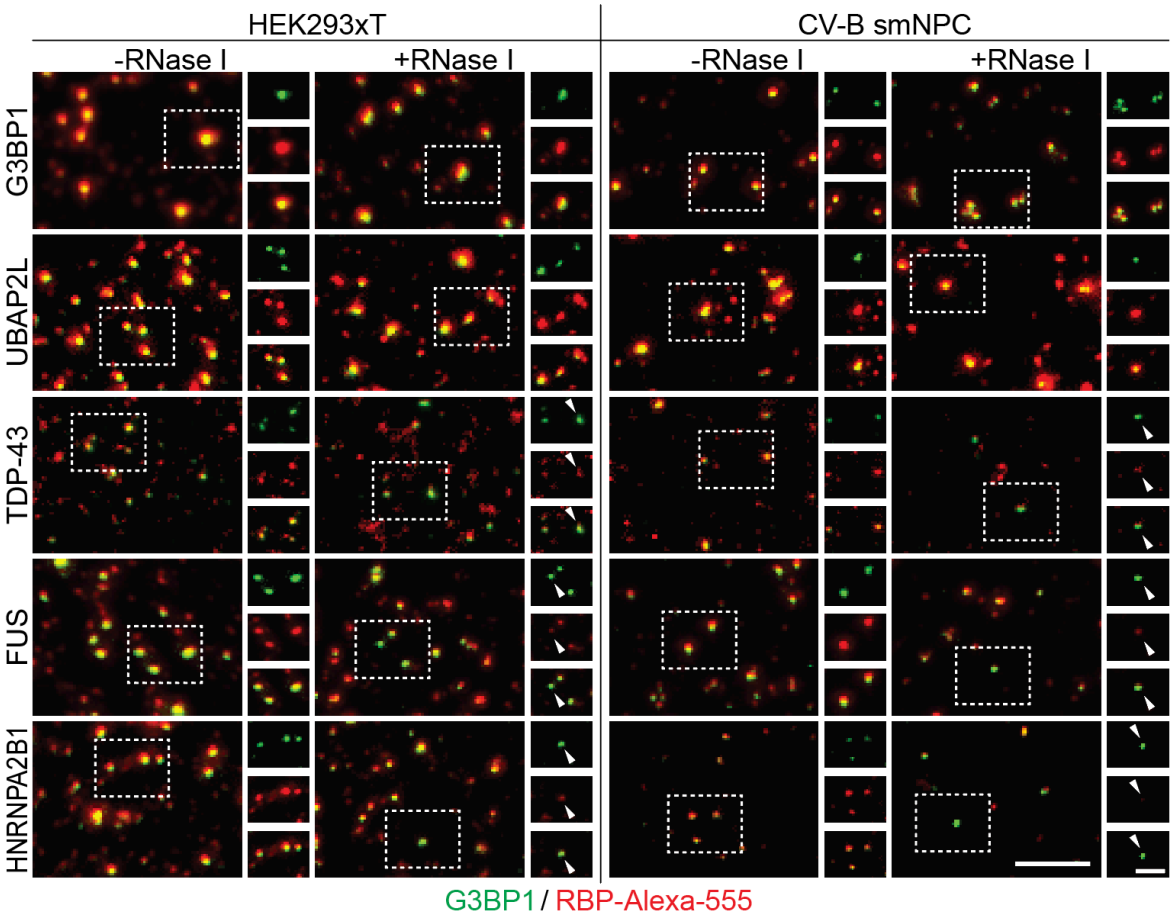

Figure 2.5.7: Representative wide-field fluorescence microscopy of $NaAsO_2$ SG-enriched fractions probed by immunofluorescence for ALS-associated RBPs and SG-associated proteins, in the absence or presence of RNase I digestion. Scale bar is 10 μm (5 μm for inset).

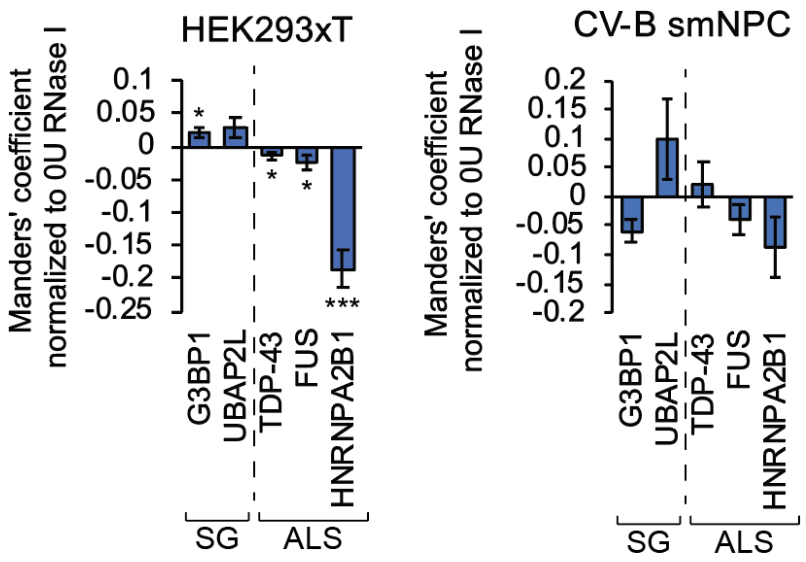

Figure 2.5.8: Histograms quantifying the co-localization in Figure 2.5.7 of G3BP1-GFP SGs and immunofluorescence probing of ALS-associated RBPs and SG-associated proteins in $NaAsO_2$ SG-enriched fractions, in the absence or presence of RNase I digestion. Histogram values are normalized to samples treated with 0 Units of RNase I. Significance levels are from two-tailed one sample Student's t-tests: * $p < 0.05$, *** $p < 0.001$. Error bars are estimated standard error of the means of 18 biological replicates from two experimental replicates.

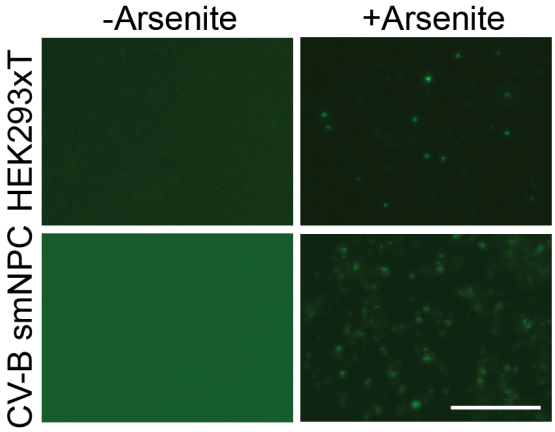

Figure 2.5.9: Representative wide-field fluorescence microscopy of SG-enriched fractions isolated from G3BP1-GFP HEK293xT cells and CV-B small molecule neural precursor cells, under unstressed or $NaAsO_2$ -stressed conditions. Scale bar is 20 μm. NPC: small molecule neural precursor cells.

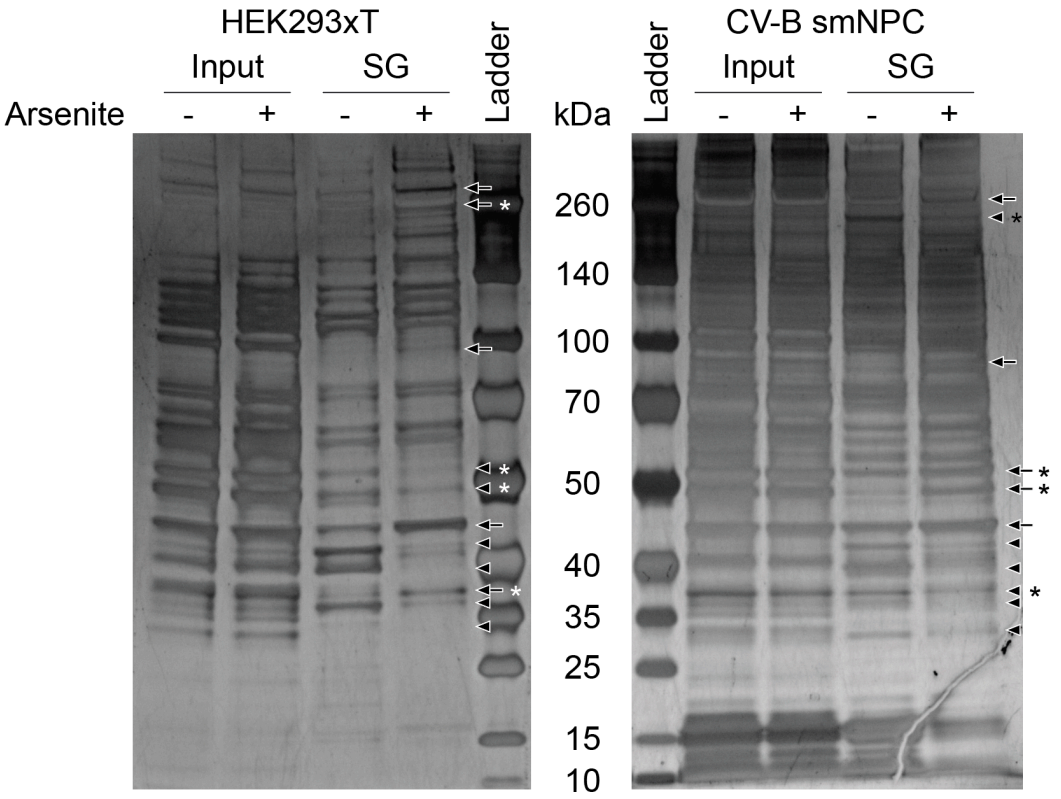

Figure 2.5.10: Representative silver staining of whole-cell lysate inputs or SG-enriched fractions isolated from HEK293xT cells and CV-B small molecule neural precursor cells under unstressed or $NaAsO_2$-stressed conditions. Arrows denote bands which appear stronger in SG-enriched fractions isolated from stressed cells. Arrowheads denote bands which appear fainter in SG-enriched fractions isolated from stressed cells. Stars next to arrows or arrowheads indicate divergences between samples from HEK293xT cells and NPCs. SG: stress granule.

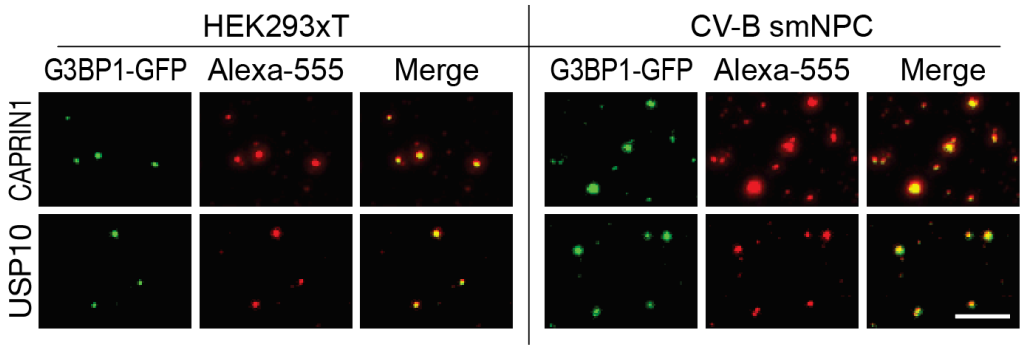

Figure 2.5.11: Representative wide-field fluorescence microscopy of $NaAsO_2$ SG-enriched fractions probed by immunofluorescence for CAPRIN1 or USP10. Scale bar is 10 μm.

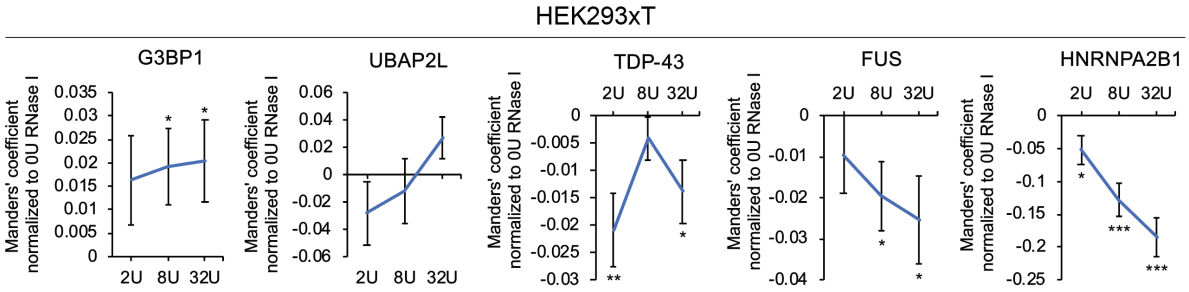

Figure 2.5.12: Scatterplots quantifying the co-localization of G3BP1-GFP SGs and immunofluorescence probing of ALS-associated RBPs and SG-associated proteins in $NaAsO_2$ SG-enriched fractions, in the presence of increasing amounts of RNase I digestion. Scatterplot values are normalized to samples treated with 0 Units of RNase I. Significance levels are from two-tailed one sample Student's t-tests: * $p < 0.05$, ** $p < 0.01$, *** $p < 0.001$. Error bars are estimated standard error of the means of 18 biological replicates from two experimental replicates

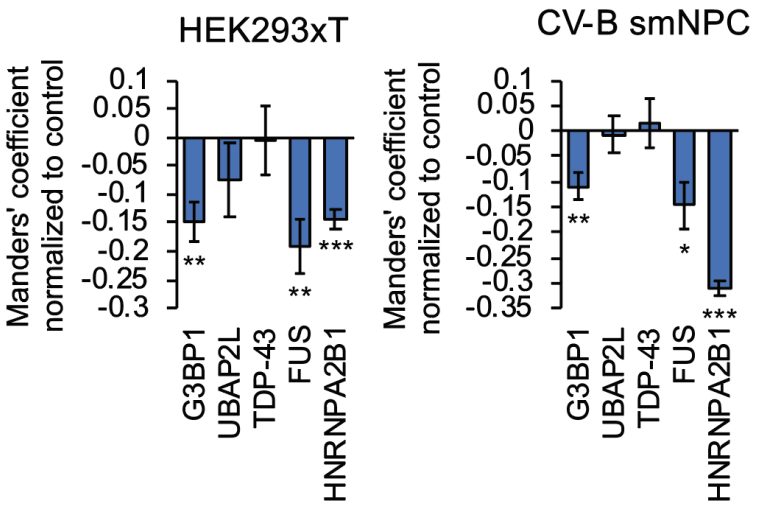

Figure 2.5.13: Histograms quantifying the co-localization of G3BP1-GFP SGs and immunofluorescence probing of ALS-associated RBPs and SG-associated proteins in $NaAsO_2$ SG-enriched fractions, in the absence or presence of overnight incubation with 5% 1,6-hexanediol followed by RNase I digestion. Histogram values are normalized to samples treated with 0% 1,6-hexanediol and 0 Units of RNase I. Significance levels are from two-tailed one sample Student's t-tests: * $p < 0.05$, ** $p < 0.01$, *** $p < 0.001$. Error bars are estimated standard error of the means from 18 biological replicates from two experimental replicates.

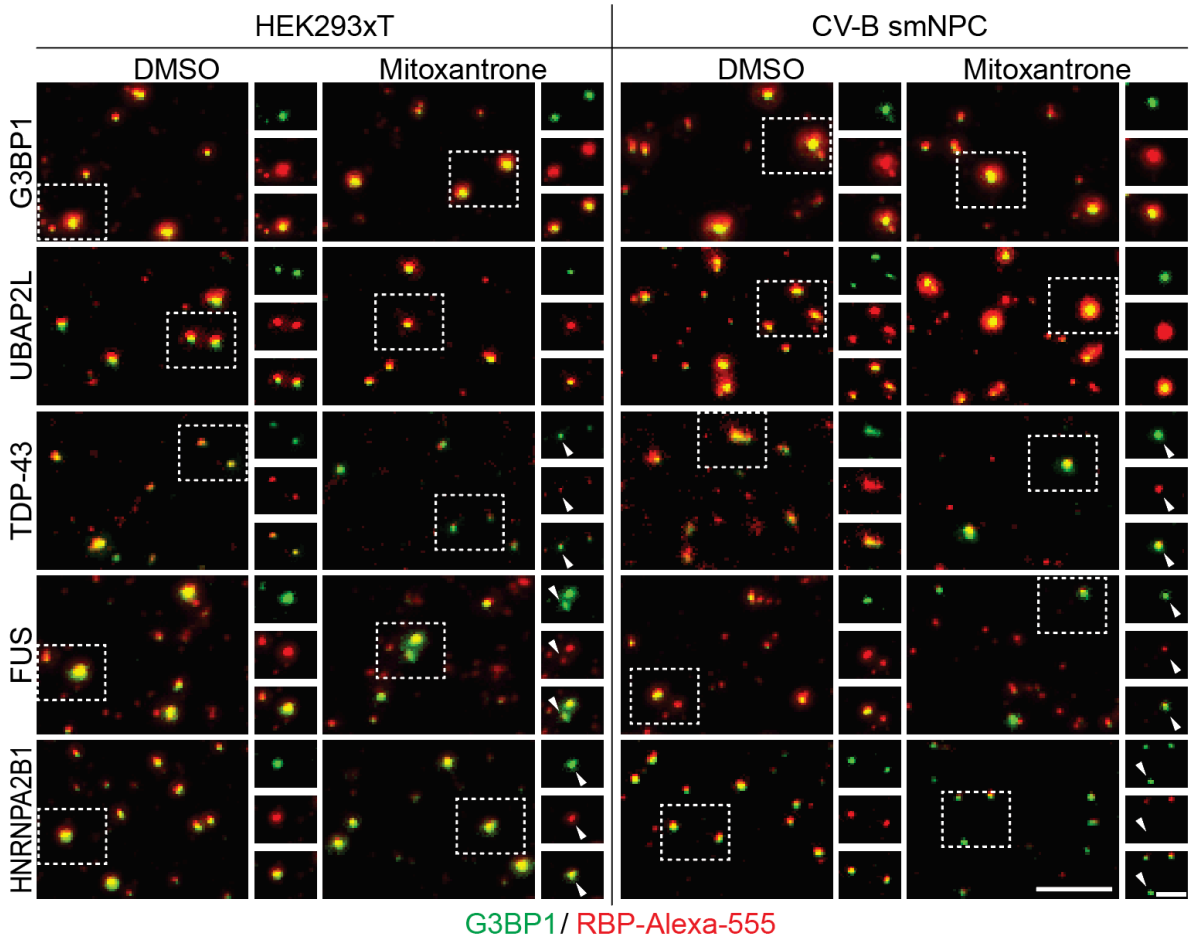

Figure 2.6.1: Representative wide-field fluorescence microscopy of $NaAsO_2$ SG-enriched fractions probed by immunofluorescence for TDP-43 in the absence or presence of overnight incubation with 100 μM mitoxantrone. Scale bar is 10 μm (5 μm for inset). NPC: small molecule neural precursor cells, RBP: RNA-binding protein.

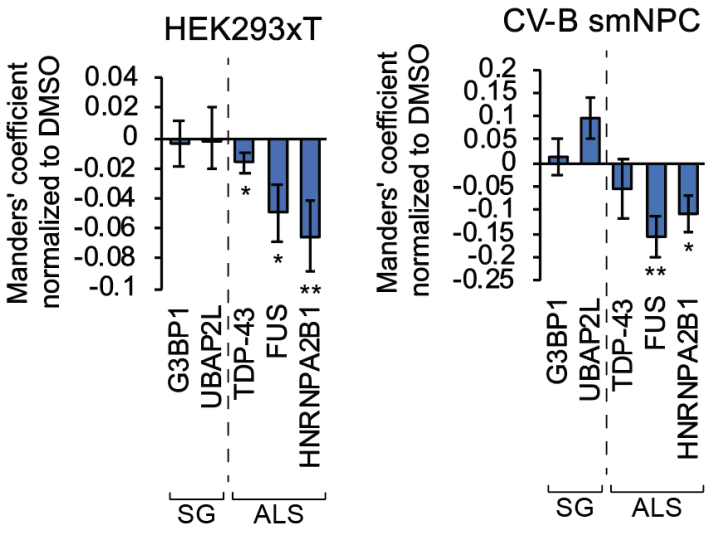

Figure 2.6.2: Histograms quantifying the change in co-localization in Figure 2.6.1 of G3BP1-GFP SGs and immunofluorescence probing of TDP-43 in $NaAsO_2$ SG-enriched fractions, in the absence or presence of overnight incubation with 100 μM mitoxantrone. Histogram values are normalized to samples treated with the vehicle control DMSO. Significance levels are from two-tailed one sample Student's t-tests: * $p < 0.05$, ** $p < 0.01$. Error bars are estimated standard error of the means from 18 biological replicates from two experimental replicates. SG: stress granule.

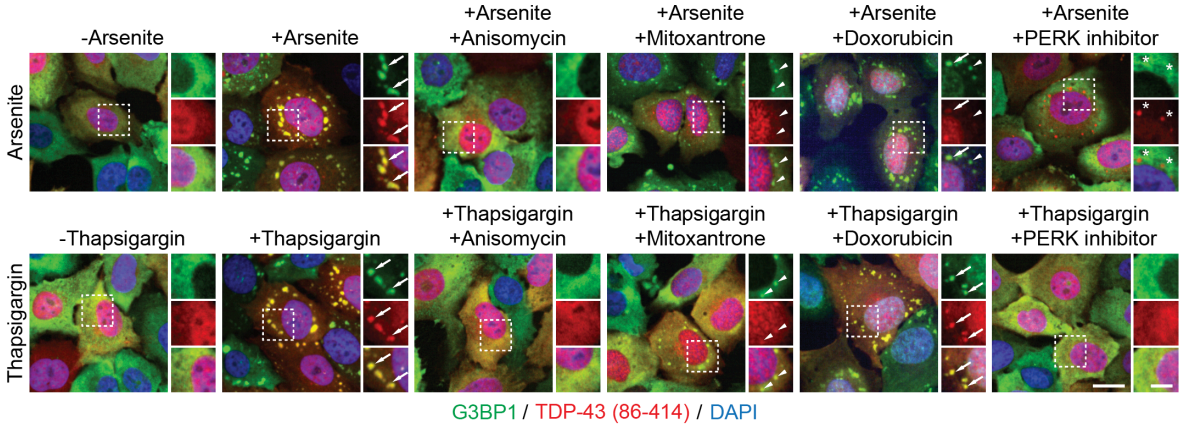

Figure 2.6.3: Representative wide-field fluorescence microscopy of H4 cells transiently expressing G3BP1-mCherry (false-colored green for consistency with other fluorescent imaging of G3BP1) and GFP-TDP-43ΔNLS (amino acid residues 86-414/no nuclear localization signal; false-colored red), stressed with $NaAsO_2$ or thapsigargin, in the absence and presence of SG-modulating compounds. Arrows denote co-localized G3BP1-mCherry SG-like puncta and GFP-TDP-43ΔNLS foci. Arrowheads denote G3BP1-mCherry puncta that are largely devoid of co-localized GFP-TDP-43ΔNLS. Stars denote GFP-TDP-43ΔNLS foci that are largely devoid of co-localized G3BP1-mCherry. Scale bar is 50 μm (20 μm for insets).

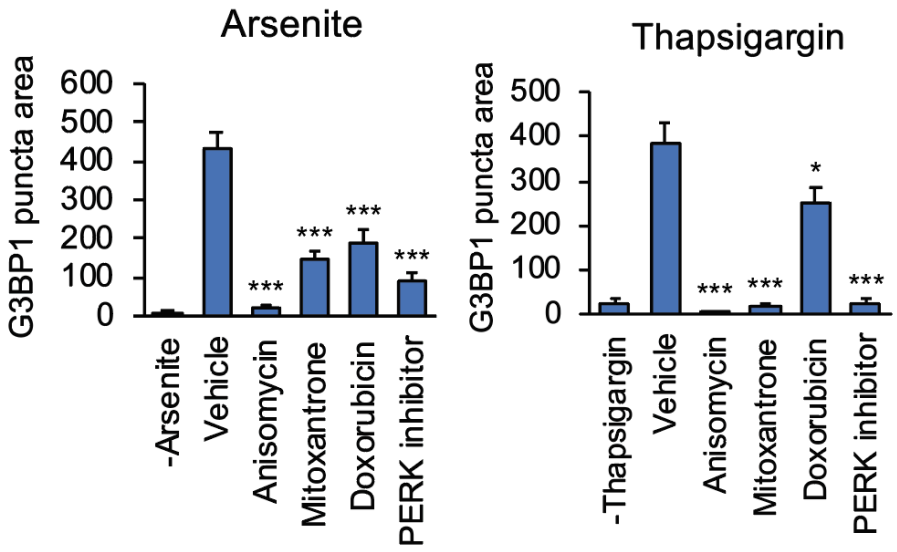

Figure 2.6.4: Histograms quantifying the formation in Figure 2.6.3 of G3BP1-mCherry SG-like puncta in H4 cells transiently expressing G3BP1-mCherry and GFP-TDP-43ΔNLS and stressed with $NaAsO_2$ or thapsigargin, in the absence or presence of SG-modulating compounds. Significance levels are from two-tailed two sample Student's t-tests to vehicle control: * $p < 0.05$, *** $p < 0.001$. Error bars are estimated standard error of the means from $n \geq 35$ cells.

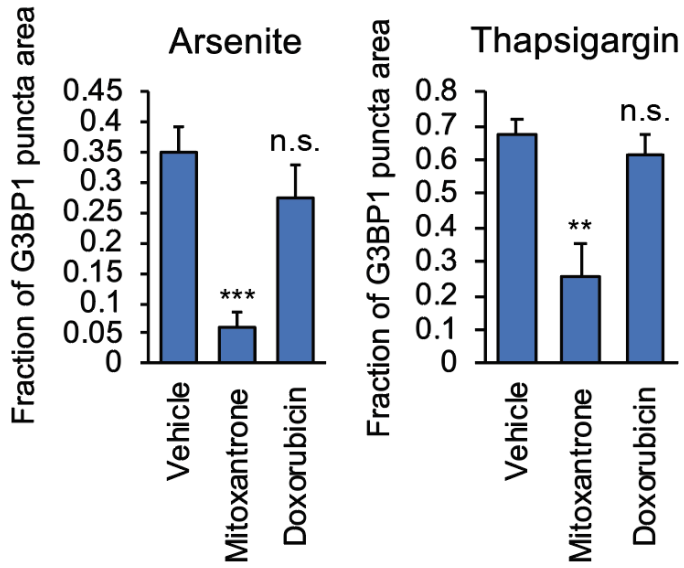

Figure 2.6.5: Histograms quantifying in Figure 2.6.3 the fraction of G3BP1-mCherry SG-like puncta that have GFP-TDP-43ΔNLS co-localization in H4 cells transiently expressing G3BP1-mCherry and GFP-TDP-43ΔNLS and stressed with $NaAsO_2$ or thapsigargin, in the absence or presence of SG-modulating compounds. Significance levels are from two-tailed two sample Student's t-tests to vehicle control: ** $p < 0.01$, *** $p < 0.001$. Error bars are estimated standard error of the means from $n \geq 14$ cells.

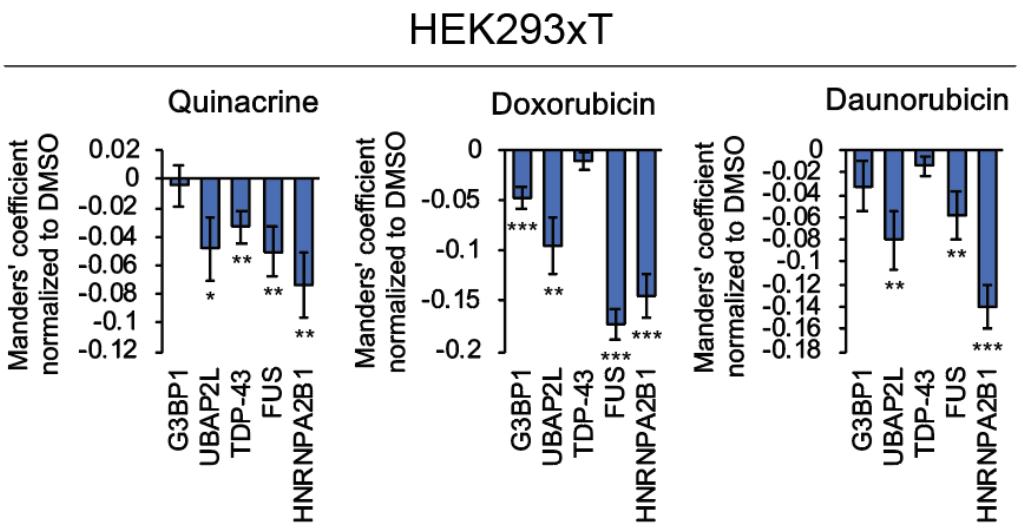

Figure 2.6.6: Histograms quantifying the change in co-localization of G3BP1-GFP SGs and immunofluorescence probing of G3BP1, UBAP2L, TDP-43, FUS, and HNRNPA2B1 in $NaAsO_2$ SG-enriched fractions, in the absence or presence of overnight incubation with 100 μM quinacrine, doxorubicin, or daunorubicin. Histogram values are normalized to samples treated with the vehicle control DMSO. Significance levels are from two-tailed one sample Student's t-tests: * $p < 0.05$, ** $p < 0.01$, *** $p < 0.001$. Error bars are estimated standard error of the means from 18 biological replicates from two experimental replicates.

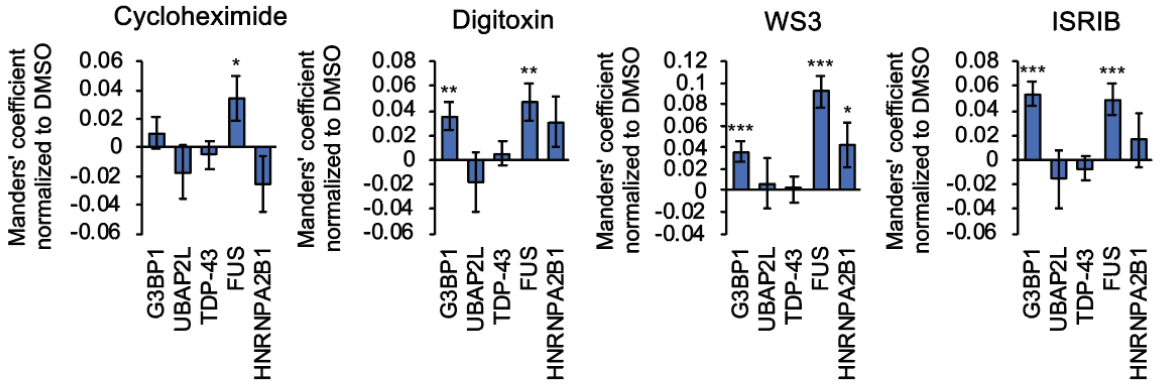

Figure 2.6.7: Histograms quantifying the change in co-localization of G3BP1-GFP SGs and immunofluorescence probing of G3BP1, UBAP2L, TDP-43, FUS, and HNRNPA2B1 in $NaAsO_2$ SG-enriched fractions, in the absence or presence of overnight incubation with 100 μM cycloheximide, digitoxin, WS3, or ISRIB. Histogram values are normalized to samples treated with the vehicle control DMSO. Significance levels are from two-tailed one sample Student's t-tests: * $p < 0.05$, ** $p < 0.01$, *** $p < 0.001$. Error bars are estimated standard error of the means from 18 biological replicates from two experimental replicates.

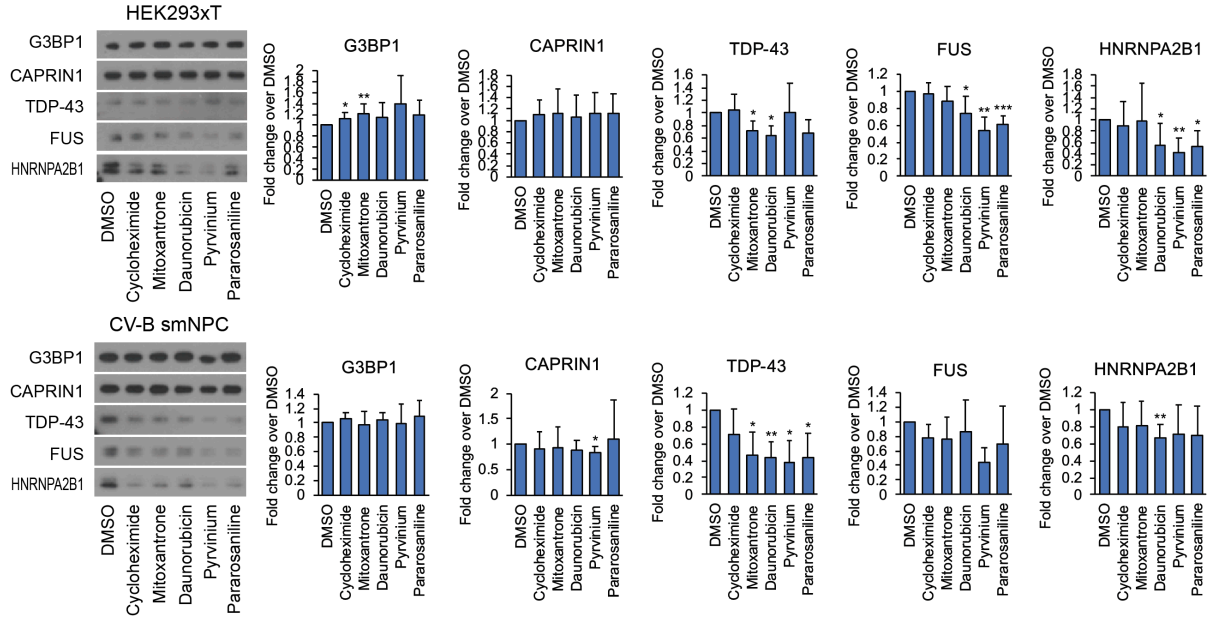

Figure 2.6.8: Representative Western blots and histograms quantifying the amounts of SG-associated proteins G3BP1 and CAPRIN1 as well as ALS-associated RBPs TDP-43, FUS, and HNRNPA2B1 in $NaAsO_2$ SG-enriched fractions after overnight incubation with 100 μM of one of five SG modifying compounds or vehicle control DMSO. Histogram values are normalized to samples treated with the vehicle control DMSO. Significance levels are from two-tailed one sample Student's t-tests: * $p < 0.05$, ** $p < 0.01$, *** $p < 0.001$. Error bars are sample standard deviations from at least three experimental replicates.

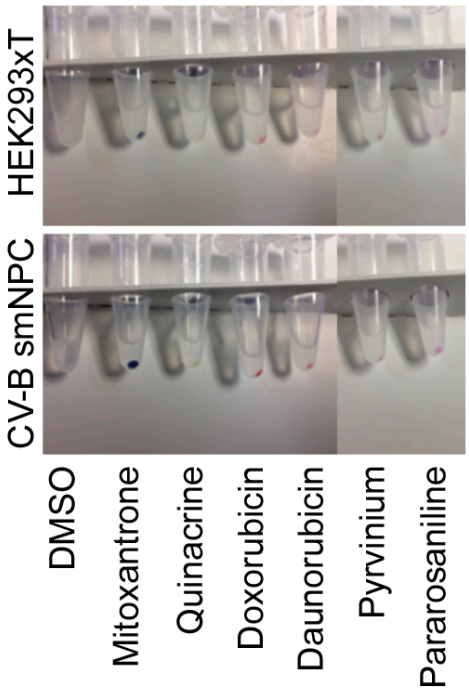

Figure 2.6.9: SG-enriched fractions after overnight incubation with nucleic acid intercalating compounds and SG pelleting by centrifugation.

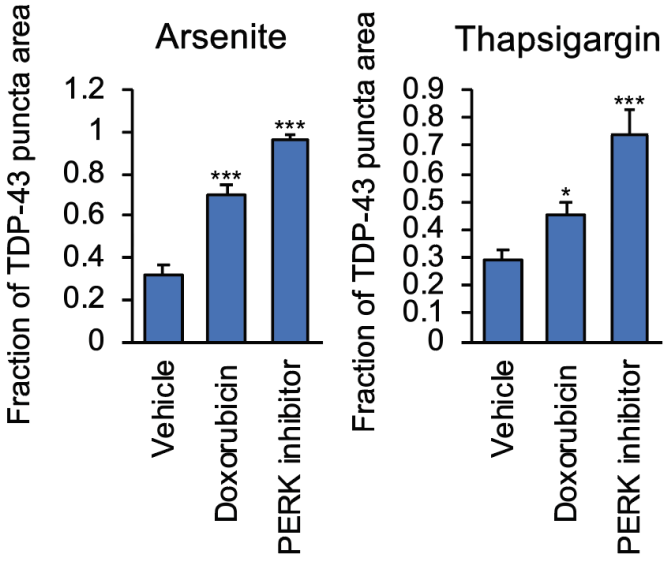

Figure 2.6.10: Histograms quantifying in Figure 2.6.5 the fraction of GFP-TDP-43ΔNLS foci (false colored red for consistency) that do not have G3BP1-mCherry (false colored green for consistency) co-localization in H4 cells transiently expressing G3BP1-mCherry and GFP-TDP-43ΔNLS and stressed with $NaAsO_2$ or thapsigargin, in the absence or presence of SG-modulating compounds. Significance levels are from two-tailed two sample Student's t-tests to vehicle control: * $p < 0.05$, *** $p < 0.001$. Error bars are estimated standard error of the means from $n \geq 25$ cells.

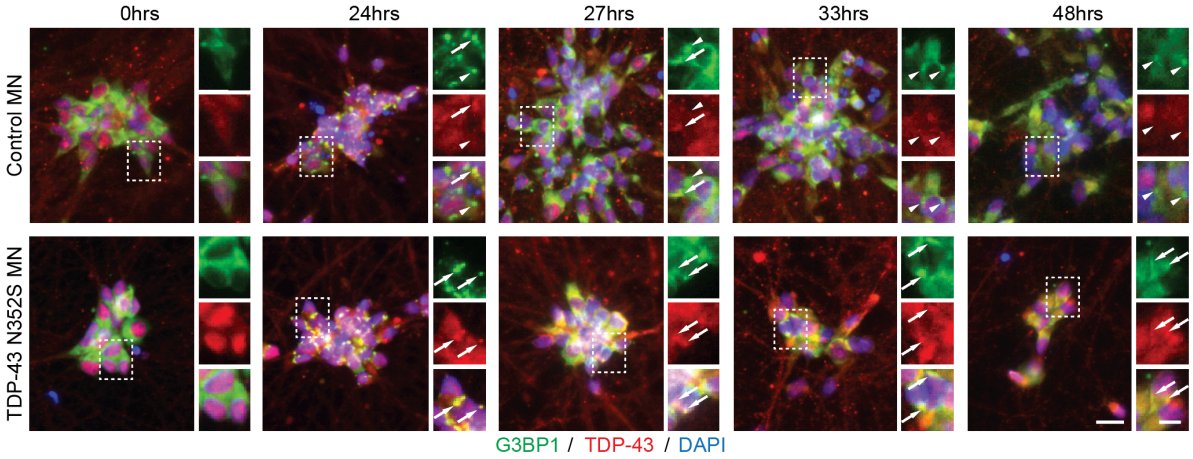

Figure 3.7.1: Representative wide-field fluorescence microscopy of iPS-MNs probed by immunofluorescence for G3BP1 and TDP-43 and stained with DAPI at several time points during puromycin stress and puromycin washout. Arrows denote co-localized G3BP1 SGs and TDP-43 puncta. Arrowheads denote G3BP1 SGs that are largely devoid of co-localized TDP-43. Scale bar is 20 μm (10 μm for insets). MN: motor neuron.

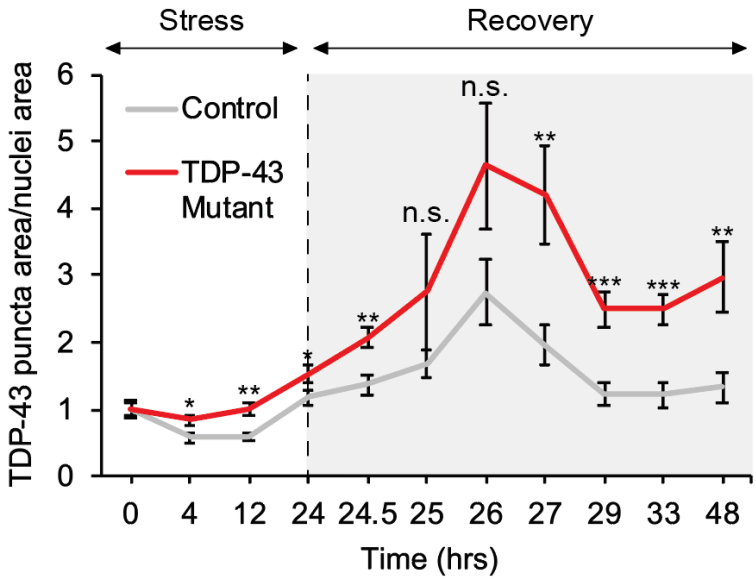

Figure 3.7.2: Scatterplot quantifying the formation in Figure 3.7.1 of cytoplasmic TDP-43 foci in iPS-MNs from individuals carrying ALS-associated mutations in *TARDBP* or control iPS-MNs. Scatterplot values are normalized to samples at the 0 hour time point. Significance levels are from two-tailed two sample Student's t-tests to control iPS-MNs: * $p < 0.05$, ** $p < 0.01$, *** $p < 0.001$. Error bars are estimated standard error of the means from five biological replicates of four control lines and four *TARDBP* mutant lines.

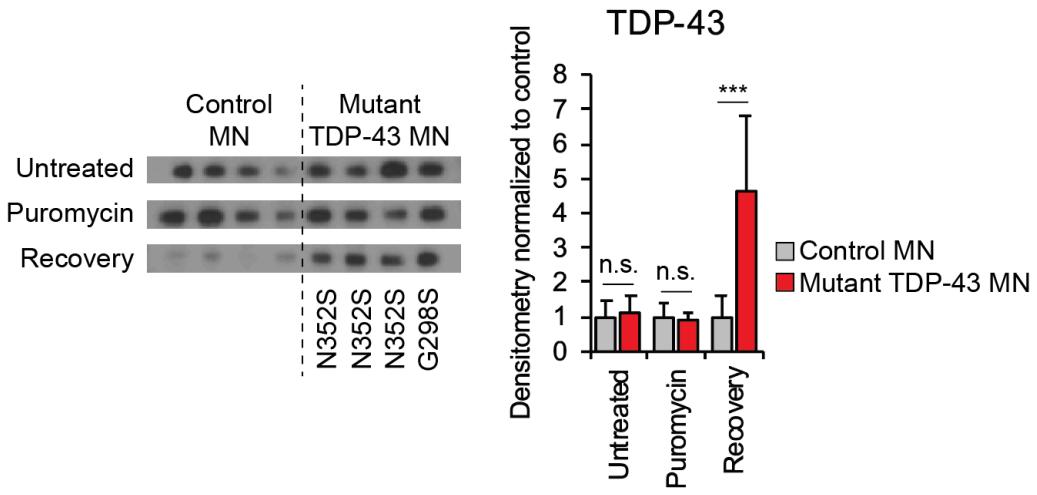

Figure 3.7.3: Representative Western blots and histogram quantifying the amount of TDP-43 in SG-enriched fractions isolated from *TARDBP* mutant or control iPS-MNs under no stress conditions, after 24 hours of puromycin stress, or after 24 hours of washout following 24 hours of puromycin stress. Histogram values are normalized to the control line samples. Significance levels are from two-tailed two sample Student's t-tests to control iPS-MNs: * $p < 0.05$. Error bars are sample standard deviations of three biological replicates across four control lines and four *TARDBP* mutant lines.

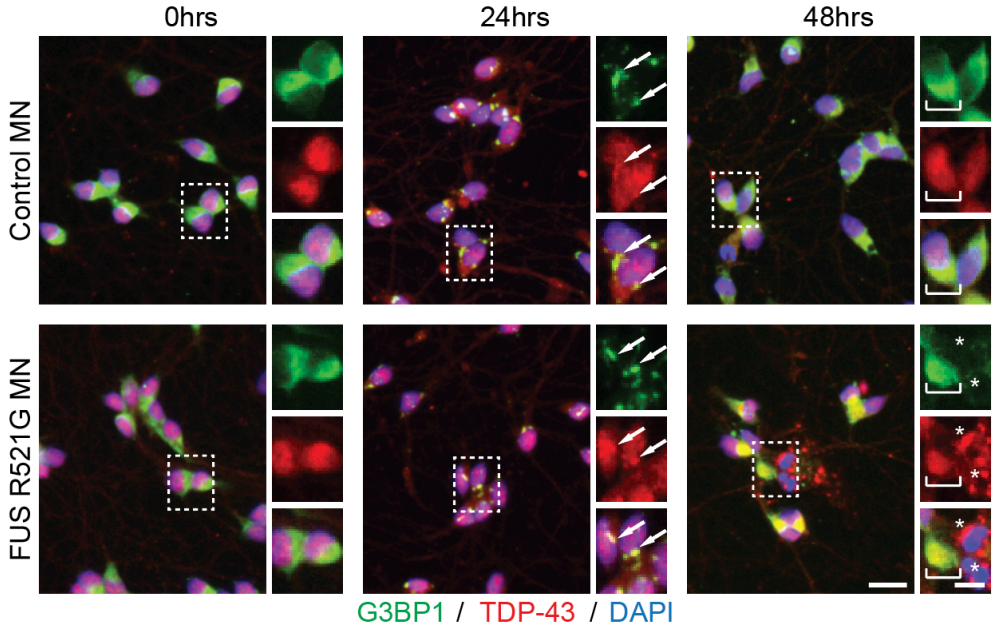

Figure 3.7.4: Representative wide-field fluorescence microscopy of iPS-MNs probed by immunofluorescence for G3BP1 and TDP-43 and stained with DAPI at several time points during puromycin stress and puromycin washout. Arrows denote co-localized G3BP1 SGs and TDP-43 puncta. Brackets denote broad regions of cytoplasmic TDP-43. Stars denote cytoplasmic TDP-43 puncta that are largely devoid of co-localized G3BP1. Scale bar is 20 μm (10 μm for insets).

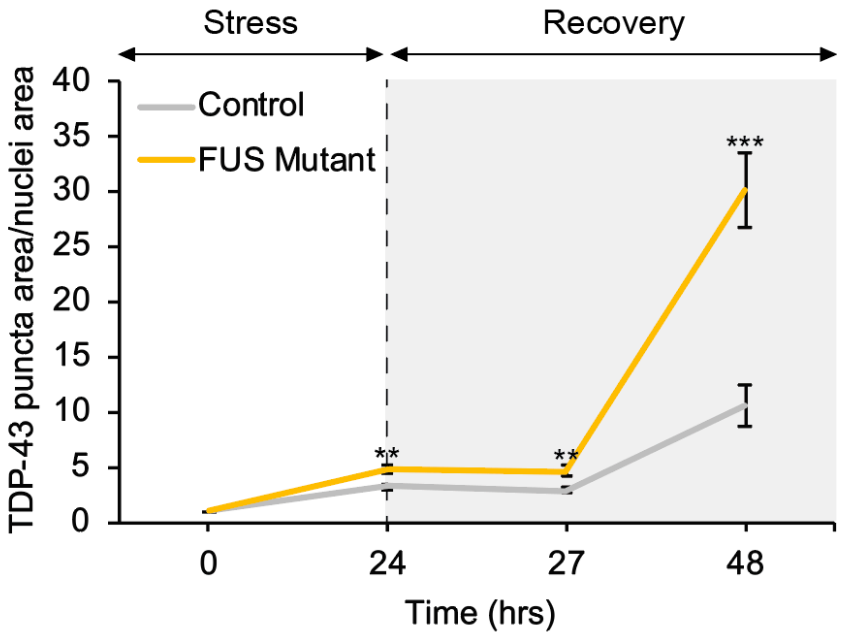

Figure 3.7.5: Scatterplot quantifying the formation in Figure 3.7.4 of cytoplasmic TDP-43 foci in iPS-MNs from individuals carrying ALS-associated mutations in *FUS* or control iPS-MNs. Scatterplot values are normalized to samples at the 0 hour time point. Significance levels are from two-tailed two sample Student's t-tests to control iPS-MNs: ** $p < 0.01$, *** $p < 0.001$. Error bars are estimated standard error of the means from five biological replicates of four control lines and two *FUS* mutant lines.

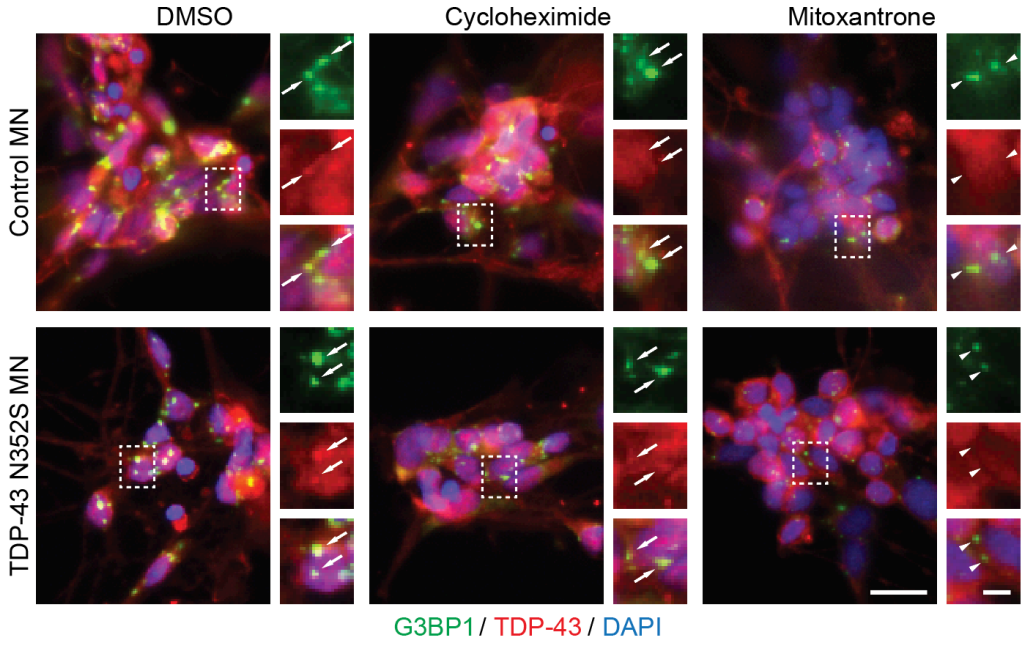

Figure 3.7.6: Representative wide-field fluorescence microscopy of iPS-MNs probed by immunofluorescence for G3BP1 and TDP-43 and stained with DAPI; iPS-MNs were incubated with SG-inhibiting compounds cycloheximide or mitoxantrone or DMSO control and stressed with puromycin. Arrows denote co-localized G3BP1 SGs and TDP-43 puncta. Arrowheads denote G3BP1 SGs that are largely devoid of co-localized TDP-43. Scale bar is 20 μm (5 μm for insets).

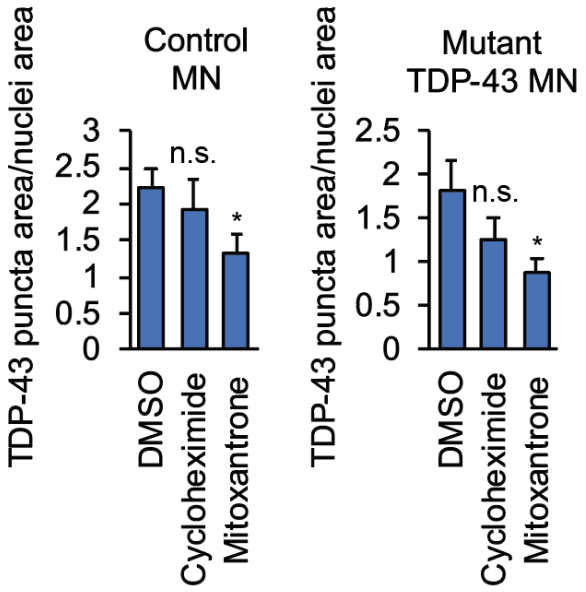

Figure 3.7.7: Histograms quantifying the formation in Figure 3.7.6 of cytoplasmic TDP-43 foci in iPS-MNs from individuals carrying ALS-associated mutations in *TARDBP,* or control iPS-MNs; cells were incubated with SG-inhibiting compounds cycloheximide or mitoxantrone or DMSO control and stressed with puromycin. Significance levels are from two-tailed two sample Student's t-tests to DMSO control: * $p < 0.05$. Error bars are estimated standard error of the means from five biological replicates of four control lines and four *TARDBP* mutant lines.

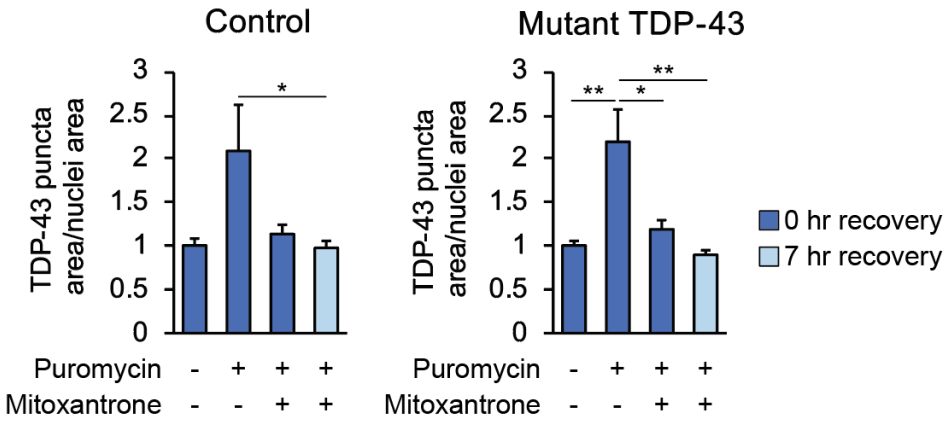

Figure 3.7.8: Histograms quantifying the formation of cytoplasmic TDP-43 foci in iPS-MNs from individuals carrying ALS-associated mutations in *TARDBP,* or control iPS-MNs; cells were incubated with the planar moiety-containing compound mitoxantrone or DMSO control in the absence or presence of puromycin stress. Significance levels are from two-tailed two sample Student's t-tests to unstressed, DMSO-treated control: * $p < 0.05$, ** $p < 0.01$. Error bars are estimated standard error of the means from 12 biological replicates of four control lines and four *TARDBP* mutant lines.

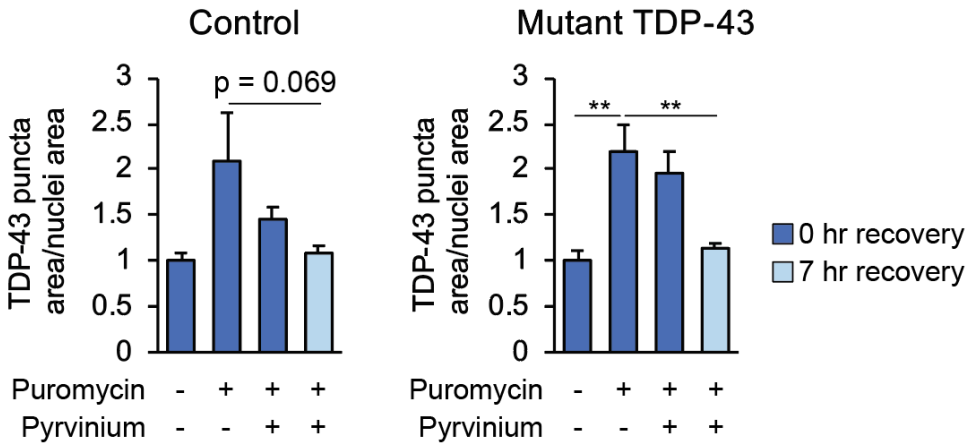

Figure 3.7.9: Histograms quantifying the formation of cytoplasmic TDP-43 foci in iPS-MNs from individuals carrying ALS-associated mutations in *TARDBP,* or control iPS-MNs; cells were incubated with the planar moiety-containing compound pyrvinium or DMSO control in the absence or presence of puromycin stress. Significance levels are from two-tailed two sample Student's t-tests to unstressed, DMSO-treated control: ** $p < 0.01$. Error bars are estimated standard error of the means from 12 biological replicates of four control lines and four *TARDBP* mutant lines. Unstressed, DMSO-treated and puromycin stressed, DMSO-treated controls are duplicated from Figure 3.7.8.

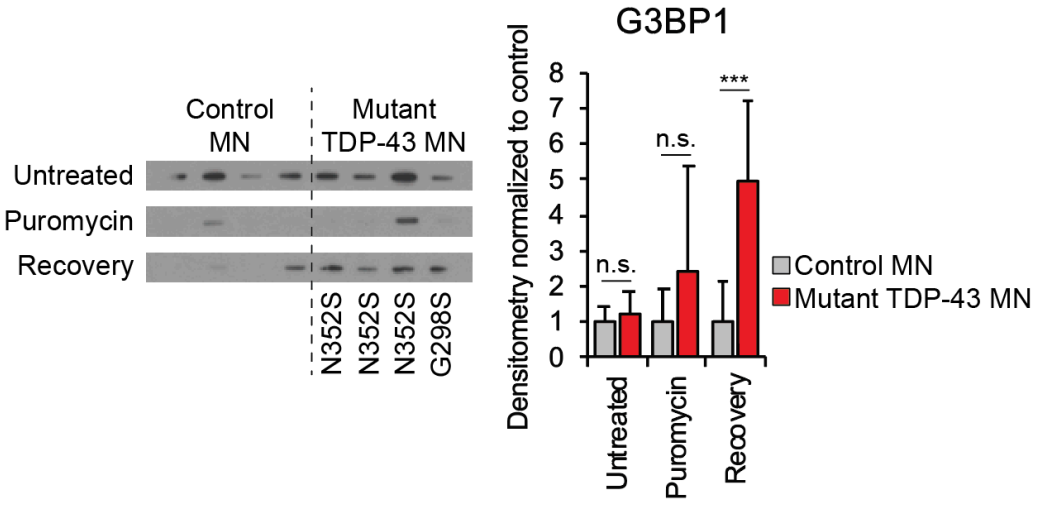

Figure 3.7.10: Representative Western blots and histogram quantifying the amount of G3BP1 in SG-enriched fractions isolated from TARDBP mutant or control iPS-MNs under no stress conditions, after 24 hours of puromycin stress, or after 24 hours of washout following 24 hours of puromycin stress. MN: motor neuron. Histogram values are normalized to the control line samples. Significance levels are from two-tailed two sample Student's t-tests to control iPS-MNs: * $p < 0.05$, ** $p < 0.01$, *** $p < 0.001$. Error bars are sample standard deviations from three biological replicates of control lines and four *TARDBP* mutant lines.

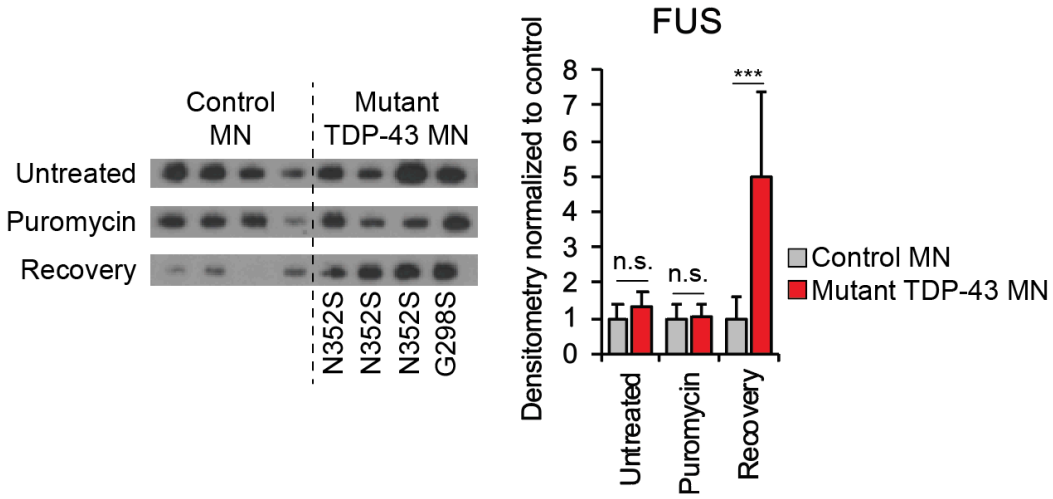

Figure 3.7.11: Representative Western blots and histogram quantifying the amount of FUS in SG-enriched fractions isolated from *TARDBP* mutant or control iPS-MNs under no stress conditions, after 24 hours of puromycin stress, or after 24 hours of washout following 24 hours of puromycin stress. Histogram values are normalized to the control line samples. Significance levels are from two-tailed two sample Student's t-tests to control iPS-MNs: * $p < 0.05$, ** $p < 0.01$, *** $p < 0.001$. Error bars are sample standard deviations from three biological replicates of control lines and four *TARDBP* mutant lines.

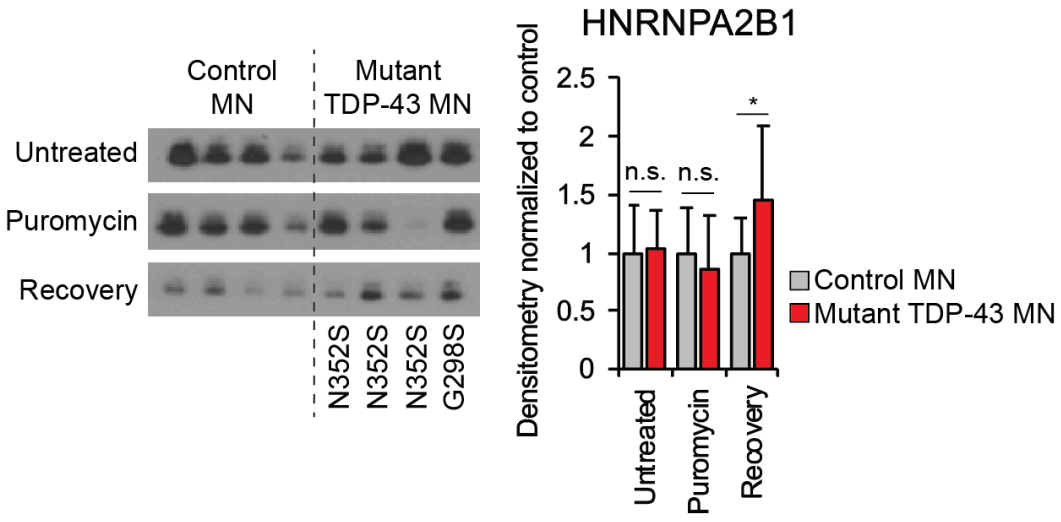

Figure 3.7.12: Representative Western blots and histogram quantifying the amount of HNRNPA2B1 in SG-enriched fractions isolated from *TARDBP* mutant or control iPS-MNs under no stress conditions, after 24 hours of puromycin stress, or after 24 hours of washout following 24 hours of puromycin stress. Histogram values are normalized to the control line samples. Significance levels are from two-tailed two sample Student's t-tests to control iPS-MNs: * $p < 0.05$, ** $p < 0.01$, *** $p < 0.001$. Error bars are sample standard deviations from three biological replicates of control lines and four *TARDBP* mutant lines.

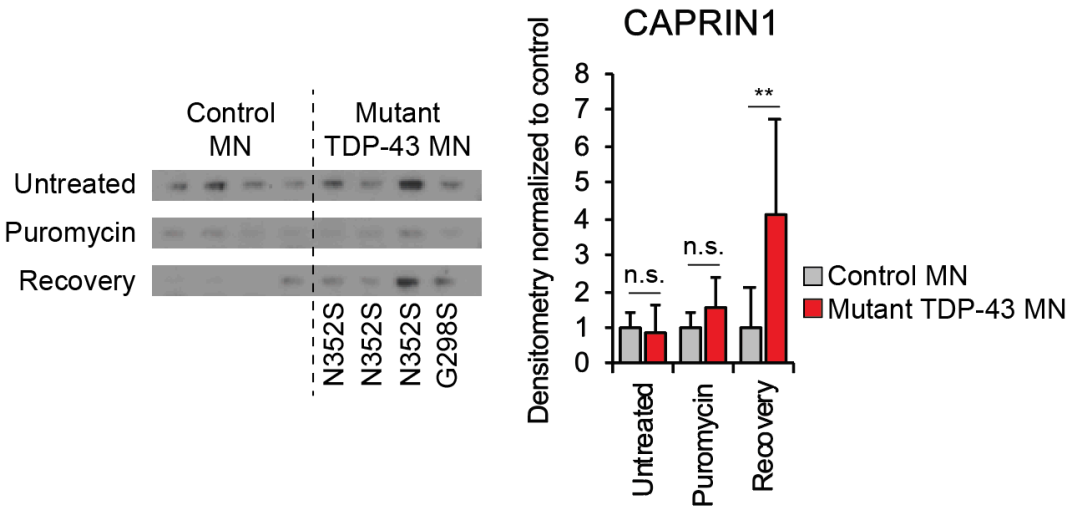

Figure 3.7.13: Representative Western blots and histogram quantifying the amount of CAPRIN1 in SG-enriched fractions isolated from *TARDBP* mutant or control iPS-MNs under no stress conditions, after 24 hours of puromycin stress, or after 24 hours of washout following 24 hours of puromycin stress. Histogram values are normalized to the control line samples. Significance levels are from two-tailed two sample Student's t-tests to control iPS-MNs: * $p < 0.05$, ** $p < 0.01$, *** $p < 0.001$. Error bars are sample standard deviations from three biological replicates of control lines and four *TARDBP* mutant lines.

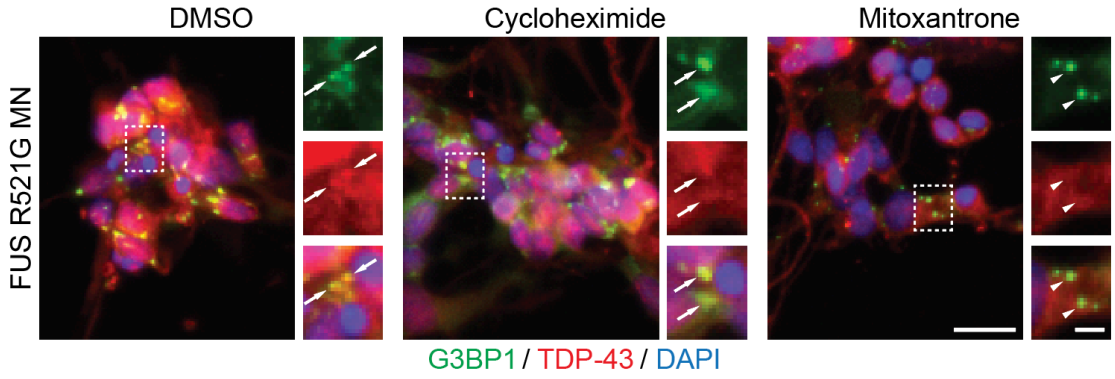

Figure 3.7.14: Representative wide-field fluorescence microscopy of iPS-MNs probed by immunofluorescence for G3BP1 and TDP-43 and stained with DAPI; iPS-MNs were incubated with SG inhibiting compounds cycloheximide or mitoxantrone or DMSO control and stressed with puromycin. Arrows denote co-localized G3BP1 SGs and TDP-43 puncta. Arrowheads denote G3BP1 SGs that are largely devoid of co-localized TDP-43. Scale bar is 20 μm (5 μm for insets).

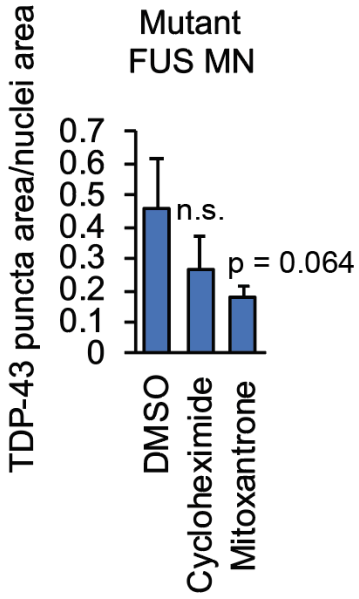

Figure 3.7.15: Histograms quantifying the formation in Figure 3.7.14 of cytoplasmic TDP-43 foci in iPS-MNs from individuals carrying ALS-associated mutations in *FUS* or control iPS-MNs; iPS-MNs were incubated with SG inhibiting compounds cycloheximide or mitoxantrone or DMSO control and stressed with puromycin. Significance levels are from two-tailed two sample Student's t-tests to DMSO control. Error bars are estimated standard error of the means from five biological replicates of four control lines and two *FUS* mutant lines.

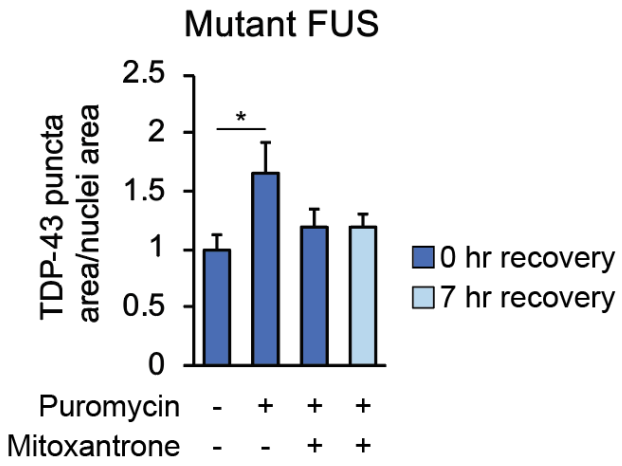

Figure 3.7.16: Histograms quantifying the formation of cytoplasmic TDP-43 foci in iPS-MNs from individuals carrying ALS-associated mutations in *FUS,* or control iPS-MNs; cells were incubated with the planar moiety-containing compound mitoxantrone or DMSO control in the absence or presence of puromycin stress. Significance levels are from two-tailed two sample Student's t-tests to unstressed, DMSO-treated control: * $p < 0.05$. Error bars are estimated standard error of the means from 12 biological replicates of four control lines and two *FUS* mutant lines.

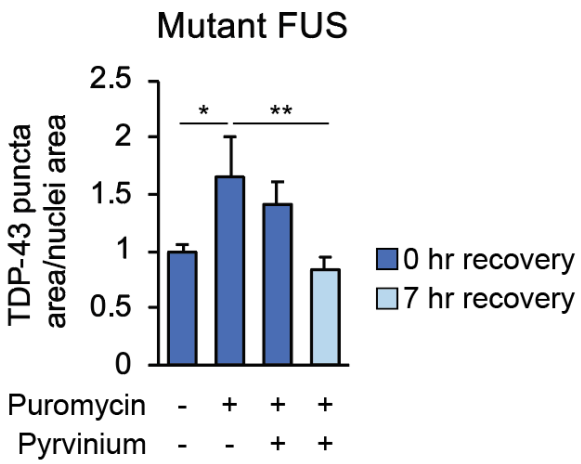

Figure 3.7.17: Histograms quantifying the formation of cytoplasmic TDP-43 foci in iPS-MNs from individuals carrying ALS-associated mutations in *FUS,* or control iPS-MNs; cells were incubated with the planar moiety-containing compound pyrvinium or DMSO control in the absence or presence of puromycin stress. Significance levels are from two-tailed two sample Student's t-tests to unstressed, DMSO-treated control: * $p < 0.05$, ** $p < 0.01$. Error bars are estimated standard error of the means from 12 biological replicates of four control lines and two *FUS* mutant lines. Unstressed, DMSO-treated and puromycin stressed, DMSO-treated controls are duplicated from Figure 3.7.16.

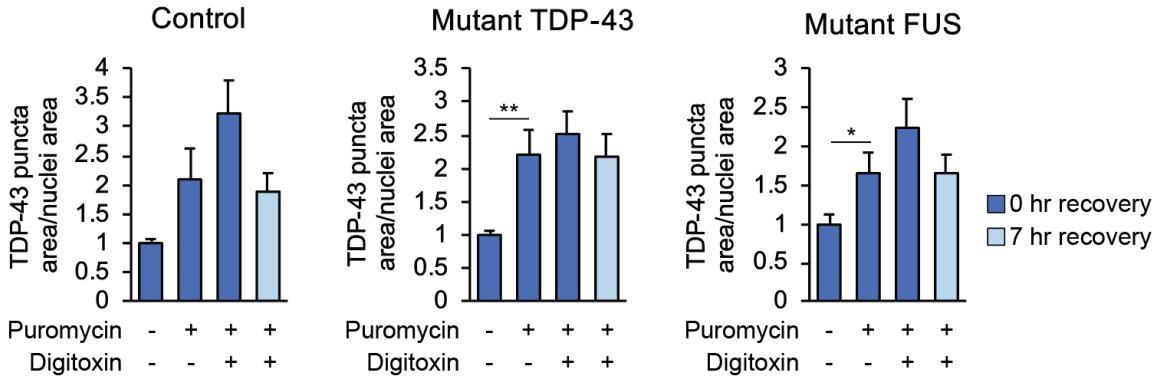

Figure 3.7.18: Histograms quantifying the formation of cytoplasmic TDP-43 foci in iPS-MNs from individuals carrying ALS-associated mutations in *TARDBP, FUS*, or control iPS-MNs; cells were incubated with digitoxin, a molecule which does not have extended planar moieties, or DMSO control in the absence or presence of puromycin stress. Significance levels are from two-tailed two sample Student's t-tests to unstressed, DMSO-treated control: * $p < 0.05$, ** $p < 0.01$. Error bars are estimated standard error of the means from 12 biological replicates of four control lines, four *TARDBP* mutant lines, and two *FUS* mutant lines. Unstressed, DMSO-treated and puromycin stressed, DMSO-treated controls are duplicated from Figures 3.7.8 and 3.7.16.

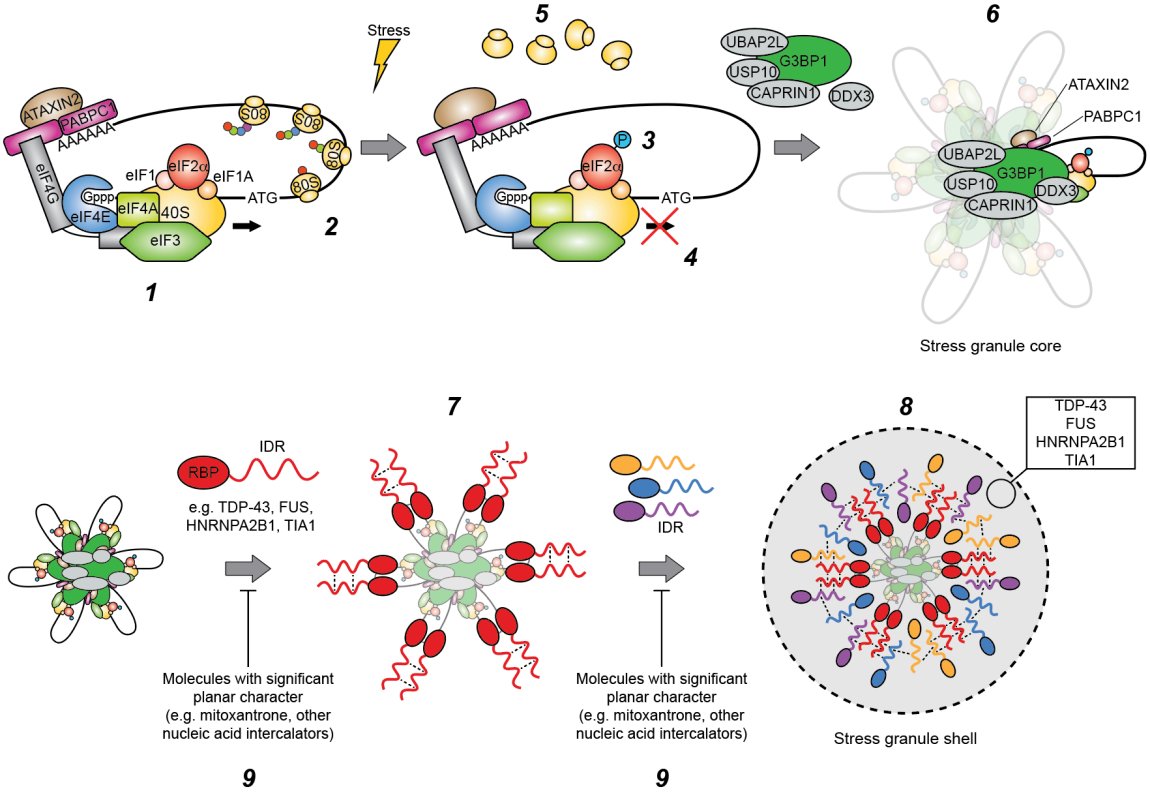

Figure 3.8.1: Under unstressed conditions, the 48S pre-initiation ribosome complex assembles on the 5' cap of actively translation mRNAs (1) and scans the 5' untranslated region for the start codon, upon which the full 80S ribosome assembles and translates the coding sequence (2). Following cellular stress such as exposure to $NaAsO_2$ or thapsigargin, stress-activated kinases phosphorylate eIF2α on serine 51 (3), freezing ribosomes at the 48S pre-initiation complex stage at the 5' cap (4). Elongating 80S ribosomes eventually fall off transcripts (5). Classical SG-associated RBPs such as G3BP1, TIA1, UBAP2L, USP10, CAPRIN1, and DDX3 can bind to the 40S ribosome subunit, the 5' or 3' untranslated regions, or G3BP1, and these proteins mediate assembly of several of these ribonucleoproteins into a core SG structure, possibly through a combination of protein-protein interactions via well-ordered protein domains as well as liquid-liquid phase separation interactions of the intrinsically disordered regions of these proteins (6). This core structure contains mRNA whose coding sequences may act as landing sites for the assembly of RBPs , including ALS-associated proteins such as TDP-43, FUS, and HNRNPA2B1 (7). The intrinsically disordered regions (IDR) of these RBPs may then further mediate assembly of other proteins with intrinsically disordered regions, which may or may not be RBPs, forming a shell SG structure (8). This shell structure may lead to a local high concentration of mutant protein in cells carrying mutations in the intrinsically disordered regions of ALS-associated proteins such as TDP-43, and may nucleate the formation of more insoluble and potentially cytotoxic aggregates. (9) SG screen hit compounds disrupt association of ALS-associated proteins with the SG shell, potentially reducing the nucleation and formation of insoluble protein aggregates.

Table 1.1.1: Enumerating the known cellular targets of SG-modulating compounds identified in the SG screen, corresponding to the table in Figure 1.2.4 and the pie charts of Figure 1.2.6. Related cellular targets have been grouped together and cellular target superclasses have been color-coded.

	MOLECULES WITH PLANAR MOIETIES, INTERACT WITH NUCLEIC ACIDS
	DNA methyltransferase
	DNA topoisomerase
	molcules with planar moieties
	PARylation
	INTERACT WITH PROTEIN INTRINSICALLY DISORDERED REGIONS
	LCD/PrLD
	ION CHANNELS, RECEPTORS, TRANSPORTERS
	adrenergic receptors (alpha1, alpha2)
	calcitriol receptor (vitamin D receptor)
	cannabinoid receptor (CB1)
	cholinergic receptors (muscarinic, nicotinic)
	dopamine receptors (D2, D3, D4)
	estrogen receptor
	G-protein-coupled estrogen receptor 1 (GPER)
	GABA-A receptor
	imidazoline receptors (I1, I2)
	Na+/Cl- cotransporter
	Na+/K+ ATPase
	OATP (OATP1B1 and OATP1B3)
	receptor tyrosine kinase
	SERCA
	serotonin receptors (5HT1A, 5HT2)
	serotonin reuptake transporter (SERT)
	transferrin receptor
	TRPV1
	voltage gated Na+ channels
	INTRACELLULAR SIGNALING, TRANSCRIPTION FACTORS
	adenylate cyclase
	Akt
	CK1alpha, Wnt
	DYRK
	FKBP12
	HIF-1 (hypoxia inducible factor-1)
	JAK-STAT
	JNK/SAPK, p38 MAPK, RACK1, MTK1
	NFkappaB
	PAK (p21 activated kinase)
	PGC1alpha
	PKC
	sirtuin1
	Zn2+ finger proteins
	LIPID MEMBRANES
	plasma membrane

Table 1.1.1: Enumerating the known cellular targets of SG-modulating compounds identified in the SG screen, corresponding to the table in Figure 1.2.4 and the pie charts of Figure 1.2.6. Related cellular targets have been grouped together and cellular target superclasses have been color-coded. (Continued.)

	INFLAMMATION
	COX1, COX2
	histamine N-methyltransferase
	histamine receptor (H1)
	myeloperoxidase
	phospholipase A2
	METABOLISM, RESPIRATION, REDOX
	aldehyde dehydrogenase
	autophagosome
	carbonic anhydrase
	dihydropteroate synthase
	dopamine beta hydroxylase
	electron transport chain
	glutathione reductase and GSH
	glycolytic enzymes
	Hsp60/chaperonin, Hsp90
	monoamine oxidase
	proteasome-chemotrypsin-like subunit
	pyruvate dehydrogenase
	reactive with thiols and amines
	SOD2 (Mn2+ dependent SOD)
	CYTOSKELETON
	microfilaments
	microtubules
	TRANSLATION
	PERK
	ribosome
	UNKNOWN TARGET

Table 1.1.2: Enumerating SG-modulating compounds identified in HEK293xT cells, color-coded by cellular target superclasses as in Table 1.1.1.

	DECREASED SG AREA/NUCLEI AREA	MECHANISM OF ACTION
	acriflavine hydrochloride	molecule with planar moieties and interferes with transcription and DNA replication; may bind to HIF-1 (hypoxia inducible factor-1)
	bergaptene	psoralen derivative that is molecule with planar moieties
	dihydrocelastrol	the derivative of celastrol, which is a triterpenoid that may modulate: p38 pathway; inhibit Hsp90; proteasome chymotrypsin-like activity; NFkappaB; PARylation
	mitoxantrone	induces phosphorylation of PERK at threonine 980 leading to eIF2alpha phosphorylation (ER stress inducer), DNA topoisomerase II inhibitor, DNA synthesis inhibitor, molecule with planar moieties
	pararosaniline	2 molecules: pararosaniline has antihelminthic activity, pamoate may be counter ion for many drugs, pararosanline is molecule with planar moieties
	pyrvinium pamoate	binds to and potentiates CK1alpha, inhibiting Wnt signaling, molecule with planar moieties
	quinacrine	binds to prion protein and inhibits aggregation, MAO inhibitor, inhibits Nf-kappa beta, activates p53 (intercalating agent), inhibits histamine N methyltransferase, intercalates, inhibits phospholipase A2
	chlorothiazide	blocks Na+/Cl- cotransporter (e.g. distal convoluted tubule), carbonic anhydrase inhibitor
	chukrasin	may inhibit the organic anion transport peptide (OATP1B1 and OATP1B3)
	digitoxin	inhibits Na+/K+ ATPase
	digoxin	inhibits Na+/K+ ATPase
	gambogic acid	binds to transferrin receptor, inhibits NFkappaB; inhibits cell proliferation and inhibits telomerase upregulation of human lung carcinoma cell line
	gitoxigenin	inhibits Na+/K+ ATPase
	lanatoside C	inhibits Na+/K+ ATPase
	ouabain	inhibits Na+/K+ ATPase
	peruvoside	inhibits Na+/K+ ATPase
	proscillaridin	inhibits Na+/K+ ATPase
	strophanthidinic acid lactone	inhibits Na+/K+ ATPase
	strophantidin	inhibits Na+/K+ ATPase
	adenylate cyclase inhib (NKH477)	forskolin derivative that activates adenylate cyclase and increases intracellular cAMP
	chrysanthellin A	saponin (therefore probably surfactant in the class of digitonin)
	digitonin	amphipathic detergent that selectively breaks up cholesterol rich lipid rafts
	gramicidin S	forms pores in lipid membrane that allow monovalent but not divalent cations and not anions through
	phenylmercuric acetate	thought to prevent stomata closing by inhibiting solute transport to stomata guard cells, thereby inhibiting osmotic-turgidity
	oxyphenbutazone	inhibits cyclooxygenase (COX)
	dapsone	inhibits bacterial dihydropteroate synthase which produces dihydrofolate; inhibits myeloperoxidase
	disulfiram	competitive inhibitor of aldehyde dehydrogenase; research on inhibition of dopamine beta hydroxylase; research on binding to Zn2+ finger peptides in Giardia; research on reducing PTEN protein levels in some cells
	sumatrol acetate	structurally very similar to rotenone
	chelidonine (+)	inhibits IPP complex which connects integrins to actin cytoskeleton; activates p38 and inhibits JAK-STAT and Akt signaling
	fenbendazole	benzimidazole class antihelminthic that binds to microtubules (same place as colchicine) and inhibit assembly
	mebendazole	benzimidazole class antihelminthic that binds to microtubules (same place as colchicine) and inhibit assembly
	podophyllotoxin	structural derivative of etoposide but whereas etoposide binds to DNA topoisomerase + DNA in a ternary complex, podophyllotoxin destabilizes microtubules; podophyllotoxin may bind to HSP60 a chaperonin
	prieurianin	aka endocidin 1, inhibits actin filament severing and depolymerization and inhibits endocytosis
	vinblastine sulfate	vinca alkaloid that binds to tubulin and inhibits microtubule assembly
	vincristine sulfate	vinca alkaloid that binds to tubulin and inhibits microtubule assembly
	WS3	inhibits ebp1/pa2g4, which regulates Rb and E2F, as well as being a dsRBP, a component of RNPs, associates with ribosomes, inhibits eIF2alpha ser51 phos, and can be phosphorylated by PKR
	neomycin sulfate	part of family of aminoglycoside antibiotics that block bacterial protein synthesis and can also disrupt bacterial membrane
	CA61	(unknown mechanism of action)
	ST1	(unknown mechanism of action)

Table 1.1.2: Enumerating SG-modulating compounds identified in HEK293xT cells, color-coded by cellular target superclasses as in Table 1.1.1. (Continued.)

	DECREASED SG AREA/NUCLEI AREA	**MECHANISM OF ACTION**
	ST23	(unknown mechanism of action)
	INCREASED SG AREA/NUCLEI AREA	**MECHANISM OF ACTION**
	CA81	(unknown mechanism of action)
	DECREASED SG COUNT/NUCLEI AREA	**MECHANISM OF ACTION**
	acriflavine hydrochloride	molecule with planar moieties and interferes with transcription and DNA replication; may bind to HIF-1 (hypoxia inducible factor-1)
	mitoxantrone hydrochloride	induces phosphorylation of PERK at threonine 980 leading to eIF2alpha phosphorylation (ER stress inducer), DNA topoisomerase II inhibitor, DNA synthesis inhibitor, molecule with planar moieties
	pararosaniline pamoate	2 molecules: pararosaniline has antihelminthic activity, pamoate may be counter ion for many drugs, pararosanline is molecule with planar moieties
	pyrvinium pamoate	binds to and potentiates CK1alpha, inhibiting Wnt signaling, molecule with planar moieties
	chlorothiazide (hydrochlorothiazide)	blocks Na+/Cl- cotransporter (e.g. distal convoluted tubule), carbonic anhydrase inhibitor
	digitoxin	inhibits Na+/K+ ATPase
	digoxin	inhibits Na+/K+ ATPase
	gitoxigenin diacetate	inhibits Na+/K+ ATPase
	lanatoside C	inhibits Na+/K+ ATPase
	ouabain (dihydroouabain, g strophanthin)	inhibits Na+/K+ ATPase
	peruvoside	inhibits Na+/K+ ATPase
	proscillaridin A	inhibits Na+/K+ ATPase
	strophanthidinic acid lactone acetate	inhibits Na+/K+ ATPase
	strophantidin (k strophanthidin)	inhibits Na+/K+ ATPase
	digitonin	amphipathic detergent that selectively breaks up cholesterol rich lipid rafts
	gramicidin S? or D? (mixture of A, B, and C is called D)	forms pores in lipid membrane that allow monovalent but not divalent cations and not anions through
	oxyphenbutazone	inhibits cyclooxygenase (COX)
	disulfiram	competitive inhibitor of aldehyde dehydrogenase; research on inhibition of dopamine beta hydroxylase; research on binding to Zn2+ finger peptides in Giardia; research on reducing PTEN protein levels in some cells
	thimerosal	organomercury compound with ethylmercury moiety that can bind thiols and amines (oligodynamic effect)
	fenbendazole	benzimidazole class antihelminthic that binds to microtubules (same place as colchicine) and inhibit assembly
	vinblastine sulfate	vinca alkaloid that binds to tubulin and inhibits microtubule assembly
	WS3	inhibits ebp1/pa2g4, which regulates Rb and E2F, as well as being a dsRBP, a component of RNPs, associates with ribosomes, inhibits eIF2alpha ser51 phos, and can be phosphorylated by PKR
	neomycin sulfate	part of family of aminoglycoside antibiotics that block bacterial protein synthesis and can also disrupt bacterial membrane
	ST1	(unknown mechanism of action)
	INCREASED SG COUNT/NUCLEI AREA	**MECHANISM OF ACTION**
	doxorubicin	molecule with planar moieties that intercalates DNA and inhibits DNA replication and DNA topoisomerase II
	epirubicin hydrochloride	molecule with planar moieties that intercalates DNA and inhibits DNA replication and DNA topoisomerase II
	nocodazole	benzimidazole antineoplastic that binds to microtubules and inhibit assembly; also inhibits Wnt driven cell proliferation by increasing expression of LATS2 which blocks beta catenin binding to BCL9
	SD22	(unknown mechanism of action)
	DECREASED AVERAGE SG SIZE	**MECHANISM OF ACTION**
	acriflavine hydrochloride	molecule with planar moieties and interferes with transcription and DNA replication; may bind to HIF-1 (hypoxia inducible factor-1)
	acrisorcin	2 molecules: 9-aminoacridine (structurally similar to acriflavine) that is molecule with planar moieties and can intercalate, hexylresorcinol inhibits NfkappaB phosphorylation and may act as weak estrogen mimic
	dactinomycin	inhibits elongation of RNA polymerase, intercalating
	daunorubicin	molecule with planar moieties; intercalates DNA and inhibits DNA replication, inhibits DNA topoisomerase II, and promotes histone eviction thereby altering transcription
	doxorubicin	molecule with planar moieties that intercalates DNA and inhibits DNA replication and DNA topoisomerase II

Table 1.1.2: Enumerating SG-modulating compounds identified in HEK293xT cells, color-coded by cellular target superclasses as in Table 1.1.1. (Continued.)

	DECREASED AVERAGE SG SIZE	**MECHANISM OF ACTION**
	epirubicin hydrochloride	molecule with planar moieties that intercalates DNA and inhibits DNA replication and DNA topoisomerase II
	mitoxantrone hydrochloride	induces phosphorylation of PERK at threonine 980 leading to eIF2alpha phosphorylation (ER stress inducer), DNA topoisomerase II inhibitor, DNA synthesis inhibitor, molecule with planar moieties
	pararosaniline pamoate	2 molecules: pararosaniline has antihelminthic activity, pamoate may be counter ion for many drugs, pararosanline is molecule with planar moieties
	pyrvinium pamoate	binds to and potentiates CK1alpha, inhibiting Wnt signaling, molecule with planar moieties
	sennoside A	may increase fluid secretion and contraction of large intestine; structural derivative of anthraquinone which is molecule with planar moieties and which can inhibit Tau aggregation and dissolve paired helical filaments in vitro and in cells
	tilorone	molecule with planar moieties; induces interferon production; may induce expression of BMP-7 in BMP signaling
	quinacrine	binds to prion protein and inhibits aggregation, MAO inhibitor, inhibits Nf-kappa beta, activates p53 (intercalating agent), inhibits histamine N methyltransferase, intercalates, inhibits phospholipase A2
	cholecalciferol/vitamin D3	activates calcitriol receptor/vitamine D receptor
	digitoxin	inhibits Na+/K+ ATPase
	metaxalone	general CNS depression (no specific MOA reported in literature)
	penfluridol	diphenylbutylpiperidine that blocks D2 receptors
	proscillaridin A	inhibits Na+/K+ ATPase
	forskolin/coleoforsin	activates adenylyl cyclase
	rapamycin	inhibits mTORC1 by binding to FKBP12
	gramicidin S? or D? (mixture of A, B, and C is called D)	forms pores in lipid membrane that allow monovalent but not divalent cations and not anions through
	albendazole	benzimidazole class antihelminthic that binds to microtubules (same place as colchicine) and inhibit assembly
	colchicine	binds to tubulin and inhibits microtubule assembly; can also inhibit neutrophil motility
	fenbendazole	benzimidazole class antihelminthic that binds to microtubules (same place as colchicine) and inhibit assembly
	mebendazole	benzimidazole class antihelminthic that binds to microtubules (same place as colchicine) and inhibit assembly
	nocodazole	benzimidazole antineoplastic that binds to microtubules and inhibit assembly; also inhibits Wnt driven cell proliferation by increasing expression of LATS2 which blocks beta catenin binding to BCL9
	paclitaxel	inhibits tubulin disassembly
	podophyllotoxin	structural derivative of etoposide but whereas etoposide binds to DNA topoisomerase + DNA in a ternary complex, podophyllotoxin destabilizes microtubules; podophyllotoxin may bind to HSP60 a chaperonin
	vinblastine sulfate	vinca alkaloid that binds to tubulin and inhibits microtubule assembly
	vincristine sulfate	vinca alkaloid that binds to tubulin and inhibits microtubule assembly
	azacitidine	chemical analog of cytidine; suicide inhibitor of DNA methyltransferase at low doses after getting incorporated into DNA; at higher doses gets incorporated into RNA and promotes polysome disassembly, inhibition of methylation, and translational inhibition
	WS3	inhibits ebp1/pa2g4, which regulates Rb and E2F, as well as being a dsRBP, a component of RNPs, associates with ribosomes, inhibits eIF2alpha ser51 phos, and can be phosphorylated by PKR
	CA61	(unknown mechanism of action)
	INCREASED AVERAGE SG SIZE	**MECHANISM OF ACTION**
	mebeverine hydrochloride	muscarinic cholinergic receptor antagonist; may prevent calcium store replenishment
	thiram	in human skin fibroblasts and yeast, inhibits glutathione reductase and depletes glutathione (GSH) by being reduced at its disulfide bridge and subsequently reoxidized (in yeast by cytochrome c), thereby disrupting cellular respiration and inducing lipid peroxidation (in human cells); at low doses inhibits pyruvate dehydrogenation

Table 1.1.3: Enumerating SG-modulating compounds identified in CV-B small molecule neural precursor cells, color-coded by cellular target superclasses as in Table 1.1.1.

	DECREASED SG AREA/NUCLEI AREA	**MECHANISM OF ACTION**
	8 hydroxyquinoline	chelating agent, stabilizes hydrogen peroxide, transcription inhibitor
	acriflavine hydrochloride	molecule with planar moieties and interferes with transcription and DNA replication; may bind to HIF-1 (hypoxia inducible factor-1)
	actinomycin D	inhibits elongation of RNA polymerase, intercalating
	alexidine hydrochloride	biguanide-containing antimicrobial; related biguanide-containing antimicrobials bind to negatively charged membranes and disrupt the membrane and also bind bacterial DNA and alter transcription
	ethopropazine hydrochloride	phenothiazine derivative that may intercalate RNA (note that methylene blue is a phenothiazine derivative though ethopropazine is not quite as planar); has anticholinergic/antimuscarinic, antihistamine, antiadrenergic effects
	mitoxantrone	induces phosphorylation of PERK at threonine 980 leading to eIF2alpha phosphorylation (ER stress inducer), DNA topoisomerase II inhibitor, DNA synthesis inhibitor, molecule with planar moieties
	pararosaniline	2 molecules: pararosaniline has antihelminthic activity, pamoate may be counter ion for many drugs, pararosanline is molecule with planar moieties
	trimeprazine tartrate	phenothiazine derivative; has antihistamine activity
	quinacrine	binds to prion protein and inhibits aggregation, MAO inhibitor, inhibits Nf-kappa beta, activates p53 (intercalating agent), inhibits histamine N methyltransferase, intercalates
	digitoxin	inhibits Na+/K+ ATPase
	ivermectin	potentiates GABA-A receptor
	lanatoside C	inhibits Na+/K+ ATPase
	ouabain	inhibits Na+/K+ ATPase
	penfluridol	diphenylbutylpiperidine that blocks D2 receptors
	proscillaridin	inhibits Na+/K+ ATPase
	suloctidil	inhibits platelet aggregation; may inhibit Na/K ATPase and increase membrane fluidity by binding to acidic phospholipids (e.g. phosphatidylinositol, which are slightly negatively charged)
	tyrphostin A9	receptor tyrosine kinase inhibitor (selective for PDGFR)
	benzalkonium chloride	quaternary ammonium cationic surfactant
	benzethonium chloride	quaternary ammonium cationic surfactant; may have nicotinic and muscarinic anticholinergic activity; may cause loss of mitochondrial membrane potential and incr cytosolic Ca
	tomatine	precipitates cholesterol and disrupts membranes (structurally similar to digitonin), immune adjuvant
	oxyphenbutazone	inhibits cyclooxygenase (COX)
	paclitaxel	inhibits tubulin disassembly
	anisomycin	strongly activates JNK/SAPK and p38 MAPK, inhibits peptidyltransferase of 80S ribosome, at high concentration can inhibit DNA synthesis
	WS3	inhibits ebp1/pa2g4, which regulates Rb and E2F, as well as being a dsRBP, a component of RNPs, associates with ribosomes, inhibits eIF2alpha ser51 phos, and can be phosphorylated by PKR
	A538	(unknown mechanism of action)
	CA4	(unknown mechanism of action)
	ST1	(unknown mechanism of action)
	INCREASED SG AREA/NUCLEI AREA	**MECHANISM OF ACTION**
	doxorubicin	molecule with planar moieties that intercalates DNA and inhibits DNA replication and DNA topoisomerase II
	epirubicin hydrochloride	molecule with planar moieties that intercalates DNA and inhibits DNA replication and DNA topoisomerase II
	buspirone	serotonin 5HT1A receptor agonist; presynaptic dopamine antagonist for D2, D3, D4 receptors; partial alpha1 adrenergic receptor agonist
	e-capsaicin	binds to TRPV1 (vanilloid receptor subtype 1) ion channel to allow cations to enter neuron, depolarizing the neuron; TRPV1 can be opened by capsaicin, temperature, protons, and physical abrasion; depletes substance P which transmits pain sensation; neurotoxic
	estriol benzyle ether	estriol derivative
	idazoxan	inhibits both alpha2 adrenergic receptor and I1 imidazoline receptors while activating I2 imidazoline receptors (note that benzimidazoles bind to tubulin; perhaps this molecule can also weakly bind to tubulin?)
	cetrimonium bromide	quaternary ammonium cationic surfactant

Table 1.1.3: Enumerating SG-modulating compounds identified in CV-B small molecule neural precursor cells, color-coded by cellular target superclasses as in Table 1.1.1. (Continued.)

	INCREASED SG AREA/NUCLEI AREA	**MECHANISM OF ACTION**
	phenylmercuric acetate	thought to prevent stomata closing by inhibiting solute transport to stomata guard cells, thereby inhibiting osmotic-turgidity
	albendazole	benzimidazole class antihelminthic that binds to microtubules (same place as colchicine) and inhibit assembly
	colchicine	binds to tubulin and inhibits microtubule assembly; can also inhibit neutrophil motility
	mebendazole	benzimidazole class antihelminthic that binds to microtubules (same place as colchicine) and inhibit assembly
	podophyllotoxin	structural derivative of etoposide but whereas etoposide binds to DNA topoisomerase + DNA in a ternary complex, podophyllotoxin destabilizes microtubules; podophyllotoxin may bind to HSP60 a chaperonin
	vinblastine sulfate	vinca alkaloid that binds to tubulin and inhibits microtubule assembly
	gentamicin sulfate	part of family of aminoglycoside antibiotics that block bacterial protein synthesis and can also disrupt bacterial membrane
	SD28	(unknown mechanism of action)
	DECREASED SG COUNT/NUCLEI AREA	**MECHANISM OF ACTION**
	acriflavine hydrochloride	molecule with planar moieties and interferes with transcription and DNA replication; may bind to HIF-1 (hypoxia inducible factor-1)
	dactinomycin	inhibits elongation of RNA polymerase, intercalating
	mitoxantrone hydrochloride	induces phosphorylation of PERK at threonine 980 leading to eIF2alpha phosphorylation (ER stress inducer), DNA topoisomerase II inhibitor, DNA synthesis inhibitor, molecule with planar moieties
	oxyquinoline sulfate (8 hydroxyquinoline)	chelating agent, stabilizes hydrogen peroxide, transcription inhibitor
	pararosaniline pamoate	2 molecules: pararosaniline has antihelminthic activity, pamoate may be counter ion for many drugs, pararosanline is molecule with planar moieties
	quinacrine	binds to prion protein and inhibits aggregation, MAO inhibitor, inhibits Nf-kappa beta, activates p53 (intercalating agent), inhibits histamine N methyltransferase, intercalates
	digitoxin	inhibits Na+/K+ ATPase
	lanatoside C	inhibits Na+/K+ ATPase
	ouabain (dihydroouabain, g strophanthin)	inhibits Na+/K+ ATPase
	penfluridol	diphenylbutylpiperidine that blocks D2 receptors
	proscillaridin A	inhibits Na+/K+ ATPase
	suloctidil	inhibits platelet aggregation; may inhibit Na/K ATPase and increase membrane fluidity by binding to acidic phospholipids (e.g. phosphatidylinositol, which are slightly negatively charged)
	tyrphostin A9	receptor tyrosine kinase inhibitor (selective for PDGFR)
	benzalkonium chloride	quaternary ammonium cationic surfactant
	benzethonium chloride	quaternary ammonium cationic surfactant; may have nicotinic and muscarinic anticholinergic activity; may cause loss of mitochondrial membrane potential and incr cytosolic Ca
	chrysanthellin A	saponin (therefore probably surfactant in the class of digitonin)
	oxyphenbutazone	inhibits cyclooxygenase (COX)
	paclitaxel	inhibits tubulin disassembly
	roxithromycin	macrolide class antibiotic that binds to and inhibits 50S ribosome in bacteria
	A538	(unknown mechanism of action)
	CA4	(unknown mechanism of action)
	INCREASED SG COUNT/NUCLEI AREA	**MECHANISM OF ACTION**
	daunorubicin	molecule with planar moieties; intercalates DNA and inhibits DNA replication, inhibits DNA topoisomerase II, and promotes histone eviction thereby altering transcription
	doxorubicin	molecule with planar moieties that intercalates DNA and inhibits DNA replication and DNA topoisomerase II
	epirubicin hydrochloride	molecule with planar moieties that intercalates DNA and inhibits DNA replication and DNA topoisomerase II
	buspirone	serotonin 5HT1A receptor agonist; presynaptic dopamine antagonist for D2, D3, D4 receptors; partial alpha1 adrenergic receptor agonist
	albendazole	benzimidazole class antihelminthic that binds to microtubules (same place as colchicine) and inhibit assembly
	mebendazole	benzimidazole class antihelminthic that binds to microtubules (same place as colchicine) and inhibit assembly

Table 1.1.3: Enumerating SG-modulating compounds identified in CV-B small molecule neural precursor cells, color-coded by cellular target superclasses as in Table 1.1.1. (Continued.)

	INCREASED SG COUNT/NUCLEI AREA	**MECHANISM OF ACTION**
	vinblastine sulfate	vinca alkaloid that binds to tubulin and inhibits microtubule assembly
	vincristine sulfate	vinca alkaloid that binds to tubulin and inhibits microtubule assembly
	SD28	(unknown mechanism of action)
	DECREASED AVERAGE SG SIZE	**MECHANISM OF ACTION**
	acriflavine hydrochloride	molecule with planar moieties and interferes with transcription and DNA replication; may bind to HIF-1 (hypoxia inducible factor-1)
	dactinomycin	inhibits elongation of RNA polymerase, intercalating
	daunorubicin	molecule with planar moieties; intercalates DNA and inhibits DNA replication, inhibits DNA topoisomerase II, and promotes histone eviction thereby altering transcription
	doxorubicin	molecule with planar moieties that intercalates DNA and inhibits DNA replication and DNA topoisomerase II
	idarubicin	molecule with planar moieties; intercalates DNA and inhibits DNA replication, inhibits DNA topoisomerase II, and promotes histone eviction thereby altering transcription
	mitoxantrone hydrochloride	induces phosphorylation of PERK at threonine 980 leading to eIF2alpha phosphorylation (ER stress inducer), DNA topoisomerase II inhibitor, DNA synthesis inhibitor, molecule with planar moieties
	oxyquinoline sulfate (8 hydroxyquinoline)	chelating agent, stabilizes hydrogen peroxide, transcription inhibitor, molecule with planar moieties
	pararosaniline pamoate	2 molecules: pararosaniline has antihelminthic activity, pamoate may be counter ion for many drugs, pararosanline is molecule with planar moieties
	quinacrine	binds to prion protein and inhibits aggregation, MAO inhibitor, inhibits Nf-kappa beta, activates p53 (intercalating agent), inhibits histamine N methyltransferase, intercalates
	digitoxin	inhibits Na+/K+ ATPase
	crinamine	inhibits HIF1 transcriptional activity but not HIF2
	paclitaxel	inhibits tubulin disassembly
	anisomycin	strongly activates JNK/SAPK and p38 MAPK, inhibits peptidyltransferase of 80S ribosome, at high concentration can inhibit DNA synthesis
	haloprogin	moderately disrupts c albicans membrane but not erythrocytes membrane; moderately inhibits O2 uptake by c albicans; moderately inhibits protein and nucleic acid synthesis in c albicans
	CA4	(unknown mechanism of action)
	INCREASED AVERAGE SG SIZE	**MECHANISM OF ACTION**
	celastrol	a triterpenoid that may modulate: p38 pathway; inhibit Hsp90; proteasome chymotrypsin-like activity; NFkappaB; PARylation
	thioridazine	phenothiazine derivative; has antihistamine and anticholinergic effect; weak dopamine D2 antagonist
	trans-resveratrol	molecule with planar moieties; may activate sirtuin1 and PGC1alpha (master regulator of mitochondrial biogenesis); may activate SOD2 (Mn2+ dependent SOD) and GPER (G-protein-coupled estrogen receptor 1)
	trimeprazine tartrate	phenothiazine derivative; has antihistamine activity
	butriptyline	strong antihistamine and anticholinergic; moderate serotonin 5HT2 receptor and alpha1 adrenergic receptor antagonist; and weak serotonin reuptake transporter SERT antagonist
	chukrasin	may inhibit the organic anion transport peptide (OATP1B1 and OATP1B3)
	e-capsaicin	binds to TRPV1 (vanilloid receptor subtype 1) ion channel to allow cations to enter neuron, depolarizing the neuron; TRPV1 can be opened by capsaicin, temperature, protons, and physical abrasion; depletes substance P which transmits pain sensation; neurotoxic
	eslicarbazepine acetate	prodrug of eslicarbazepine that binds to closed form of voltage gated Na+ channel, preventing it from opening
	estriol benzyl ether	estriol derivative
	ropinirole	dopamine D2, D3, D4 agonist (strongest for D2); mild serotonin 5HT2 and alpha2 adrenergic agonist
	chelerythrine chloride	molecule with planar moieties; PKC inhibitor; cannabinoid receptor CB1 antagonist; structurally very similar to sanguinarine which inhibits Na/K ATPase; somewhat similar structurally to chelidonine
	IPA-3	p21 activated kinase (PAK) inhibitor (p21 is a cyclin dependent kinase inhibitor that is a target of p53)

Table 1.1.3: Enumerating SG-modulating compounds identified in CV-B small molecule neural precursor cells, color-coded by cellular target superclasses as in Table 1.1.1. (Continued.)

	INCREASED AVERAGE SG SIZE	MECHANISM OF ACTION
	PMA (phorbol 12-myristate 13-acetate)	activates PKC; induces formation of superoxide radical; after infection with KSHV will activate early immediate viral protein RTA which leads to MAPK activation
	benzalkonium chloride	quaternary ammonium cationic surfactant
	chrysanthellin A	saponin (therefore probably surfactant in the class of digitonin)
	thonzonium bromide	quaternary ammonium cationic surfactant
	pargyline	MAO inhibitor, binds to I2
	rotenone	mitochondrial poison that inhibits transfer of electrons from complex 1 to ubiquinone/CoQ, leading to reduction of O2 to oxygen radicals and oxidative stress
	suramin	binds to lipoproteins as well as trypanosomal glycolytic proteins
	thapsigargin	noncompetitive inhibitor of sarco-/endoplasmic reticulum Ca2+ ATPase SERCA; inhibits autophagosome fusion with lysoome in the final step of autophagy leading to ER stress
	thimerosal	organomercury compound with ethylmercury moiety that can bind thiols and amines (oligodynamic effect)
	albendazole	benzimidazole class antihelminthic that binds to microtubules (same place as colchicine) and inhibit assembly
	mebendazole	benzimidazole class antihelminthic that binds to microtubules (same place as colchicine) and inhibit assembly
	vinblastine sulfate	vinca alkaloid that binds to tubulin and inhibits microtubule assembly
	ST20	(unknown mechanism of action)

Table 1.1.4: Enumerating SG-modulating compounds identified in both HEK293xT cells and CV-B small molecule neural precursor cells, color-coded by cellular target superclasses as in Table 1.1.1.

	DECREASED SG AREA/NUCLEI AREA	**MECHANISM OF ACTION**
	acriflavine hydrochloride	molecule with planar moieties and interferes with transcription and DNA replication; may bind to HIF-1 (hypoxia inducible factor-1)
	mitoxantrone	induces phosphorylation of PERK at threonine 980 leading to eIF2alpha phosphorylation (ER stress inducer), DNA topoisomerase II inhibitor, DNA synthesis inhibitor, molecule with planar moieties
	pararosaniline	2 molecules: pararosaniline has antihelminthic activity, pamoate may be counter ion for many drugs, pararosanline is molecule with planar moieties
	quinacrine	binds to prion protein and inhibits aggregation, MAO inhibitor, inhibits Nf-kappa beta, activates p53 (intercalating agent), inhibits histamine N methyltransferase, intercalates, inhibits phospholipase A2
	digitoxin	inhibits Na+/K+ ATPase
	lanatoside C	inhibits Na+/K+ ATPase
	ouabain	inhibits Na+/K+ ATPase
	proscillaridin	inhibits Na+/K+ ATPase
	oxyphenbutazone	inhibits cyclooxygenase (COX)
	WS3	inhibits ebp1/pa2g4, which regulates Rb and E2F, as well as being a dsRBP, a component of RNPs, associates with ribosomes, inhibits eIF2alpha ser51 phos, and can be phosphorylated by PKR
	ST1	(unknown mechanism of action)
	DECREASED SG COUNT/NUCLEI AREA	**MECHANISM OF ACTION**
	acriflavine hydrochloride	molecule with planar moieties and interferes with transcription and DNA replication; may bind to HIF-1 (hypoxia inducible factor-1)
	mitoxantrone hydrochloride	induces phosphorylation of PERK at threonine 980 leading to eIF2alpha phosphorylation (ER stress inducer), DNA topoisomerase II inhibitor, DNA synthesis inhibitor, molecule with planar moieties
	pararosaniline pamoate	2 molecules: pararosaniline has antihelminthic activity, pamoate may be counter ion for many drugs, pararosanline is molecule with planar moieties
	digitoxin	inhibits Na+/K+ ATPase
	lanatoside C	inhibits Na+/K+ ATPase
	ouabain (dihydroouabain, g strophanthin)	inhibits Na+/K+ ATPase
	proscillaridin A	inhibits Na+/K+ ATPase
	oxyphenbutazone	inhibits cyclooxygenase (COX)
	INCREASED SG COUNT/NUCLEI AREA	**MECHANISM OF ACTION**
	doxorubicin	molecule with planar moieties that intercalates DNA and inhibits DNA replication and DNA topoisomerase II
	epirubicin hydrochloride	molecule with planar moieties that intercalates DNA and inhibits DNA replication and DNA topoisomerase II
	DECREASED AVERAGE SG SIZE	**MECHANISM OF ACTION**
	acriflavine hydrochloride	molecule with planar moieties and interferes with transcription and DNA replication; may bind to HIF-1 (hypoxia inducible factor-1)
	dactinomycin	inhibits elongation of RNA polymerase, intercalating
	daunorubicin	molecule with planar moieties; intercalates DNA and inhibits DNA replication, inhibits DNA topoisomerase II, and promotes histone eviction thereby altering transcription
	doxorubicin	molecule with planar moieties that intercalates DNA and inhibits DNA replication and DNA topoisomerase II
	mitoxantrone hydrochloride	induces phosphorylation of PERK at threonine 980 leading to eIF2alpha phosphorylation (ER stress inducer), DNA topoisomerase II inhibitor, DNA synthesis inhibitor, molecule with planar moieties
	pararosaniline pamoate	2 molecules: pararosaniline has antihelminthic activity, pamoate may be counter ion for many drugs, pararosanline is molecule with planar moieties
	quinacrine	binds to prion protein and inhibits aggregation, MAO inhibitor, inhibits Nf-kappa beta, activates p53 (intercalating agent), inhibits histamine N methyltransferase, intercalates, inhibits phospholipase A2
	digitoxin	inhibits Na+/K+ ATPase
	paclitaxel	inhibits tubulin disassembly

Table 1.2.5: Enumerating SG screen hit compounds that were tested in HEK293xT cells in four counterscreen assays: dose response assay against $NaAsO_2$ stress, heat shock stress assay, thapsigargin stress assay, and $NaAsO_2$ pre-stress assay. Compounds color-coded by cellular target superclasses as in Table 1.1.1.

	COMPOUND	**MECHANISM OF ACTION**
	mitoxantrone	induces phosphorylation of PERK at threonine 980 leading to eIF2alpha phosphorylation (ER stress inducer), DNA topoisomerase II inhibitor, DNA synthesis inhibitor, molecule with planar moieties
	pararosaniline	2 molecules: pararosaniline has antihelminthic activity, pamoate may be counter ion for many drugs, pararosanline is molecule with planar moieties
	pyrvinium pamoate	binds to and potentiates CK1alpha, inhibiting Wnt signaling, molecule with planar moieties
	chlorothiazide (hydrochlorothiazide)	blocks Na+/Cl- cotransporter (e.g. distal convoluted tubule), carbonic anhydrase inhibitor
	digitoxin	inhibits Na+/K+ ATPase
	digoxin	inhibits Na+/K+ ATPase
	gitoxigenin	inhibits Na+/K+ ATPase
	lanatoside C	inhibits Na+/K+ ATPase
	ouabain	inhibits Na+/K+ ATPase
	peruvoside	inhibits Na+/K+ ATPase
	proscillaridin	inhibits Na+/K+ ATPase
	strophanthidinic acid lactone	inhibits Na+/K+ ATPase
	strophantidin	inhibits Na+/K+ ATPase
	gramicidin S	forms pores in lipid membrane that allow monovalent but not divalent cations and not anions through
	WS3	inhibits ebp1/pa2g4, which regulates Rb and E2F, as well as being a dsRBP, a component of RNPs, associates with ribosomes, inhibits eIF2alpha ser51 phos, and can be phosphorylated by PKR
	ST1	(unknown mechanism of action)

Table 1.2.6: Enumerating SG screen hit compounds that were tested in NPCs in four counterscreen assays: dose response assay against $NaAsO_2$, heat shock and thapsigargin stress assays as well as $NaAsO_2$ pre-stress assay. Compounds color-coded by cellular target superclasses as in Table 1.1.1.

	COMPOUND	MECHANISM OF ACTION
	8 hydroxyquinoline	chelating agent, stabilizes hydrogen peroxide, transcription inhibitor
	dactinomycin	inhibits elongation of RNA polymerase, intercalating
	mitoxantrone	induces phosphorylation of PERK at threonine 980 leading to eIF2alpha phosphorylation (ER stress inducer), DNA topoisomerase II inhibitor, DNA synthesis inhibitor, molecule with planar moieties
	pararosaniline	2 molecules: pararosaniline has antihelminthic activity, pamoate may be counter ion for many drugs, pararosanline is molecule with planar moieties
	quinacrine	binds to prion protein and inhibits aggregation, MAO inhibitor, inhibits Nf-kappa beta, activates p53 (intercalating agent), inhibits histamine N methyltransferase, intercalates
	digitoxin	inhibits Na+/K+ ATPase
	ivermectin	potentiates GABA-A receptor
	lanatoside C	inhibits Na+/K+ ATPase
	ouabain	inhibits Na+/K+ ATPase
	penfluridol	diphenylbutylpiperidine that blocks D2 receptors
	proscillaridin	inhibits Na+/K+ ATPase
	tyrphostin A9	receptor tyrosine kinase inhibitor (selective for PDGFR)
	tomatine	precipitates cholesterol and disrupts membranes (structurally similar to digitonin), immune adjuvant
	oxyphenbutazone	inhibits cyclooxygenase (COX)
	paclitaxel	inhibits tubulin disassembly
	anisomycin	strongly activates JNK/SAPK and p38 MAPK, inhibits peptidyltransferase of 80S ribosome, at high concentration can inhibit DNA synthesis
	WS3	inhibits ebp1/pa2g4, which regulates Rb and E2F, as well as being a dsRBP, a component of RNPs, associates with ribosomes, inhibits eIF2alpha ser51 phos, and can be phosphorylated by PKR
	ST1	(unknown mechanism of action)

Table 1.3.7: Enumerating SG screen hit compounds that were tested in control, *TARDBP* mutant, or *FUS* mutant iPS-MNs against $NaAsO_2$ stress, thapsigargin stress, or puromycin stress. Compounds color-coded by cellular target superclasses as in Table 1.1.1.

	COMPOUND	**MECHANISM OF ACTION**
	DMSO	negative control; vehicle
	cycloheximide	positive control; inhibits ribosomal translocation
	8 hydroxyquinoline	chelating agent, stabilizes hydrogen peroxide, transcription inhibitor
	daunorubicin	molecule with planar moieties; intercalates DNA and inhibits DNA replication, inhibits DNA topoisomerase II, and promotes histone eviction thereby altering transcription
	mitoxantrone	induces phosphorylation of PERK at threonine 980 leading to eIF2alpha phosphorylation (ER stress inducer), DNA topoisomerase II inhibitor, DNA synthesis inhibitor, molecule with planar moieties
	pyrvinium pamoate	binds to and potentiates CK1alpha, inhibiting Wnt signaling, molecule with planar moieties
	quinacrine	binds to prion protein and inhibits aggregation, MAO inhibitor, inhibits Nf-kappa beta, activates p53 (intercalating agent), inhibits histamine N methyltransferase, intercalates
	digitoxin	inhibits Na+/K+ ATPase
	penfluridol	diphenylbutylpiperidine that blocks D2 receptors
	benzethonium chloride	quaternary ammonium cationic surfactant; may have nicotinic and muscarinic anticholinergic activity; may cause loss of mitochondrial membrane potential and incr cytosolic Ca
	anisomycin	strongly activates JNK/SAPK and p38 MAPK, inhibits peptidyltransferase of 80S ribosome, at high concentration can inhibit DNA synthesis
	WS3	inhibits ebp1/pa2g4, which regulates Rb and E2F, as well as being a dsRBP, a component of RNPs, associates with ribosomes, inhibits eIF2alpha ser51 phos, and can be phosphorylated by PKR

REFERENCES

1. N. Kedersha, P. Anderson, Mammalian Stress Granules and Processing Bodies. **431**, 61-81 (2007).

2. N. Kedersha, P. Ivanov, P. Anderson, Stress granules and cell signaling: more than just a passing phase? *Trends in biochemical sciences* **38**, 494-506 (2013).

3. A. Khong, T. Matheny, S. Jain, S. F. Mitchell, J. R. Wheeler, R. Parker, The Stress Granule Transcriptome Reveals Principles of mRNA Accumulation in Stress Granules. *Molecular cell* **68**, 808-820 e805 (2017).

4. N. Kedersha, S. Chen, N. Gilks, W. Li, I. J. Miller, J. Stahl, P. Anderson, Evidence that ternary complex (eIF2-GTP-tRNA(i)(Met))-deficient preinitiation complexes are core constituents of mammalian stress granules. *Molecular biology of the cell* **13**, 195-210 (2002).

5. C. Sidrauski, A. M. McGeachy, N. T. Ingolia, P. Walter, The small molecule ISRIB reverses the effects of eIF2alpha phosphorylation on translation and stress granule assembly. *Elife* **4**, (2015).

6. H. P. Harding, I. Novoa, Y. Zhang, H. Zeng, R. Wek, M. Schapira, D. Ron, Regulated translation initiation controls stress-induced gene expression in mammalian cells. *Molecular cell* **6**, 1099-1108 (2000).

7. K. Arimoto, H. Fukuda, S. Imajoh-Ohmi, H. Saito, M. Takekawa, Formation of stress granules inhibits apoptosis by suppressing stress-responsive MAPK pathways. *Nature cell biology* **10**, 1324-1332 (2008).

8. F. Wippich, B. Bodenmiller, M. G. Trajkovska, S. Wanka, R. Aebersold, L. Pelkmans, Dual specificity kinase DYRK3 couples stress granule condensation/dissolution to mTORC1 signaling. *Cell* **152**, 791-805 (2013).

9. J. R. Wheeler, T. Matheny, S. Jain, R. Abrisch, R. Parker, Distinct stages in stress granule assembly and disassembly. *Elife* **5**, (2016).

10. S. Jain, J. R. Wheeler, R. W. Walters, A. Agrawal, A. Barsic, R. Parker, ATPase-Modulated Stress Granules Contain a Diverse Proteome and Substructure. *Cell* **164**, 487-498 (2016).

11. S. Markmiller, S. Soltanieh, K. L. Server, R. Mak, W. Jin, M. Y. Fang, E. C. Luo, F. Krach, D. Yang, A. Sen, A. Fulzele, J. M. Wozniak, D. J. Gonzalez, M. W. Kankel, F. B. Gao, E. J. Bennett, E. Lecuyer, G. W. Yeo, Context-Dependent and Disease-

Specific Diversity in Protein Interactions within Stress Granules. *Cell* **172**, 590-604 e513 (2018).

12. J. Y. Youn, W. H. Dunham, S. J. Hong, J. D. R. Knight, M. Bashkurov, G. I. Chen, H. Bagci, B. Rathod, G. MacLeod, S. W. M. Eng, S. Angers, Q. Morris, M. Fabian, J. F. Cote, A. C. Gingras, High-Density Proximity Mapping Reveals the Subcellular Organization of mRNA-Associated Granules and Bodies. *Molecular cell* **69**, 517-532 e511 (2018).

13. K. W. Brannan, W. Jin, S. C. Huelga, C. A. Banks, J. M. Gilmore, L. Florens, M. P. Washburn, E. L. Van Nostrand, G. A. Pratt, M. K. Schwinn, D. L. Daniels, G. W. Yeo, SONAR Discovers RNA-Binding Proteins from Analysis of Large-Scale Protein-Protein Interactomes. *Molecular cell* **64**, 282-293 (2016).

14. A. Castello, B. Fischer, K. Eichelbaum, R. Horos, B. M. Beckmann, C. Strein, N. E. Davey, D. T. Humphreys, T. Preiss, L. M. Steinmetz, J. Krijgsveld, M. W. Hentze, Insights into RNA biology from an atlas of mammalian mRNA-binding proteins. *Cell* **149**, 1393-1406 (2012).

15. A. Castello, B. Fischer, C. K. Frese, R. Horos, A. M. Alleaume, S. Foehr, T. Curk, J. Krijgsveld, M. W. Hentze, Comprehensive Identification of RNA-Binding Domains in Human Cells. *Molecular cell* **63**, 696-710 (2016).

16. A. S. Chen-Plotkin, V. M. Lee, J. Q. Trojanowski, TAR DNA-binding protein 43 in neurodegenerative disease. *Nat Rev Neurol* **6**, 211-220 (2010).

17. Y. Shang, E. J. Huang, Mechanisms of FUS mutations in familial amyotrophic lateral sclerosis. *Brain Res* **1647**, 65-78 (2016).

18. V. H. Ryan, G. L. Dignon, G. H. Zerze, C. V. Chabata, R. Silva, A. E. Conicella, J. Amaya, K. A. Burke, J. Mittal, N. L. Fawzi, Mechanistic View of hnRNPA2 Low-Complexity Domain Structure, Interactions, and Phase Separation Altered by Mutation and Arginine Methylation. *Molecular cell* **69**, 465-479 e467 (2018).

19. H. J. Kim, N. C. Kim, Y. D. Wang, E. A. Scarborough, J. Moore, Z. Diaz, K. S. MacLea, B. Freibaum, S. Li, A. Molliex, A. P. Kanagaraj, R. Carter, K. B. Boylan, A. M. Wojtas, R. Rademakers, J. L. Pinkus, S. A. Greenberg, J. Q. Trojanowski, B. J. Traynor, B. N. Smith, S. Topp, A. S. Gkazi, J. Miller, C. E. Shaw, M. Kottlors, J. Kirschner, A. Pestronk, Y. R. Li, A. F. Ford, A. D. Gitler, M. Benatar, O. D. King, V. E. Kimonis, E. D. Ross, C. C. Weihl, J. Shorter, J. P. Taylor, Mutations in prion-like domains in hnRNPA2B1 and hnRNPA1 cause multisystem proteinopathy and ALS. *Nature* **495**, 467-473 (2013).

20. T. J. Kwiatkowski, Jr., D. A. Bosco, A. L. Leclerc, E. Tamrazian, C. R. Vanderburg, C. Russ, A. Davis, J. Gilchrist, E. J. Kasarskis, T. Munsat, P. Valdmanis, G. A. Rouleau, B. A. Hosler, P. Cortelli, P. J. de Jong, Y. Yoshinaga, J. L. Haines, M. A. Pericak-Vance,

J. Yan, N. Ticozzi, T. Siddique, D. McKenna-Yasek, P. C. Sapp, H. R. Horvitz, J. E. Landers, R. H. Brown, Jr., Mutations in the FUS/TLS gene on chromosome 16 cause familial amyotrophic lateral sclerosis. *Science* **323**, 1205-1208 (2009).

21. J. Sreedharan, I. P. Blair, V. B. Tripathi, X. Hu, C. Vance, B. Rogelj, S. Ackerley, J. C. Durnall, K. L. Williams, E. Buratti, F. Baralle, J. de Belleroche, J. D. Mitchell, P. N. Leigh, A. Al-Chalabi, C. C. Miller, G. Nicholson, C. E. Shaw, TDP-43 mutations in familial and sporadic amyotrophic lateral sclerosis. *Science* **319**, 1668-1672 (2008).

22. C. Vance, B. Rogelj, T. Hortobagyi, K. J. De Vos, A. L. Nishimura, J. Sreedharan, X. Hu, B. Smith, D. Ruddy, P. Wright, J. Ganesalingam, K. L. Williams, V. Tripathi, S. Al-Saraj, A. Al-Chalabi, P. N. Leigh, I. P. Blair, G. Nicholson, J. de Belleroche, J. M. Gallo, C. C. Miller, C. E. Shaw, Mutations in FUS, an RNA processing protein, cause familial amyotrophic lateral sclerosis type 6. *Science* **323**, 1208-1211 (2009).

23. F. J. Martinez, G. A. Pratt, E. L. Van Nostrand, R. Batra, S. C. Huelga, K. Kapeli, P. Freese, S. J. Chun, K. Ling, C. Gelboin-Burkhart, Protein-RNA Networks Regulated by Normal and ALS-Associated Mutant HNRNPA2B1 in the Nervous System. *Neuron* **92**, 780-795 (2016).

24. S. C. Ling, M. Polymenidou, D. W. Cleveland, Converging mechanisms in ALS and FTD: disrupted RNA and protein homeostasis. *Neuron* **79**, 416-438 (2013).

25. T. Murakami, S. Qamar, J. Q. Lin, G. S. Schierle, E. Rees, A. Miyashita, A. R. Costa, R. B. Dodd, F. T. Chan, C. H. Michel, D. Kronenberg-Versteeg, Y. Li, S. P. Yang, Y. Wakutani, W. Meadows, R. R. Ferry, L. Dong, G. G. Tartaglia, G. Favrin, W. L. Lin, D. W. Dickson, M. Zhen, D. Ron, G. Schmitt-Ulms, P. E. Fraser, N. A. Shneider, C. Holt, M. Vendruscolo, C. F. Kaminski, P. St George-Hyslop, ALS/FTD Mutation-Induced Phase Transition of FUS Liquid Droplets and Reversible Hydrogels into Irreversible Hydrogels Impairs RNP Granule Function. *Neuron* **88**, 678-690 (2015).

26. A. Patel, H. O. Lee, L. Jawerth, S. Maharana, M. Jahnel, M. Y. Hein, S. Stoynov, J. Mahamid, S. Saha, T. M. Franzmann, A. Pozniakovski, I. Poser, N. Maghelli, L. A. Royer, M. Weigert, E. W. Myers, S. Grill, D. Drechsel, A. A. Hyman, S. Alberti, A Liquid-to-Solid Phase Transition of the ALS Protein FUS Accelerated by Disease Mutation. *Cell* **162**, 1066-1077 (2015).

27. M. Kato, T. W. Han, S. Xie, K. Shi, X. Du, L. C. Wu, H. Mirzaei, E. J. Goldsmith, J. Longgood, J. Pei, N. V. Grishin, D. E. Frantz, J. W. Schneider, S. Chen, L. Li, M. R. Sawaya, D. Eisenberg, R. Tycko, S. L. McKnight, Cell-free formation of RNA granules: low complexity sequence domains form dynamic fibers within hydrogels. *Cell* **149**, 753-767 (2012).

28. M. A. Farg, K. Y. Soo, S. T. Warraich, V. Sundaramoorthy, I. P. Blair, J. D. Atkin, Ataxin-2 interacts with FUS and intermediate-length polyglutamine expansions enhance FUS-related pathology in amyotrophic lateral sclerosis. *Hum Mol Genet* **22**, 717-728 (2013).

29. A. M. Blokhuis, E. J. Groen, M. Koppers, L. H. van den Berg, R. J. Pasterkamp, Protein aggregation in amyotrophic lateral sclerosis. *Acta Neuropathol* **125**, 777-794 (2013).

30. B. A. Keller, K. Volkening, C. A. Droppelmann, L. C. Ang, R. Rademakers, M. J. Strong, Co-aggregation of RNA binding proteins in ALS spinal motor neurons: evidence of a common pathogenic mechanism. *Acta Neuropathol* **124**, 733-747 (2012).

31. E. Bentmann, M. Neumann, S. Tahirovic, R. Rodde, D. Dormann, C. Haass, Requirements for stress granule recruitment of fused in sarcoma (FUS) and TAR DNA-binding protein of 43 kDa (TDP-43). *The Journal of biological chemistry* **287**, 23079-23094 (2012).

32. L. Liu-Yesucevitz, A. Bilgutay, Y. J. Zhang, T. Vanderweyde, A. Citro, T. Mehta, N. Zaarur, A. McKee, R. Bowser, M. Sherman, L. Petrucelli, B. Wolozin, Tar DNA binding protein-43 (TDP-43) associates with stress granules: analysis of cultured cells and pathological brain tissue. *PloS one* **5**, e13250 (2010).

33. D. J. Apicco, P. E. A. Ash, B. Maziuk, C. LeBlang, M. Medalla, A. Al Abdullatif, A. Ferragud, E. Botelho, H. I. Ballance, U. Dhawan, S. Boudeau, A. L. Cruz, D. Kashy, A. Wong, L. R. Goldberg, N. Yazdani, C. Zhang, C. Y. Ung, Y. Tripodis, N. M. Kanaan, T. Ikezu, P. Cottone, J. Leszyk, H. Li, J. Luebke, C. D. Bryant, B. Wolozin, Reducing the RNA binding protein TIA1 protects against tau-mediated neurodegeneration in vivo. *Nature neuroscience* **21**, 72-80 (2018).

34. H. J. Kim, A. R. Raphael, E. S. LaDow, L. McGurk, R. A. Weber, J. Q. Trojanowski, V. M. Lee, S. Finkbeiner, A. D. Gitler, N. M. Bonini, Therapeutic modulation of eIF2alpha phosphorylation rescues TDP-43 toxicity in amyotrophic lateral sclerosis disease models. *Nature genetics* **46**, 152-160 (2014).

35. L. A. Becker, B. Huang, G. Bieri, R. Ma, D. A. Knowles, P. Jafar-Nejad, J. Messing, H. J. Kim, A. Soriano, G. Auburger, S. M. Pulst, J. P. Taylor, F. Rigo, A. D. Gitler, Therapeutic reduction of ataxin-2 extends lifespan and reduces pathology in TDP-43 mice. *Nature* **544**, 367-371 (2017).

36. N. Kedersha, M. D. Panas, C. A. Achorn, S. Lyons, S. Tisdale, T. Hickman, M. Thomas, J. Lieberman, G. M. McInerney, P. Ivanov, P. Anderson, G3BP-Caprin1-USP10 complexes mediate stress granule condensation and associate with 40S subunits. *The Journal of cell biology* **212**, 845-860 (2016).

37. J. H. Zhang, T. D. Chung, K. R. Oldenburg, A Simple Statistical Parameter for Use in Evaluation and Validation of High Throughput Screening Assays. *Journal of biomolecular screening* **4**, 67-73 (1999).

38. P. A. Ivanov, E. M. Chudinova, E. S. Nadezhdina, Disruption of microtubules inhibits cytoplasmic ribonucleoprotein stress granule formation. *Exp Cell Res* **290**, 227-233 (2003).

39. M. F. Burkhardt, F. J. Martinez, S. Wright, C. Ramos, D. Volfson, M. Mason, J. Garnes, V. Dang, J. Lievers, U. Shoukat-Mumtaz, R. Martinez, H. Gai, R. Blake, E. Vaisberg, M. Grskovic, C. Johnson, S. Irion, J. Bright, B. Cooper, L. Nguyen, I. Griswold-Prenner, A. Javaherian, A cellular model for sporadic ALS using patient-derived induced pluripotent stem cells. *Mol Cell Neurosci* **56**, 355-364 (2013).

40. Y. M. Yang, S. K. Gupta, K. J. Kim, B. E. Powers, A. Cerqueira, B. J. Wainger, H. D. Ngo, K. A. Rosowski, P. A. Schein, C. A. Ackeifi, A. C. Arvanites, L. S. Davidow, C. J. Woolf, L. L. Rubin, A small molecule screen in stem-cell-derived motor neurons identifies a kinase inhibitor as a candidate therapeutic for ALS. *Cell stem cell* **12**, 713-726 (2013).

41. A. Patel, L. Malinovska, S. Saha, J. Wang, S. Alberti, Y. Krishnan, A. A. Hyman, ATP as a biological hydrotrope. *Science* **356**, 753-756 (2017).

42. S. F. Banani, H. O. Lee, A. A. Hyman, M. K. Rosen, Biomolecular condensates: organizers of cellular biochemistry. *Nature reviews. Molecular cell biology* **18**, 285-298 (2017).

43. J. B. Rayman, K. A. Karl, E. R. Kandel, TIA-1 Self-Multimerization, Phase Separation, and Recruitment into Stress Granules Are Dynamically Regulated by Zn(2). *Cell Rep* **22**, 59-71 (2018).

44. J. R. Buchan, R. M. Kolaitis, J. P. Taylor, R. Parker, Eukaryotic stress granules are cleared by autophagy and Cdc48/VCP function. *Cell* **153**, 1461-1474 (2013).

45. A. Turakhiya, S. R. Meyer, G. Marincola, S. Bohm, J. T. Vanselow, A. Schlosser, K. Hofmann, A. Buchberger, ZFAND1 Recruits p97 and the 26S Proteasome to Promote the Clearance of Arsenite-Induced Stress Granules. *Molecular cell* **70**, 906-919 e907 (2018).

46. N. Gilks, N. Kedersha, M. Ayodele, L. Shen, G. Stoecklin, L. M. Dember, P. Anderson, Stress granule assembly is mediated by prion-like aggregation of TIA-1. *Molecular biology of the cell* **15**, 5383-5398 (2004).

47. A. Jain, R. D. Vale, RNA phase transitions in repeat expansion disorders. *Nature* **546**, 243-247 (2017).

48. C. Korth, B. C. May, F. E. Cohen, S. B. Prusiner, Acridine and phenothiazine derivatives as pharmacotherapeutics for prion disease. *Proceedings of the National Academy of Sciences of the United States of America* **98**, 9836-9841 (2001).

49. F. Krach, R. Batra, E. C. Wheeler, A. Q. Vu, R. Wang, K. Hutt, S. J. Rabin, M. W. Baughn, R. T. Libby, S. Diaz-Garcia, J. Stauffer, E. Pirie, S. Saberi, M. Rodriguez, A. A. Madrigal, Z. Kohl, B. Winner, G. W. Yeo, J. Ravits, Transcriptome-pathology correlation identifies interplay between TDP-43 and the expression of its kinase CK1E in sporadic ALS. *Acta Neuropathol* **136**, 405-423 (2018).

50. N. H. Alami, R. B. Smith, M. A. Carrasco, L. A. Williams, C. S. Winborn, S. S. W. Han, E. Kiskinis, B. Winborn, B. D. Freibaum, A. Kanagaraj, A. J. Clare, N. M. Badders, B. Bilican, E. Chaum, S. Chandran, C. E. Shaw, K. C. Eggan, T. Maniatis, J. P. Taylor, Axonal transport of TDP-43 mRNA granules is impaired by ALS-causing mutations. *Neuron* **81**, 536-543 (2014).

51. K. Kapeli, G. A. Pratt, A. Q. Vu, K. R. Hutt, F. J. Martinez, B. Sundararaman, R. Batra, P. Freese, N. J. Lambert, S. C. Huelga, S. J. Chun, T. Y. Liang, J. Chang, J. P. Donohue, L. Shiue, J. Zhang, H. Zhu, F. Cambi, E. Kasarskis, S. Hoon, M. Ares, Jr., C. B. Burge, J. Ravits, F. Rigo, G. W. Yeo, Distinct and shared functions of ALS-associated proteins TDP-43, FUS and TAF15 revealed by multisystem analyses. *Nat Commun* **7**, 12143 (2016).

52. P. Reinhardt, M. Glatza, K. Hemmer, Y. Tsytsyura, C. S. Thiel, S. Hoing, S. Moritz, J. A. Parga, L. Wagner, J. M. Bruder, G. Wu, B. Schmid, A. Ropke, J. Klingauf, J. C. Schwamborn, T. Gasser, H. R. Scholer, J. Sterneckert, Derivation and expansion using only small molecules of human neural progenitors for neurodegenerative disease modeling. *PloS one* **8**, e59252 (2013).

53. A. E. Carpenter, T. R. Jones, M. R. Lamprecht, C. Clarke, I. H. Kang, O. Friman, D. A. Guertin, J. H. Chang, R. A. Lindquist, J. Moffat, P. Golland, D. M. Sabatini, CellProfiler: image analysis software for identifying and quantifying cell phenotypes. *Genome Biol* **7**, R100 (2006).

54. N. Malo, J. A. Hanley, S. Cerquozzi, J. Pelletier, R. Nadon, Statistical practice in high-throughput screening data analysis. *Nature biotechnology* **24**, 167-175 (2006).

55. A. Birmingham, L. M. Selfors, T. Forster, D. Wrobel, C. J. Kennedy, E. Shanks, J. Santoyo-Lopez, D. J. Dunican, A. Long, D. Kelleher, Q. Smith, R. L. Beijersbergen, P. Ghazal, C. E. Shamu, Statistical methods for analysis of high-throughput RNA interference screens. *Nat Methods* **6**, 569-575 (2009).

56. T. Aittokallio, Dealing with missing values in large-scale studies: microarray data imputation and beyond. *Brief Bioinform* **11**, 253-264 (2010).

57. F. Mosteller, J. W. Tukey, *Data analysis and regression : a second course in statistics*. Addison-Wesley series in behavioral science (Addison-Wesley Pub. Co., Reading, Mass., 1977), pp. xvii, 588 pages.

58. C. Brideau, B. Gunter, B. Pikounis, A. Liaw, Improved statistical methods for hit selection in high-throughput screening. *Journal of biomolecular screening* **8**, 634-647 (2003).

59. G. W. Wright, R. M. Simon, A random variance model for detection of differential gene expression in small microarray experiments. *Bioinformatics* **19**, 2448-2455 (2003).

60. C. A. Schneider, W. S. Rasband, K. W. Eliceiri, NIH Image to ImageJ: 25 years of image analysis. *Nat Methods* **9**, 671-675 (2012).

61. U. Nonhoff, M. Ralser, F. Welzel, I. Piccini, D. Balzereit, M. L. Yaspo, H. Lehrach, S. Krobitsch, Ataxin-2 interacts with the DEAD/H-box RNA helicase DDX6 and interferes with P-bodies and stress granules. *Molecular biology of the cell* **18**, 1385-1396 (2007).

62. S. C. Gopinath, A. Matsugami, M. Katahira, P. K. Kumar, Human vault-associated non-coding RNAs bind to mitoxantrone, a chemotherapeutic compound. *Nucleic Acids Res* **33**, 4874-4881 (2005).

63. R. J. White, F. E. Durr, Development of mitoxantrone. *Invest New Drugs* **3**, 85-93 (1985).

64. S. Zheng, Y. Chen, C. P. Donahue, M. S. Wolfe, G. Varani, Structural basis for stabilization of the tau pre-mRNA splicing regulatory element by novantrone (mitoxantrone). *Chem Biol* **16**, 557-566 (2009).

65. W. D. Wilson, L. Ratmeyer, M. Zhao, L. Strekowski, D. Boykin, The search for structure-specific nucleic acid-interactive drugs: effects of compound structure on RNA versus DNA interaction strength. *Biochemistry* **32**, 4098-4104 (1993).

66. J. Wang, J. Du, Z. Wu, Q. Jin, Quinacrine impairs enterovirus 71 RNA replication by preventing binding of polypyrimidine-tract binding protein with internal ribosome entry sites. *PloS one* **8**, e52954 (2013).

67. M. Shen, S. Bellaousov, M. Hiller, P. de La Grange, T. P. Creamer, O. Malina, R. Sperling, D. H. Mathews, P. Stoilov, S. Stamm, Pyrvinium pamoate changes alternative splicing of the serotonin receptor 2C by influencing its RNA structure. *Nucleic Acids Res* **41**, 3819-3832 (2013).

68. J. Schindelin, I. Arganda-Carreras, E. Frise, V. Kaynig, M. Longair, T. Pietzsch, S. Preibisch, C. Rueden, S. Saalfeld, B. Schmid, J. Y. Tinevez, D. J. White, V. Hartenstein, K. Eliceiri, P. Tomancak, A. Cardona, Fiji: an open-source platform for biological-image analysis. *Nat Methods* **9**, 676-682 (2012).

69. E. M. M. V. Manders, F.J.; Aten J.A., Measurement of co-localization of objects in dual-colour confocal images. *Journal of Microscopy* **169**, 375-382 (1993).

70. S. J. Parker, J. Meyerowitz, J. L. James, J. R. Liddell, P. J. Crouch, K. M. Kanninen, A. R. White, Endogenous TDP-43 localized to stress granules can subsequently form protein aggregates. *Neurochem Int* **60**, 415-424 (2012).

71. S. J. Barmada, G. Skibinski, E. Korb, E. J. Rao, J. Y. Wu, S. Finkbeiner, Cytoplasmic mislocalization of TDP-43 is toxic to neurons and enhanced by a mutation associated with familial amyotrophic lateral sclerosis. *J Neurosci* **30**, 639-649 (2010).

72. H. Wils, G. Kleinberger, J. Janssens, S. Pereson, G. Joris, I. Cuijt, V. Smits, C. Ceuterick-de Groote, C. Van Broeckhoven, S. Kumar-Singh, TDP-43 transgenic mice develop spastic paralysis and neuronal inclusions characteristic of ALS and frontotemporal lobar degeneration. *Proceedings of the National Academy of Sciences of the United States of America* **107**, 3858-3863 (2010).

73. L. M. Igaz, L. K. Kwong, E. B. Lee, A. Chen-Plotkin, E. Swanson, T. Unger, J. Malunda, Y. Xu, M. J. Winton, J. Q. Trojanowski, V. M. Lee, Dysregulation of the ALS-associated gene TDP-43 leads to neuronal death and degeneration in mice. *J Clin Invest* **121**, 726-738 (2011).

74. K. Zhang, J. G. Daigle, K. M. Cunningham, A. N. Coyne, K. Ruan, J. C. Grima, K. E. Bowen, H. Wadhwa, P. Yang, F. Rigo, J. P. Taylor, A. D. Gitler, J. D. Rothstein, T. E. Lloyd, Stress Granule Assembly Disrupts Nucleocytoplasmic Transport. *Cell*, (2018).

75. C. Sidrauski, D. Acosta-Alvear, A. Khoutorsky, P. Vedantham, B. R. Hearn, H. Li, K. Gamache, C. M. Gallagher, K. K. Ang, C. Wilson, V. Okreglak, A. Ashkenazi, B. Hann, K. Nader, M. R. Arkin, A. R. Renslo, N. Sonenberg, P. Walter, Pharmacological brake-release of mRNA translation enhances cognitive memory. *Elife* **2**, e00498 (2013).

76. E. M. Langdon, Y. Qiu, A. Ghanbari Niaki, G. A. McLaughlin, C. A. Weidmann, T. M. Gerbich, J. A. Smith, J. M. Crutchley, C. M. Termini, K. M. Weeks, S. Myong, A. S. Gladfelter, mRNA structure determines specificity of a polyQ-driven phase separation. *Science* **360**, 922-927 (2018).

77. S. Maharana, J. Wang, D. K. Papadopoulos, D. Richter, A. Pozniakovsky, I. Poser, M. Bickle, S. Rizk, J. Guillen-Boixet, T. M. Franzmann, M. Jahnel, L. Marrone, Y. T. Chang, J. Sterneckert, P. Tomancak, A. A. Hyman, S. Alberti, RNA buffers the phase separation behavior of prion-like RNA binding proteins. *Science* **360**, 918-921 (2018).

78. S. Alberti, R. Halfmann, O. King, A. Kapila, S. Lindquist, A systematic survey identifies prions and illuminates sequence features of prionogenic proteins. *Cell* **137**, 146-158 (2009).

79. J. Wang, J. M. Choi, A. S. Holehouse, H. O. Lee, X. Zhang, M. Jahnel, S. Maharana, R. Lemaitre, A. Pozniakovsky, D. Drechsel, I. Poser, R. V. Pappu, S. Alberti, A. A. Hyman, A Molecular Grammar Governing the Driving Forces for Phase Separation of Prion-like RNA Binding Proteins. *Cell* **174**, 688-699 e616 (2018).

80. G. T. Dolphin, S. Chierici, M. Ouberai, P. Dumy, J. Garcia, A multimeric quinacrine conjugate as a potential inhibitor of Alzheimer's beta-amyloid fibril formation. *Chembiochem* **9**, 952-963 (2008).